Diploma Thesis

Low carbon concrete: Design of a CEM III high-performance concrete (CEM III-UHPC)

submitted in satisfaction of the requirements for the degree
Diplom-Ingenieur
of the TU Wien, Faculty of Civil and Environmental Engineering

---

Diplomarbeit

Kohlenstoffarmer Beton: Entwurf eines CEM III-Hochleistungsbetons (CEM III-UHPC)

ausgeführt zum Zwecke der Erlangung des akademischen Grads
Diplom-Ingenieur
eingereicht an der TU Wien, Fakultät für Bau- und Umweltingenieurwesen

Thomas Seiringer, BSc

Matr.Nr.: 01426248

Betreuung: Univ.Prof.in **Agathe Robisson**, PhD
Senior Scientist Dipl.-Ing. Dr.techn **Johannes Kirnbauer**
Institut für Werkstofftechnologie, Bauphysik und Bauökologie
Forschungsbereich Baustofflehre und Werkstofftechnologie
Technische Universität Wien
Karlsplatz 13/E207-01, 1040 Wien, Österreich

Wien, im Oktober 2024

Danksagung

Ich möchte mich an dieser Stelle bei Frau Univ.-Prof.in Agathe Robisson, PhD für die Möglichkeit zu dieser interessanten Diplomarbeit an ihrem Institut bedanken. Ein besonderer Dank gilt meinem Betreuer Dipl.-Ing. Dr.techn. Johannes Kirnbauer, der mir nicht nur zahlreiche wertvolle Inputs geliefert hat, sondern mich gemeinsam mit Benjamin Marksteiner durchgehend bei der Versuchsdurchführung sowie der Vorbereitung unterstützt hat. Beide haben immer ein sehr angenehmes Arbeitsklima geschaffen. Weiters möchte ich mich bei allen am Institut beschäftigten Kolleginnen und Kollegen für ihre Denkanstöße und hilfsbereite Zusammenarbeit bedanken.

Der größte Dank gilt meinen Eltern, Alfons und Lydia, meiner Partnerin Jasmine, sowie meinen Geschwistern Nadine, Mario, Victoria und Madleine für ihre andauernde Unterstützung und ihr Verständnis. Zu guter Letzt möchte ich mich bei allen Freunden, Kollegen und Bekannten bedanken, die mich auf meinem Weg begleitet haben.

Abstract

In order to reach net zero emissions by the year 2050, as stated in the *Paris Agreement*, the sector *Building Materials and Construction*, which contributes 11% to the total emissions, needs to develop by reducing the Kilograms of Carbon Dioxide Equivalent ($kgCO_2e$) emissions [66][69].

A major pollution factor is the cement industry, particularly the production of Portland cement clinker [7]. Due to a chemical reaction, where the embodied carbon in the limestone's atomic structure gets released, this process cannot simply turn carbon dioxide (CO_2)-neutral by running it with green energy [24]. One alternative to conventional Portland Cement (CEM I) is the so called *Blast Furnace Cement with 66-80% Slag (CEM III/B)*. Consisting mostly of Blast Furnace Slag (BFS), a byproduct of steel production, it is considered as an environmentally friendly alternative [19].

This thesis explores whether CEM III/B is suitable for producing usable Ultra High Performance Concrete (UHPC) and experiments with different amounts of additives added to the mixture to observe how they influence the fresh and hardened concrete properties. Different mixes were tested with a Water to Cement Ratio (w/c) of 0.25, which is typical for UHPC, to ensure a good balance between workability and compressive strength. The replacement of 10 to 30 percent of the cement mass with Limestone Powder (LS), and 10 to 40 percent with Microsilica (MS), was also studied to observe the impact on the mixtures properties.

In this work, we further focused on the mixture design, especially regarding packing density. Workability issues, in form of strong shear thickening effects, were addressed by implementing the *surplus water* factor, which provides direct information on whether the amount of water is sufficient to fill the voids in the bulk volume.

With the promising strength results of this thesis, further research is recommended, particularly focusing on the addition of steel fibres for reinforcement, with the perspective to significantly enhance the strength, especially the bending tensile strength. Additionally, a subsequent thesis should investigate whether factors other than packing density contribute to the shear thickening, as this phenomenon was more pronounced than in CEM I UHPC mixtures. Further, a larger specimen series should also be tested with the updated calculation to highlight the importance of the amount of surplus water in the mixture design.

Since a considerable proportion of slag is already utilized in various applications, CEM III/B does not have the potential to revolutionize the cement industry alone. Therefore, additional alternatives are required, and luckily, a lot of research is going on right now. The goal should be to have a range of different alternatives, each for its own special application.

The research for cement technology in the last decades has put a huge gap on the map between the potential strengths of the material and the actual strengths used by the industry [9]. This makes it an opportune time to focus on developing alternatives that can achieve the same strengths already obtained with conventional concrete.

Kurzfassung

Wie im *Pariser Abkommen* beschlossen, sollen bis zum Jahre 2050 Netto-Null-Emissionen erreicht werden. Dafür muss sich der Sektor *Baustoffe und Bauwesen*, der 11% zu den Gesamtemissionen beiträgt, weiterentwickeln und die kgCO_2e Emissionen deutlich reduzieren [66][69].

Ein Großteil der Emissionen wird durch die Zementindustrie verursacht, insbesondere durch die Herstellung von Portlandzementklinker [7]. Da bei diesem Prozess durch eine chemische Reaktion der in Kalkstein gebundene Kohlenstoff freigesetzt wird, kann dieses Verfahren nicht gänzlich CO_2-neutral betrieben werden [24]. Eine Alternative zu Portlandzement ist CEM III/B. Er besteht großteils aus Hochofenschlacke, einem Nebenprodukt der Stahlproduktion, und wird daher als umweltfreundliche Alternative betrachtet [19].

Diese Arbeit untersucht, ob CEM III/B für die Herstellung von UHPC geeignet ist und wie unterschiedliche Mengen an Zusatzstoffen die Frisch- und Festbetoneigenschaften beeinflussen. Es wurden verschiedene Mischungen mit einem, für UHPC typischen, Wasser zu Zement-Verhältnis von 0,25 getestet. Dies soll ein gutes Gleichgewicht zwischen Verarbeitbarkeit und Druckfestigkeit gewährleisten. Schrittweise wurden 10 bis 30 Prozent der Zementmasse mit Kalksteinmehl, und 10 bis 40 Prozent der Zementmasse mit Microsilica ersetzt und die Auswirkungen auf die Eigenschaften sowie das Verhalten der Mischung beobachtet.

Weiters fokusiert sich diese Arbeit auf die Mischungszusammensetzung, insbesondere auf die Berücksichtigung der Packungsdichte. Die Probleme mit der Verarbeitbarkeit, in Form von stark auftretenden Scherverdickungseffekten, wurden durch die Ergänzung des *Überschusswasser*-Faktors, in der Mischungsberechnung, behoben. Dieser liefert direkte Informationen darüber, ob die Wassermenge ausreicht um die Hohlräume im Gesamtvolumen zu füllen.

Aufgrund der vielversprechenden Festigkeitswerte, welche in dieser Arbeit erreicht wurden, sollten weitere Forschungsarbeiten in diesem Themenbereich durchgeführt werden. Vor allem mit Fokus auf die Zugabe von Stahlfasern als Bewehrung, die die Festigkeitswerte, vor allem die Biegezugfestigkeit, deutlich erhöhen werden. Außerdem sollte in weiteren Forschungsarbeiten untersucht werden, ob zusätzliche Faktoren, neben der Packungsdichte, zur Scherverdickung beitragen, da dieses Phänomen deutlich ausgeprägter ist als mit vergleichbaren CEM I UHPC-Mischungen. Darüber hinaus sollte eine größere Probenserie mit der aktualisierten Berechnung untersucht werden, um deren Richtigkeit zu verifizieren.

Da ein erheblicher Anteil an Schlacke bereits für verschiedenste Anwendungen eingesetzt wird, hat CEM III/B nicht das Potenzial, die Zementindustrie allein zu revolutionieren. Aus diesem Grund sind zusätzliche Alternativen zu Portlandzement erforderlich, welche zur Zeit Thema mehrerer Forschungsarbeiten sind. Das Ziel sollte eine Reihe von Zement-Alternativen für unterschiedliche Anwendungsgebiete sein.

In den letzten Jahrzehnten entstand durch die Forschung in der Zementtechnologie eine große Lücke zwischen den potenziellen Festigkeiten des Materials und den von der Industrie tatsächlich verwendeten Festigkeiten [9]. Dadurch bietet sich die Gelegenheit, die Entwicklung von Alternativen zu forcieren, die dieselben Festigkeiten erreichen können, welche bereits mit konventionellem Beton erreicht werden.

Contents

Acronyms

ACE MasterGlenium ACE 430

BFS Blast Furnace Slag

C-S-H calcium silicate hydrate

$Ca(OH)_2$ calcium hydroxide

$CaCO_3$ calcium carbonate

CEM I Portland Cement

CEM II Portland Composite Cement

CEM III/B Blast Furnace Cement with 66-80% Slag

CO_2 carbon dioxide

E-mod Modulus of Elasticity

GHG Greenhouse Gas

GWP Global Warming Potential

$kgCO_2e$ Kilograms of Carbon Dioxide Equivalent

LS Limestone Powder

MPa Megapascal

MS Microsilica

PCE Polycarboxylate Ether

PD Packing Density

pH Potential of Hydrogen

PSD Particle Size Distribution

QS Quartz Sand

RPM Revolutions per Minute

SCM Supplementary Cementitious Materials

SEM Scanning Electron Microscope

SF Silica Fume

Sky MasterSure Sky 911

SP Superplasticizers

UHPC Ultra High Performance Concrete

UN United Nations

w/c Water to Cement Ratio

Chapter 1

Introduction

This thesis explores the feasibility of producing UHPC utilizing low-carbon cement. Given the pressing issue of global warming and the significant carbon footprint of clinker production, it is imperative to explore alternative, environmentally-friendly options. CEM III/B has the potential to substitute some amount of conventional cement with a more sustainable alternative. Moreover, this study will discuss some possible mixtures and associated challenges inherent to the use of CEM III/B. Ultimately, the aim is to ascertain whether CEM III/B has the capacity to steer the construction industry towards a more sustainable trajectory.

1.1 Motivation

In times of global warming and the world trying to reach net zero carbon emissions by 2050 [69] it is inevitable to save emissions in every single aspects of life. The *Building Materials and Construction* sector is having a huge impact on the Greenhouse Gas (GHG) pollution with around 11 percent of the worldwide CO_2 emissions [66] as shown in Fig. 1.1a. With the cement industry alone being responsible for around 5-7% of the total emissions [57], it becomes clear that there is a huge potential of reducing these. The report on building materials from the United Nations (UN) goes a step further and notes that the *built environment sector* contributes a staggering amount of 37% of total emissions. For reference, the global air traffic, which is around 100,000 flights per day, is responsible for around 2.5% of the emissions, as it stands in 2024 [51].

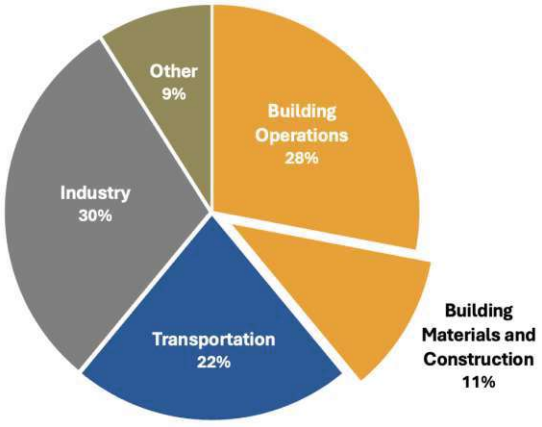

(a) CO_2 Emissions by Sector [66]

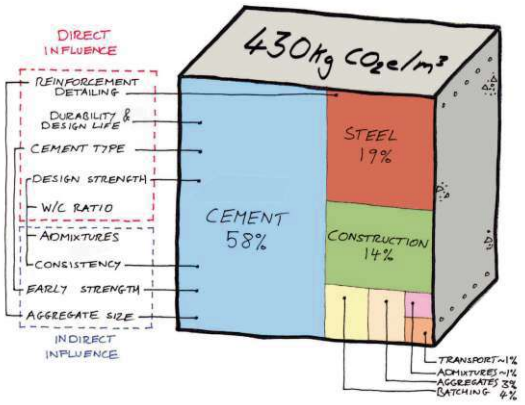

(b) CO_2 Emissions of 1m³ Concrete [7]

Fig. 1.1: CO_2 Emissions of the Building Sector Respectively Cement Production

The majority of the emissions in cement production (around 60%) is due to the chemical decarbonation of limestone and is necessary for producing Portland cement clinker. Bill Gates[1] mentioned this in his book *How to avoid a climate disaster*:

> "It's hard to get around that simple fact - *limestone plus heat* equals *calcium oxide plus carbon dioxide*", Gates [24]

$$CaCO_3 \longrightarrow CaO + CO_2 \tag{1.1}$$

Since the main part of the emissions result from the chemical reaction (Eq. 1.1), simply using green energy for the process won't eliminate them. To reduce the CO_2 emissions in the concrete or cement industry, it is necessary to find alternatives for Portland cement clinker.

1.2 Objective

The objective is to find reproducible mixtures for CO_2-reduced UHPC (>150 Megapascal (MPa)) using CEM III/B. This thesis will focus solely on the concrete mixtures themselves, without any type of reinforcement or steel fibres added. Based on experience and research, adding steel fibres can be expected to increase strength by 15-30%. For compression strength, this increase occurs because the fibres take the transverse tension forces that typically lead to failure in compression tests with concrete. The bending tensile strength also increases, as the fibres act similarly to longitudinal reinforcement, such as in beams.

There are different criteria for the compression strength at which concrete is classified as UHPC. One criterion might be anything above the highest class defined in *EN 206-1*, which is C100/115. Some research and various papers defines it as at least 120 MPa [5], while others say above 150 MPa [42], but there is no official standard. As shown in Fig. 1.2, there is a substantial supply of Supplementary Cementitious Materials (SCM) that needs to replace Portland cement with something more environmentally friendly. Most of the slag is already used, so the use of CEM III/B alone won't suffice as the sole alternative to replace Portland cement.

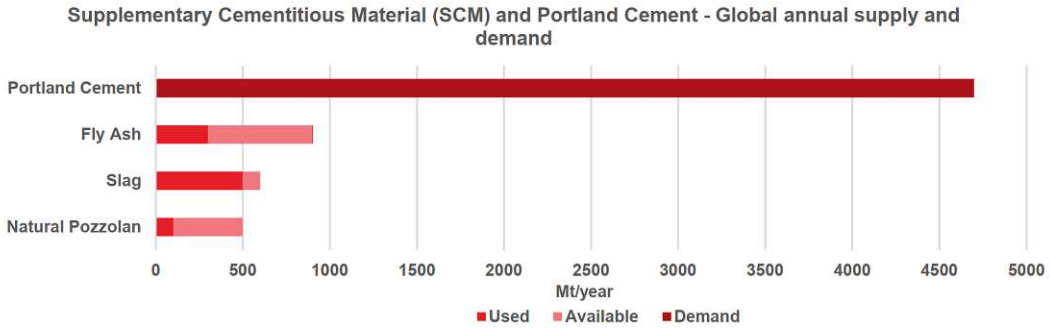

Fig. 1.2: SCM and Portland Cement - Global Annual Supply and Demand [56]

1.3 State of the Art

Concrete has been used for hundreds of years, since Roman times, although the concrete known today is different from its ancient form. Modern concrete, as we know today, was invented in

[1] Bill Gates (born in 1955), American businessman, investor, philanthropist and writer

the 19th century and extensively studied and developed in the 20th century, and became the most frequently used building material worldwide [4][9]. The extent of innovation is visible in Fig. 1.3, which shows the strength evolution of concrete over the past 100 years. In the last century, the maximum strength has increased almost 10 times. Obviously, the biggest jump was the invention of Superplasticizers (SP) and therefore the possibility to create UHPC in the 1990s, where the strength roughly doubled in less than 10 years. The graph also indicates, that the theoretical strength achievable in material development is much higher than what is used in common structural applications by the industry. However, this value also constantly increased over the last 100 years by the factor of 2 to 3.

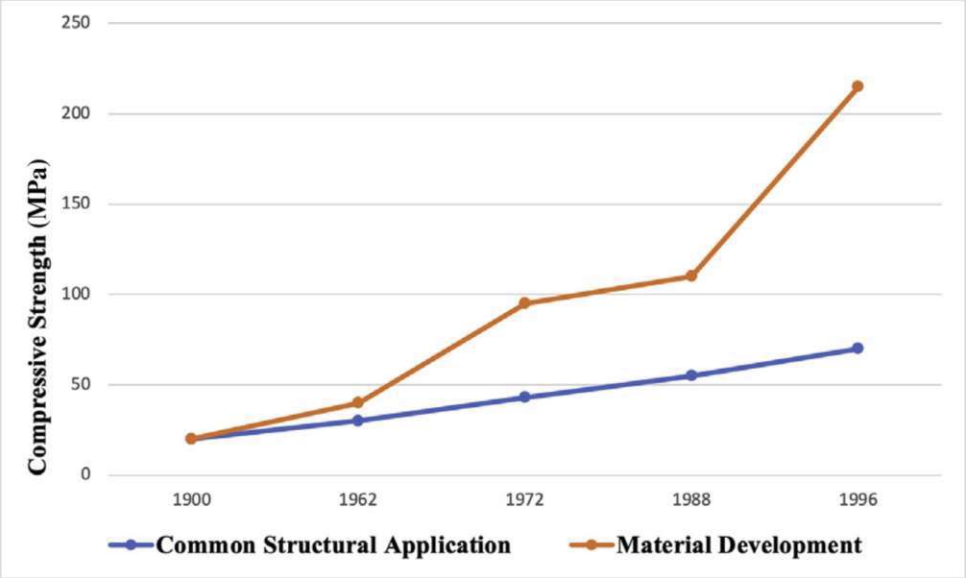

Fig. 1.3: The Increase in Compression Strength of Concrete Over 100 Years [9]

UHPC, which became famous by the turn of the century as shown in Fig. 1.4, is arguably the most significant invention in the history of concrete. For today, it is certain that the next major inventions in the concrete or cement industry have to be carbon reduced alternatives to conventional concrete and UHPC.

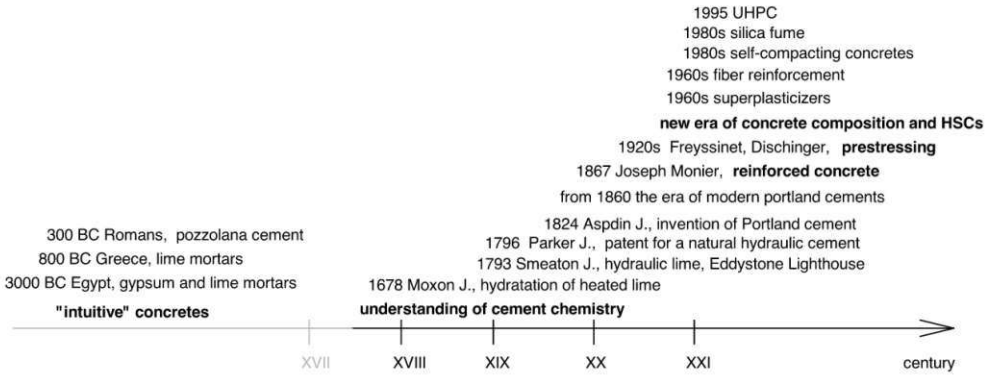

Fig. 1.4: Inventions in the Concrete Industry [64]

1.3.1 UHPC Benefits and Applications

The benefits of UHPC are extensive. Some of the most important ones are listed below, according to several sources [3][4][8][29][36]:

Compression strength The compression strength of UHPC typically exceeds 150 MPa, which is 5-10 times higher than conventional concrete. This allows the construction of lighter and slimmer structures, or conversely, much higher loads with a similar cross-section. UHPC also has improved performance under lateral loading. Wind turbine towers, bridge piles, and seismic columns are therefore typical elements built with UHPC.

Durability Due to the dense arrangement of the particles in the matrix, UHPC is showing a high resistance against penetrating factors like freeze-thaw cycles and chemical exposure. Therefore, the lifespan of UHPC is significantly extended compared to conventional concrete, making it a good choice for foundations. Further, due to this fact, also the maintenance is drastically reduced, resulting in cost savings and fewer disruptions for repairs. Also the impact resistance and abrasive strength is significantly better, making it a common choice for highway infrastructure and bridge decks or bridge girders.

Flexural performance UHPC has a high flexural strength, allowing slimmer and lighter elements, which is advantageous in applications like bridge decks and architectural facades.

Lightweight The use of thinner elements in UHPC can save up to 25-33% of weight while the construction is still maintaining the same load bearing capacity.

Emissions The high strength of UHPC allows reduced cross-sections to bear loads, leading to two positive effects: A more efficient use of space due to thinner structural elements and a reduced carbon footprint, although having a lower w/c-ratio.

Rapid construction UHPC typically exhibits a high early-strength development, allowing it to be stripped from formwork earlier than comparable concrete, ultimately saving time and therefore costs on the construction site.

Flexibility The use of UHPC provides greater architectural flexibility, that allows the creation of forms and shapes that simply wouldn't be possible with standard concrete. Compared to conventional concrete, there is no gravel but only sand in the mixture composition for UHPC. Therefore, the surface is much smoother with minimal voids and imperfections.

As mentioned above, UHPC is highly versatile, which allows a very wide range of applications. There are many more potential advantages and examples of where UHPC can be used.

1.3.2 UHPC Development

According to [4], there has been a need to find low-cost UHPC production methods for several years now. However, the latest development focus on how to create an UHPC with more environmentally friendly alternatives, which will be discussed more in detail in the following section *Eco-friendly concrete perspectives*. Another major research topic at the moment is 3D printed UHPC. The usually very good flowability and the high early strength of UHPC makes it an attractive option for 3D printing applications.

1.4 Eco-Friendly Concrete Perspectives

1.4.1 Structural Engineering Approach

UHPC is only a niche in the broader cement and concrete industry at the moment but the demand for high-quality architectural buildings in developed countries is expected to rise, leading to the need for slimmer components and more durable concretes types [4][8]. For example, a high rise building in Vienna called *Parkarpatments am Belvedere*, uses UHPC columns that are up to 20 meters high, unsupported and with a diameter of only 60 centimeters with more than 10 stories above. This geometry would simply not be possible with conventional concrete. While there are several alternatives for regular concrete, UHPC has only limited substitutes. Numerous studies have showed that it is possible to create useful concrete with CEM III/B but there is limited data available about UHPC. CEM III/B is considered carbon reduced because it contains 66-80 percent slag, a byproduct of steel-production, called BFS.

As a colleague of mine once said:

"You shouldn't underestimate the impact of a structural engineer on CO_2 emissions"

Fig. 1.5 supports this argument. It illustrates how much carbon can be saved every year by a single structural engineer by reducing structural embodied carbon by 20%. This reduction can be achieved through structural and architectural collaboration for the load-bearing system. Additionally, the industry has to adopt to alternative mixtures, which they are going to, if the alternatives will become cheaper than the currently widely spread Portland cement clinker. Considering that only one cubic meter of concrete generates around 430 kg CO_2 emissions as mentioned earlier (Fig. 1.1b), and that every structural engineer works with tons and tons of concrete throughout their career, the potential impact is significant. For instance, the reconstruction of the *Wien Museum* at Karlsplatz in Vienna used approximately 1.000 tons of concrete. Environmentally friendly alternatives could save thousands of tons of CO_2 emissions in similar projects.

Fig. 1.5: Importance of Structural Design Awareness Regarding CO_2 [25]

1.4.2 Global Warming Potential (GWP) of CEM I and CEM III/B

To provide context, a reasonable assumption is made that an equivalent mass of cement is needed in order to create concrete with CEM I and CEM III/B. When comparing a standard concrete of grade C25/30 for the phases A1-A3, it shows a GWP for CEM I of 309.6 $kgCO_2e/m^3$ compared to 134,4 $kgCO_2e/m^3$ for CEM III/B [19]. This represents a significant reduction of almost 60%. The phases A1-A3 account for approximately 50% of the total emissions and are the most critical values for planners, whether they are structural engineers, architects, or construction companies.

This is the easiest way to save emissions. Figure 1.6 shows the CO_2 emissions for all life cycle stages (*cradle to grave*) consisting of:

A1-A3: *Cradle to gate* – carbon emissions in construction material processing

A4-A5: Construction process

B1-B5: In use carbon emissions

C1-C4: End of life carbon emissions

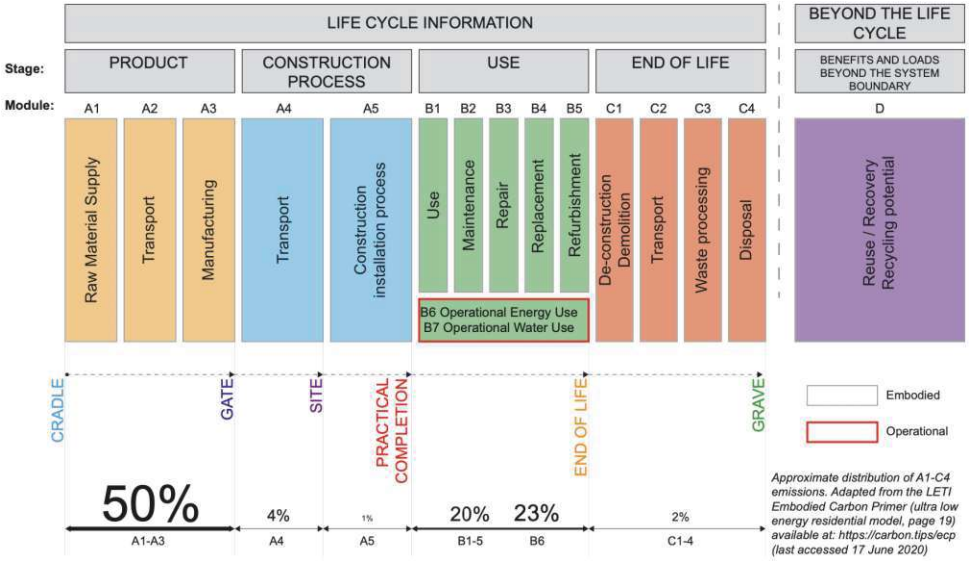

Fig. 1.6: Lifecycle Stages and Modules [45]

The crushing process of the extremely hard BFS requires a large amount of energy, resulting in emissions that can be categorized as *operational carbon*. In contrast, conventional concrete releases the majority of CO_2 emissions due to a chemical reaction, which is named *embodied carbon*. Therefore, the emissions can be further reduced by running the crushing process with green energy, theoretically up to 66-80% for CEM III/B. Fig. 1.7 indicates that in 2017 the operational and embodied carbon have been roughly the same. This highlights that around 50% of CO_2 emissions from the cement industry can be saved only by the use of green energy.

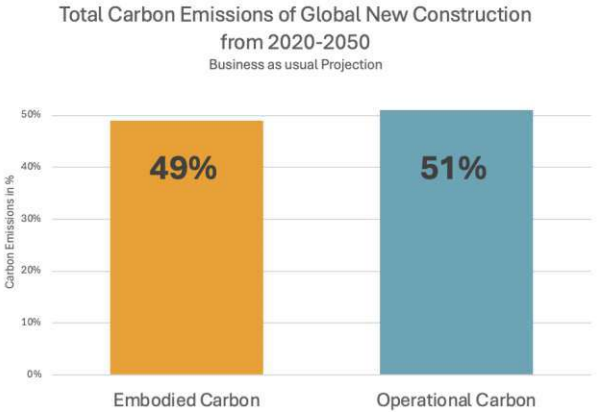

Fig. 1.7: Embodied and Operational Carbon [68]

Chapter 2

Materials

The main focus in this study was to determine whether it is possible to design UHPC using CEM III/B, specifically the product *"der Violette"* from Holcim [28]. CEM III/B is characterized by its high percentage of BFS, ranging from 66-80%. Further, a certain percentage of the cement was gradually substituted with LS and Silica Fume (SF) to observe how these substitutions affect the strength and behaviour of the concrete. The used sand had a small Particle Size Distribution (PSD). To maintain a low w/c of 0.25, the use of SP was essential.

2.1 CEM III/B (*"ECO Planet VIOLETT"*)

CEM III/B consists of 66-80% slag and 20-34% CEM I, while CEM I consists of approximately 96% Portland cement clinker and about 4% gypsum.

The properties of Holcim CEM III/B and Holcim CEM I are compared and noted in Tab. 2.1. The most noticeable difference is the much slower chemical reaction of CEM III/B, as evidenced by various parameters in the table. The solidification start takes almost twice as long. This slower reaction results in lower early strength compared to CEM I, which is around nine times higher after one day, but only 1.4 times higher after 28 days. Continuing this trend, CEM III/B could potentially match or even exceed the strength of CEM I after 56 days. Due to its lower heat of hydration because of the slower chemical reaction, CEM III/B is especially suitable for heavy mass applications. Additionally, it has a high resistance against harmful waters and soils, making CEM III/B an excellent choice for large foundations for example.

Tab. 2.1: Product Data Sheet Comparison Holcim 2023 [28][27]

Properties	CEM III/B	CEM I
Density [kg/dm³]	2,88	3,12
Blaine Value [cm²/g]	4700	4500
Solidification Start [min]	260	140
Compressive Strength 1 day [N/mm²]	3	28
Compressive Strength 7 days [N/mm²]	23	41
Compressive Strength 28 days [N/mm²]	46	64

Figure 2.1 shows the PSD of the used CEM III/B. The grain sizes range from 0.5μm to 50μm, featuring a small plateau at the smaller diameters and a prominent peak at around 10μm.

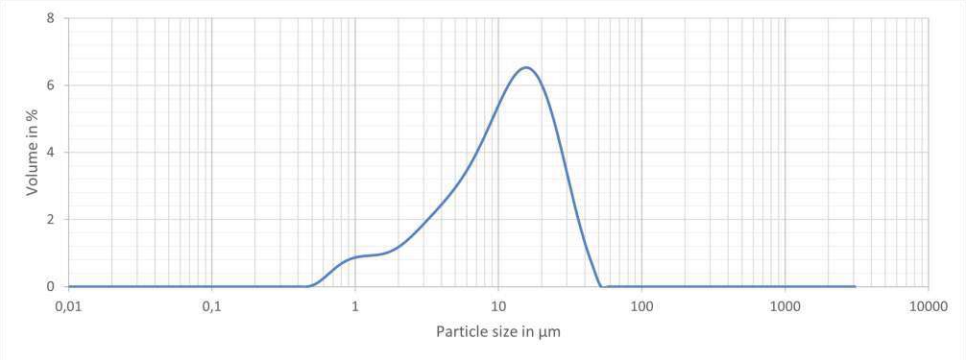

Fig. 2.1: Frequency PSD of CEM III/B via *Mastersizer 3000*

Different types of cement can show different crystal structures, but CEM I and CEM III/B exhibit a pretty similar structure with a sharply fractured shape, as shown in Scanning Electron Microscope (SEM) micrographs in Fig. 2.2.

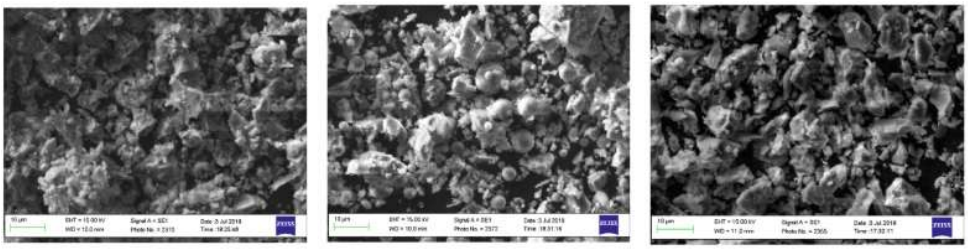

Fig. 2.2: SEM Micrographs of (a) CEM I, (b) CEM II, (c) CEM III [54]

2.2 Limestone Powder

The mainly used limestone powder (H100 from Bernegger GmbH) has a PSD similar to that of the used CEM III/B, ranging from 0.6μm to 150μm. While a prominent peak is absent, there is a much wider plateau at around 10μm (Fig. 2.3). The density of the limestone powder is 2.71kg/dm³ and due to the similar PSD the specific surface is expected to be comparable to CEM III/B.

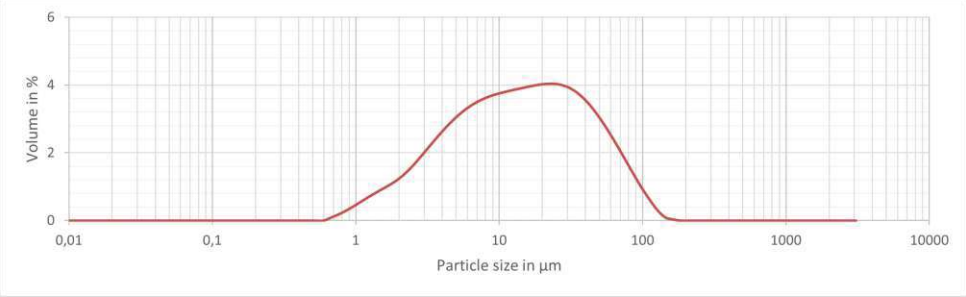

Fig. 2.3: Frequency PSD of Limestone Powder H100 via *Mastersizer 3000*

The SEM picture (Fig. 2.4) of limestone powder shows a structure comparable to the ones of cement. The particles also have sharp edges, and the grain size and shape is almost the same.

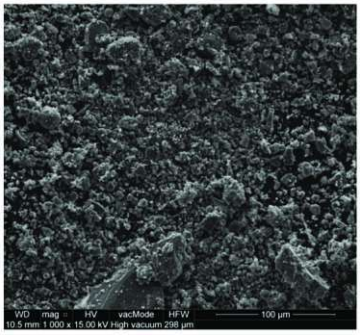

Fig. 2.4: SEM Micrograph of Limestone Powder [33]

Additionally, another limestone powder (H200MP from Bernegger GmbH) was used for a comparable mixture design to address workability issues. This powder is slightly finer, ranging from 0.3μm to 40μm. (Fig. 2.5)

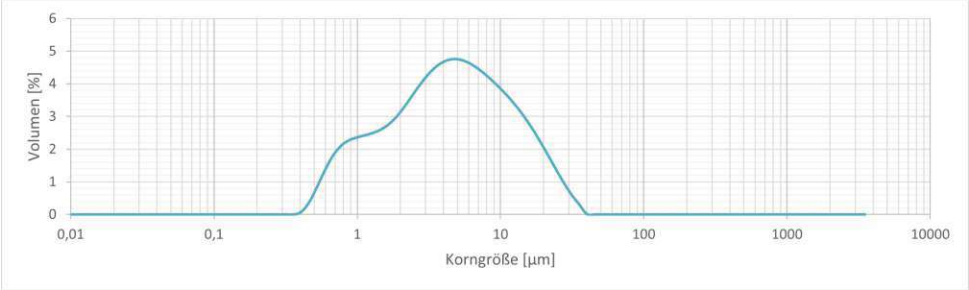

Fig. 2.5: Frequency PSD of Limestone Powder H200MP via *Mastersizer 3000*

2.3 Microsilica/Silica Fume

The microsilica powder used, Elkem 940U, is approximately 100 times finer than the cement or limestone powder, making it an excellent filler material. Unfortunately, it is also very expensive. Silica fume is extracted from the exhausts of silicon production, which is the reason for the perfect spherical form. The plot Fig. 2.6 shows the PSD of the used microsilica. The distribution is ranging from 0.01μm to 100μm with a peak at around 0.2μm and a very low plateau from 1μm to 100μm. The density is 2.30kg/dm³ making it significantly lighter than the cement and the limestone powder.

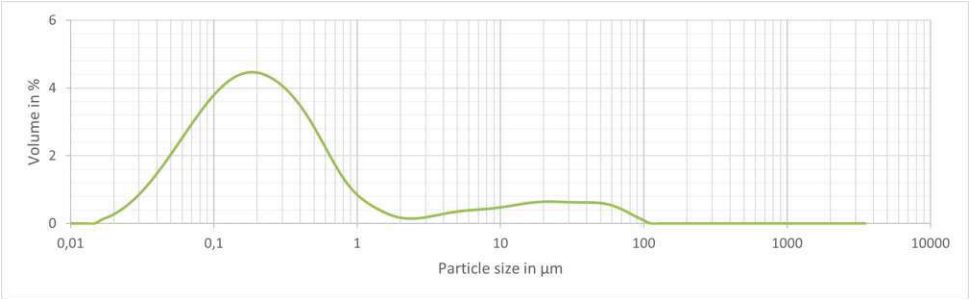

Fig. 2.6: Frequency PSD of Silica Fume via *Mastersizer 3000*

Fig. 2.7 shows a SEM picture of microsilica. The structure is completely different compared to cement and limestone powder. Silica fume has a spherical shape and a very smooth surface.

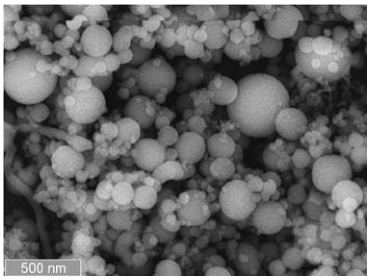

Fig. 2.7: SEM Micrograph of Silica Fume [62]

2.4 Sand

The used sand for all the tested mixtures was a Quartz Sand (QS) with particle size mainly ranging from 0.1 to 0.7mm (Fig. 2.8). Using a fine sand, with largest grains smaller than 1mm in diameter for UHPC, has several benefits. It increases the packing density, which leads to smaller voids between particles and therefore to a denser matrix. Smaller voids also means reduced water content, which results in higher strength and reduced risk of shrinkage cracks. QS has high compression strength itself and is easily available is Europe. To be a responsible construction product, it is important for the QS to have a sharp surface and irregular fractured shape.

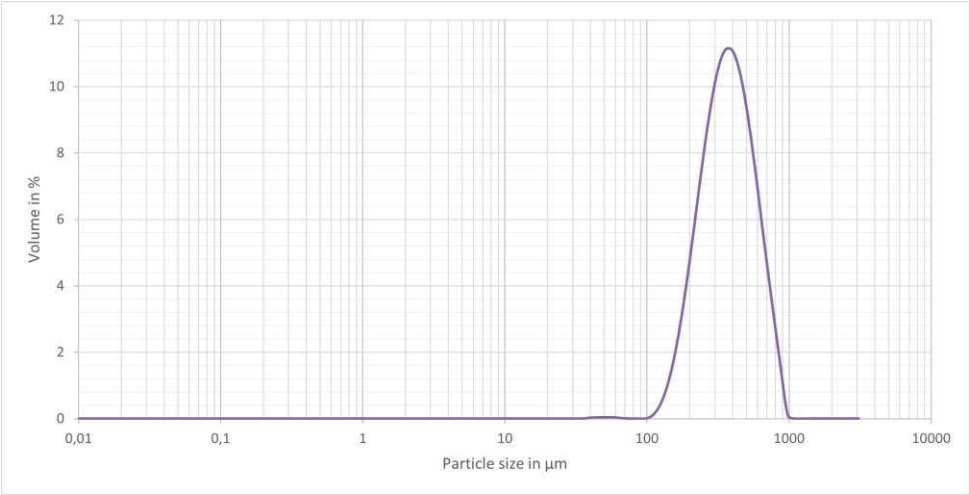

Fig. 2.8: Frequency PSD of Quartz Sand via *Mastersizer 3000*

2.5 Superplasticizer

SP in general are essential for improving workability, reducing the w/c ratio and enhancing the overall performance. The production of UHPC would not be feasible without the use SP. There are basically two types of modern superplasticizers on the market: flow agents and consistency holders, both based on Polycarboxylate Ether (PCE). The flow agent used in this study was MasterGlenium ACE 430 (ACE), with the effect to liquefy the mixture. On the other hand, the used consistency holder was MasterSure Sky 911 (Sky), having the effect to delay and slow down chemical reactions within the mix.

2.6 Mixture

The chosen w/c ratio was 25%. In this study, up to 30% of the cement mass was sequentially replaced with limestone powder and 40% of the cement mass with microsilica or a combination of both. The following plots Fig. 2.9 and 2.10 show the PSD of the mixture in orange, alongside the separate ingredients. This example mixture contains 10% LS and 20% MS

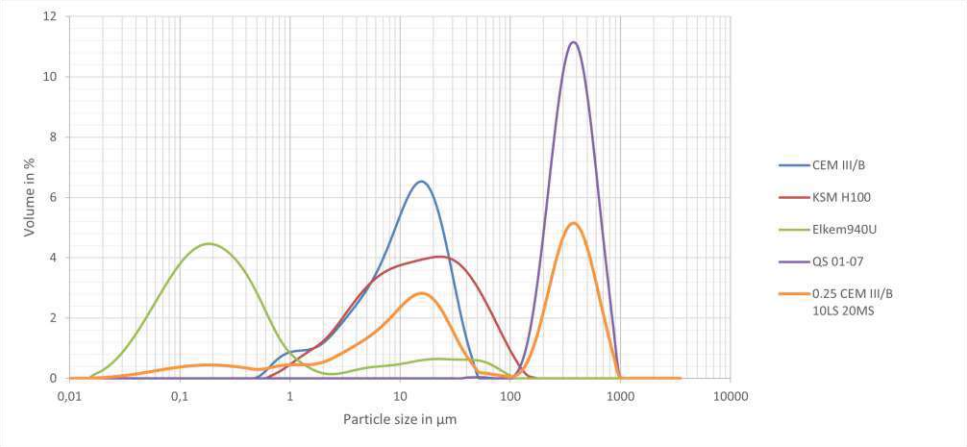

Fig. 2.9: Frequency PSD of the Mixture

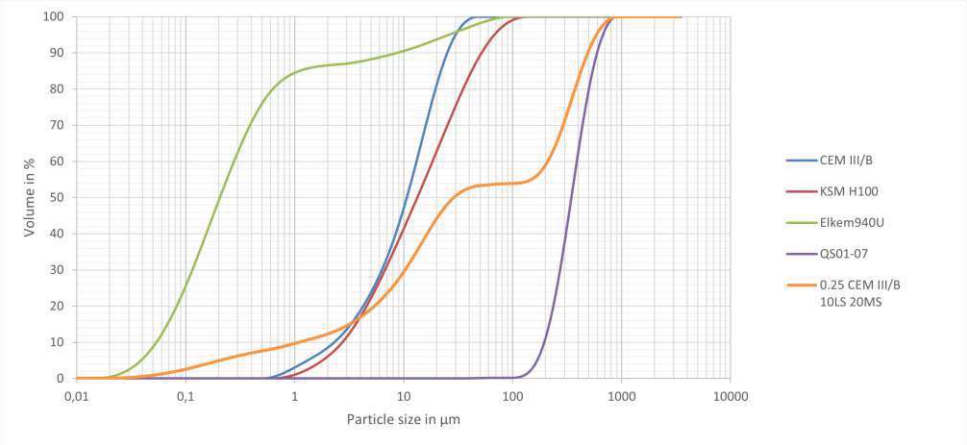

Fig. 2.10: Cumulative PSD of the Mixture

Chapter 3

Methods and Early Stage Results

3.1 Mixture Design

In concrete mixture design, additives are commonly used to replace some amount of cement. This is done to control the properties of the concrete and to reduce the mixtures GWP. In this thesis, up to 30% of concrete mass was replaced with LS and up to 40% with MS. Throughout the thesis, abbreviations are used for the mixture compositions. The following example explains how they have to be interpreted:

0.25 CEM III LS20 MS10

- w/c-ratio 0.25;
- CEM III/B;
- 20% of the cement mass replaced with limestone powder;
- 10% of the cement mass replaced with microsilica

Tab. 3.1 provides information on various mixture designs, including the quantities of individual ingredients and relevant ratios. Cement, limestone, microsilica and the solid content of superplasticizers (f_m) sum up to the powder volume (F_v). The Packing Density (PD) is calculated according to Schwanda [58][59] and will be explained shortly later in this chapter. Finally, the solid volume fraction (ϕ) is defined as the sum of all solids divided by the total container volume of $1m^3$.

As shown in Tab. 3.2, the CO_2 emissions of CEM III/B are significantly lower compared to CEM I. It further illustrates that both LS and MS have a substantially lower GWP compared to cement. This means, the higher the percentage of cement mass replaced with additives, the better (lower) the total GWP of the mixture. Superplasticizers, while showing a very high GWP, are essential for producing UHPC. However, since they are used in very small quantities, with only a few grams, their contribution to the total emissions is negligible.

Tab. 3.1: Mixture Design

Mix Design	Cement [dm^3]	LS [dm^3]	MS [dm^3]	Sand [dm^3]	f_m [dm^3]	Water [dm^3]	ACE [dm^3]	Sky [dm^3]	Air [dm^3]	PD [%]	W/F_v [-]	ϕ [-]
0.25 CEM III	364.99	-	-	350	2,21	262.80	6.75	3.54	20	74.79	0.72	0.72
0.25 CEM III MS10	339.67	-	42.53	350	3.23	244.56	9.87	5.17	20	78.31	0.63	0.74
0.25 CEM III MS10 no Sky	340.15	-	42.59	350	2.34	244.91	9.89	-	20	78.30	0.64	0.74
0.28 CEM III	348.04	-	-	350	1.31	280.66	5.52	-	20	74.98	0.80	0.70
0.28 CEM III MS10	325.36	-	40.74	350	1.53	262.37	6.45	-	20	78.42	0.71	0.72
0.37 CEM III	304.77	-	-	350	0.48	324.76	2.01	-	20	75.45	1.06	0.66
0.25 CEM III LS10	343.34	36.49	-	350	2.97	247.20	9.07	4.75	20	74.67	0.65	0.73
0.25 CEM III LS10 MS10	321.16	34.13	40.22	350	3.25	231.24	9.84	5.34	20	77.92	0.58	0.75
0.25 CEM III LS10 MS20	301.51	32.04	75.51	350	3.86	217.08	11.74	6.26	20	80.87	0.53	0.76
0.25 CEM III LS20	324.29	68.93	-	350	3.29	233.49	10.28	4.94	20	74.56	0.59	0.75
0.25 CEM III LS20 MS10	304.41	64.70	38.12	350	3.59	219.18	10.86	5.90	20	77.59	0.53	0.76
0.25 CEM III LS20 MS20	286.65	60.93	71.79	350	4.24	206.39	12.99	6.75	20	80.36	0.49	0.77
0.25 CEM III LS30	307.05	97.89	-	350	3.98	221.08	12.17	6.38	20	74.47	0.54	0.76
0.25 CEM III LS30 MS10	289.16	92.19	36.21	350	4.25	208.19	12.99	6.81	20	77.30	0.49	0.77
0.25 CEM III LS30 MS20	273.17	87.09	68.41	350	4.64	196.68	14.07	7.56	20	79.91	0.45	0.78
0.25 CEM III LS30 MS40	244.34	77.90	122.38	350	9.45	175.93	29.05	14.89	20	86.51	0.39	0.80

Values represent the contribution to 1m^3

Tab. 3.2: GWP of Additives

Additives	ρ [kg/dm^3]	GWP [kgCO$_2$e/kg]	GWP [kgCO$_2$e/dm^3]
CEM III$^{(1)}$	2.88	0.278	0.801
CEM I$^{(1)}$	3.12	0.910	2.839
LS$^{(1)}$	2.71	0.016	0.043
MS$^{(2)}$	2.30	0.052	0.120
ACE$^{(1)}$	1.09	1.880	2.049
Sky$^{(1)}$	1.04	1.880	1.955

$^{(1)}$ Values for embodied carbon including phases A1-A3 from ICE V3.0 Beta [19]
$^{(2)}$ Values from a comparable MS powder including phases A1-A3 [22]

Giving the data from Tab. 3.2 and Tab. 3.1, the total GWP of the mixtures can be calculated. For comparison the GWP values for a similar mixture with CEM I instead of CEM III/B were also evaluated. Depending on the mixture design, the GWP reduction potential ranges from approximately 60% to 70%.

Tab. 3.3: GWP of Mixtures

Mix Design	GWP$_{\text{CEM III}}$ [kgCO$_2$e]	GWP$_{\text{CEM I}}$$^{(1)}$ [kgCO$_2$e]	GWP saving [%]
0.25 CEM III	312.98	1,057.03	70
0.25 CEM III MS10	307.37	999.81	69
0.25 CEM III MS10 no Sky	297.70	991.11	70
0.28 CEM III	289.97	999.47	71
0.28 CEM III MS10	278.59	941.85	70
0.37 CEM III	248.13	869.42	71
0.25 CEM III LS10	304.32	1,004.24	70
0.25 CEM III LS10 MS10	294.01	948.71	69
0.25 CEM III LS10 MS20	288.10	902.74	68
0.25 CEM III LS20	293.31	954.39	69
0.25 CEM III LS20 MS10	284.84	905.40	69
0.25 CEM III LS20 MS20	280.51	864.86	68
0.25 CEM III LS30	287.43	913.37	69
0.25 CEM III LS30 MS10	279.72	869.19	68
0.25 CEM III LS30 MS20	274.23	831.10	67
0.25 CEM III LS30 MS40	302.24	800.34	62

Values refer to 1m^3 of concrete.
$^{(1)}$ Values are for reference, if the same amount of CEM III would be replaced with CEM I.

3.2 Workability

The reference mix *0.25 CEM III* exhibited the expected behaviour of an UHPC, though it showed stiff characteristics. This stiff appearance was due to a higher than usual shear thickening effect. Despite this, the mixture remained with an acceptable workability. In the modified mixes, the additives LS and MS were used to partially replace the cement mass.

Increasing the amount of limestone powder decreases the workability significantly due to a very strong shear thickening effect. However, LS was retained due to the numerous benefits, like reduced hydration heat, minimized shrinkage and enhanced durability [61][71]. Conversely, microsilica positively affects workability. Initially, the plan was to limit silica fume to 20% due to its high costs compared to cement or limestone powder. This amount proved insufficient, especially for high percentages of limestone powder in the mixes. The viscosity of these mixes have been so high, that it exceeded the measurement capabilities of the available laboratory equipment. To address these issues, various strategies are explored to mitigate the excessive shear thickening associated with high LS content. This involved investigating different theories and adjusting the mixture composition to achieve acceptable workability.

Packing density With a higher level of compaction, it is reasonable to expect a decrease in workability. High packing density can lead to a more compact and less fluid mixture, making it harder to work with and process.

Physical interaction There may be a physical interaction between the blast furnace slag in the CEM III/B and the ions from the limestone powder. These interactions could alter the mix's viscosity and workability [72].

Chemical interaction The CEM III/B cement might contain elements that exhibit pozzolanic effects, potentially leading to a stronger chemical reaction when mixed with limestone powder. This interaction could produce additional compounds that affect the mixture's flow characteristics [37].

Superplasticizer Research indicates that modern SP can sometimes cause issues with workability, particularly when used in combination with certain additives. These problems may arise from complex interactions between the SP and the other mix components [34][39].

Mixture calculation There is a possibility that the mixture was calculated with no focus on the packing density, resulting in insufficient water for the void volume. This miscalculation could lead to overly viscous mixtures that are difficult to handle and process.

3.2.1 Shear Thickening

Liquids can be categorized based on their behaviour into two primary groups: *Newtonian fluids* and *Non-Newtonian fluids*. A Newtonian fluid describes a liquid, or in this thesis a mixture, where the shear stress τ increases proportionally with the shear strain rate $\dot{\gamma}$, while the viscosity η stays constant for different shear strain rates, as illustrated in Fig. 3.1. This well-known liquid behaviour is shown for example by water, as its most famous representative. Every other liquid therefore is a non-Newtonian fluid and can be further categorized based on their specific behaviours. The most notable types are *pseudoplastic* (shear thinning) and *dilatant* (shear thickening) liquids. The second occurred with a very strong effect for most of the tested mixtures in this thesis.

Figure 3.1a illustrates the relation between shear strain rate $\dot{\gamma}$ and shear stress τ for different liquid behaviours. The Newtonian liquid was already discussed above and shows a constant

relation. A Bingham-fluid shows a solid behaviour until a certain shear stress is reached, known as the yield stress. After reaching it, it behaves as a Newtonian fluid and has a liquid appearance then. Last but no least, there is shear thickening (dilatant fluid) and shear thinning (pseudoplastic fluid). Shear thinning describes liquids where the shear stress rises slower with an increasing shear strain rate. On the other hand, a shear thickening fluid shows a disproportionately increase of shear stress with just a small increase of shear strain rate.

Fig. 3.1b shows the relation between shear strain rate $\dot{\gamma}$ and viscosity η. Starting with the Newtonian fluid again, it shows a horizontal line, which means the viscosity does not change and stays the same for various shear strain rates. Shear thinning liquids starts at a certain base viscosity. With increasing shear strain rate, the viscosity reduces consistently. Meaning the resistance of the fluid is getting lower the faster it gets sheared. Vice versa applies to shear thickening fluids. They start at a base viscosity, and with increased shear strain rate the viscosity increases much faster. This means, the faster the mix gets sheared, the more viscous it gets. Applied to our concrete mixture, it appeared that the concrete mixer rather crushing and crumbling the mixture, instead of a proper mixing process.

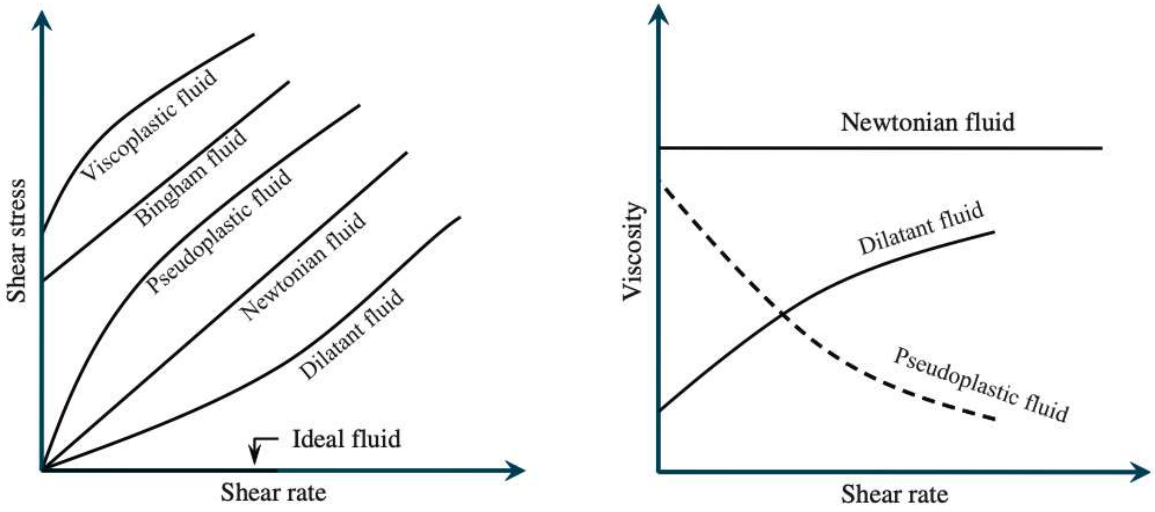

(a) Shear Strain Rate - Shear Stress

(b) Shear Strain Rate - Viscosity

Fig. 3.1: Shear Behaviour of Liquids [46]

For a clearer understanding, the following pictures (3.2) provide visual examples using everyday substances. These illustrations help to demonstrate the different types of fluid behaviour described, allowing readers to observe these phenomena with materials commonly found at home.

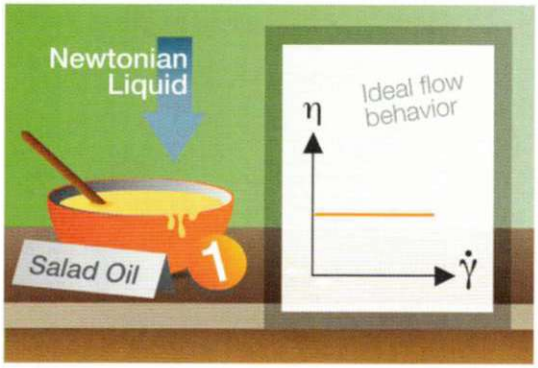

(a) Newtonian Liquid

Newtonian Liquid:
Salad oil is a typical example of a Newtonian liquid. It exhibits a consistent viscosity across all shear strain rates. This means that regardless how fast the oil is mixed or swirled, the resistance encountered on the cooking spoon remains constant.

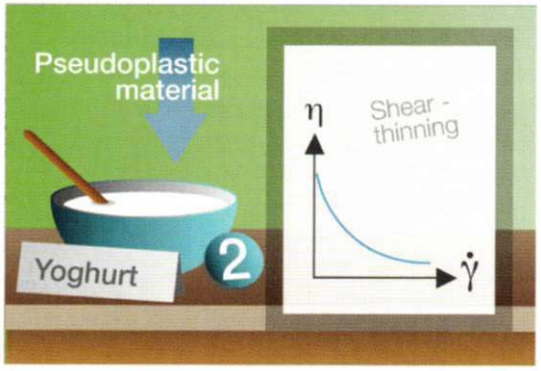

(b) Pseudoplastic Material

Pseudoplastic Material:
Yoghurt is a perfect example of a pseudoplastic material, also know as *shear-thinning* liquid. In this case, the viscosity decreases as the shear strain rate increases. Practically, this means that as you stir or swirl the yoghurt faster, it becomes thinner and the resistance you experience decreases.

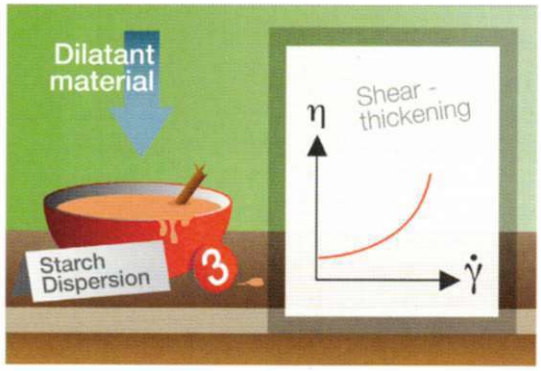

(c) Dilatant Material

Dilatant Material:
A starch dispersion is a classic example of a dilatant material, also known as a *shear-thickening* liquid. In this case, the viscosity increases as the shear strain rate rises. Practically, this means that the faster you mix or stir the starch dispersion, the thicker and stiffer it becomes, resulting in greater resistance.

Fig. 3.2: Liquid Behaviours Explained with Everyday Materials [41]

3.2.2 Packing Density

The packing density was calculated according to Schwanda [58][59][65]. This model allows to calculate the void content, and therefore the packing density of any grain size distribution. Without going to much into detail in this thesis, it is determined following these simplified steps:

1. A series of sieves is used to separate the raw material into different particle size fractions, where the biggest grain diameter is maximum twice the diameter of the smallest.
2. Mass and volume of these fractions is measured precisely

3. The bulk density of each individual fraction is calculated using the following equation:

$$Bulk\ Density_{\mathrm{i}} = \frac{Mass_{\mathrm{i}}}{Volume_{(\mathrm{Solid+Void}),\mathrm{i}}} \qquad [g/cm^3] \tag{3.1}$$

4. The different fractions are combined according to Schwanda [58][59], which involves a systematical variation of proportion of each fractions trying to minimize the void content and therefore maximize packing density.

5. After determining the optimal mixture of fractions, the overall bulk density of the mixture, which is the densest packing achievable with the given grain size distribution, is calculated using the total mass and volume:

$$Overall\ Bulk\ Density = \frac{Total\ Mass}{Total\ Volume} \qquad [g/cm^3] \tag{3.2}$$

6. The highest possible packing density with the variation of the primary grain and the considered interaction factors between different particle sizes is the final result and is calculated with:

$$Packing\ Density = \frac{Overall\ Bulk\ Density}{Density\ of\ Solids} \qquad [-] \tag{3.3}$$

The packing density alone was determined not to be the cause of shear thickening observed in the mixes. As shown in Tab. 3.1, the packing density varies by approximately 5%. Microsilica was observed to have a positive effect on the workability, although the packing density is rising with it. Limestone does not effect the packing density. It even tends to decrease it a tiny bit and still decreases workability massively. Thus, it can be concluded that packing density does not account for the reduction in workability associated with increasing limestone powder content.

3.2.3 Physical Interaction

CEM III/B consists of a small amount of CEM I and a high proportion of 66 to 80% BFS. The slag can have a negative charge, especially in alkaline environment as in concrete, while limestone contains positively charged calcium ions (Ca^{2+}) [21][31][40][72]. This suggests a potential interaction where these components attract each other. To investigate this theory, an alternative to limestone powder was tested to determine if the shear thickening effect could be reduced or eliminated. Quartz powder, which lacks any charge, was chosen as the alternative. Although quartz powder showed a slight improvement in workability, the effect was almost undetectable. Thus, it can be concluded that electrostatic interactions between limestone and slag are unlikely to be the main cause of the observed shear thickening.

3.2.4 Chemical Interaction

Another theory considered is the possibility of a chemical reaction, such as a pozzolanic effect, occurring between the slag and limestone. This theory arises from observations that similar shear thickening effects were not as pronounced in mixes using CEM I [1][23][44]. As with the physical reaction theory, this theory was also considered rather unlikely to be the main reason for the occurred shear thickening because the effect was still present when LS was replaced with quartz powder.

3.2.5 Superplasticizer

Research indicates that SP can also have an impact on the workability. Modern SP contain extremely long polymer chains, which can become entangled. This entanglement may lead to a shear thickening effect, as these tangled polymer chains can increase the resistance of the mixture to deformation under stress. Consequently, the use of certain SP may contribute to the observed decrease in workability, similar to the effects cause by high limestone powder content [26][32][34]. Alternative SP have been tested and showed only marginal changes in the workability and flowability. The influence of SP therefore was ruled out to be the major reason for the shear thickening occured in our mixes.

3.2.6 Mixture Calculation

3.2.6.1 w/c-Ratio

The w/c ratio is a key parameter for adjusting workability. Increasing the w/c generally improves workability but significantly reduces compression strength. As discussed earlier, a w/c ratio of 0.25 was chosen for the reference mix without additives (*0.25 CEM III*). Therefore, the w/c ratio alone is not the primary issue affecting the mixes with additives. As shown in **Chapter 2: Materials**, Limestone powder has a similar grain size to the CEM III/B used, whereas microsilica is approximately 100 times finer. The w/c ratio is determined using only the water and cement, not the powder. When 20% of the cement mass is replaced with limestone powder, the total cement content decreases. Consequently, the amount of water, calculated based on the reduced cement content, also decreases, while the total powder mass stood the same, leading to a drier mix and reduced workability. Despite this, microsilica positively impacts workability. This suggests that, while limestone powder decreases workability due to its effect on the w/c ratio, microsilica helps counteract this reduction.

3.2.6.2 *Apollonian* Packing

When replacing cement with microsilica, even though the total water content decreases, there is often more *free water* available. This is due to the difference in particle size between cement or limestone and microsilica. Microsilica particles are much smaller and can fill the voids created by the larger particles of cement or limestone. This phenomenon is known as Apollonian packing. The mechanism works as follows: smaller particles of microsilica fall into the voids between the larger particles of cement or limestone. This displacement of water from the voids results in a mix that appears more moist and exhibits better workability because there is more excess water available. Testing was also conducted with a limestone powder that was finer (the before mentioned H200MP) than the regularly used one (H100). Although it showed a slight improvement in workability, the effect was minimal. This is likely because the difference in particle size was not significant enough to create the pronounced Apollonian packing effect. The concept of Apollonian packing involves filling the voids created by larger, perfectly round particles with progressively smaller particles. Each size reduction aims to fill the remaining voids, thereby increasing the packing density as much as possible (Fig. 3.3). The ultimate goal is to achieve a packing density that is as efficient as possible, reducing voids and improving the overall mix properties.

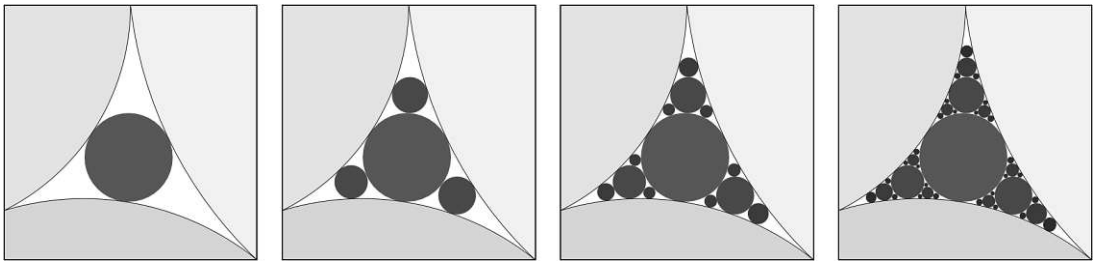

Fig. 3.3: Step by Step Creation of an Apollonian Packing [20]

The plot shown in 3.4 refers to the concept illustrated in Fig. 3.3 (first image from the left). It emphasizes the importance of the size ratio between the base grain and the filler grain. It demonstrates that if the filler grain is too large relative to the base grain, it cannot properly fill the voids created by the larger particles. Instead, it tends to push the base grain aside, resulting in larger voids and thus, lower packing density. To achieve optimal packing, the filler must be significantly smaller in diameter compared to the base grain. This allows the filler to effectively occupy the voids between the larger particles, enhancing the overall packing density of the mixture.

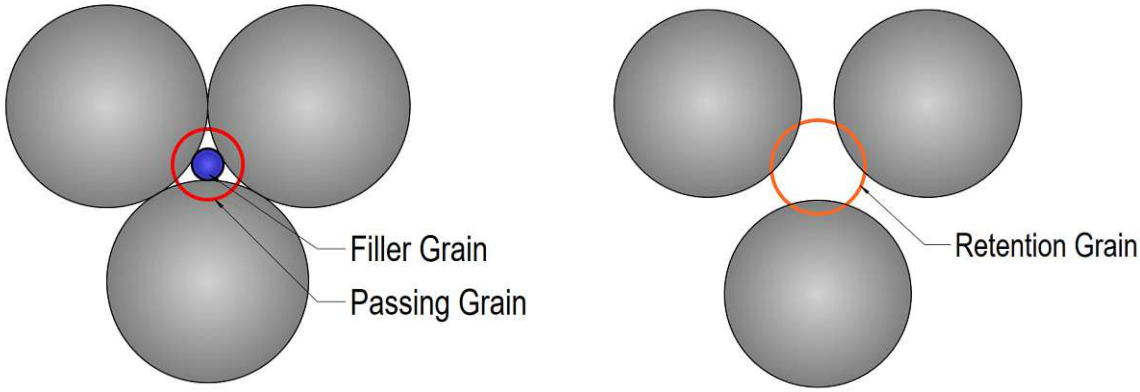

(a) Passing Grain **(b)** Retention Grain

Fig. 3.4: Passing Grain vs. Retention Grain [20]

3.2.7 Solid Volume vs. Bulk Volume

The following figure, Fig. 3.5 highlights the significance of incorporating packing density into the mixing calculation. The first plot (Fig. 3.5a) shows the composition of all ingredients of the mixture *0.25 CEM III/B 30LS 10MS*. It can clearly be seen that sand and cement constitute the biggest portions. The impact of a relatively small amount of limestone powder (30% of the cement mass) and microsilica (10% of the cement mass) becomes evident in this context. Water accounts for approximately 20% of the total volume of the mixture. When adding up the volumes of the individual components, the total equals exactly 1000 liters. This value is derived without considering packing density. However, when accounting for packing density, which theoretically corresponds to 100% solid volume, the bulk volume will be larger due to the presence of voids between particles. The packing density is calculated based on the theory of Schwanda [65].

The relation between bulk volume and solid volume is illustrated in Fig. 3.5b, which shows a calculated packing density of 77.8% for this mixture. The plot clearly indicates that the bulk

volume is significantly larger than the solid volume. Notably, the total bulk volume approaches 1000 litres. In concrete mixing, it is usually referred to the *Container Volume*, which equals a closed system with a lid. The difference between bulk volume and solid volume is the void volume. The graph reveals two problems. First, that the bulk volume can exceed the container volume, which was not the case for this mixture, but for *0.25 CEM III/B 30LS* for example. Second, the amount of water in the mixture is less than the void volume, meaning that not all voids are filled with water and there is no excess water available, which leads to a dry appearance and bad workability. This adds another important consideration to the mixture calculation: *is the container volume exceeded and is there sufficient amount of excess water available?*

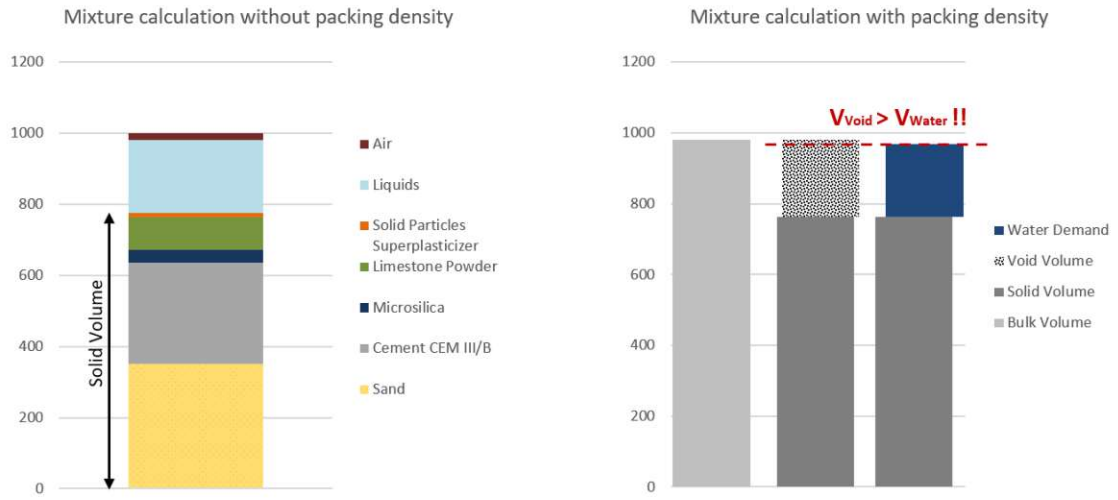

(a) Volume Composition **(b)** Bulk Volume Consideration

Fig. 3.5: Comparison Solid Volume and Bulk Volume *0.25 CEMIII/B 30LS 10MS*

This concept is further illustrated in Fig. 3.6. The first picture 3.6a, shows two scenarios. The left plot demonstrates a densely packed mix where particles form a stable structure with minimal voids. All voids are filled with water, with some excess water available to enhance workability. In contrast, the right plot shows the same particles during mixing. As particles move, the distance between them increase, thereby enlarging the voids. The excess water, which is crucial for workability, becomes insufficient to fill these increased voids, resulting in a mix with a drier appearance and reduced workability. In other words, imagine the left picture where excess water is not available for the stable structure. If the mix is then under moving, there is too less water to cover all particles.

The second image, Fig. 3.6b, emphasizes the significance of particle size differences between base grains and fillers. In *Mix 1*, where the base grain and filler are the same size, large voids are created, requiring more water. This scenario, in combination with the previously discussed plot, leads to even larger voids and thus, a higher water demand. As a result, there is not enough water to fill this voids, leading to a mix with poor workability. Conversely, the right plot illustrates the advantage of using smaller fillers, such as microsilica. Smaller fillers reduce void sizes due to improved packing density, resulting in more available excess water and, consequently, better flowability and workability [52].

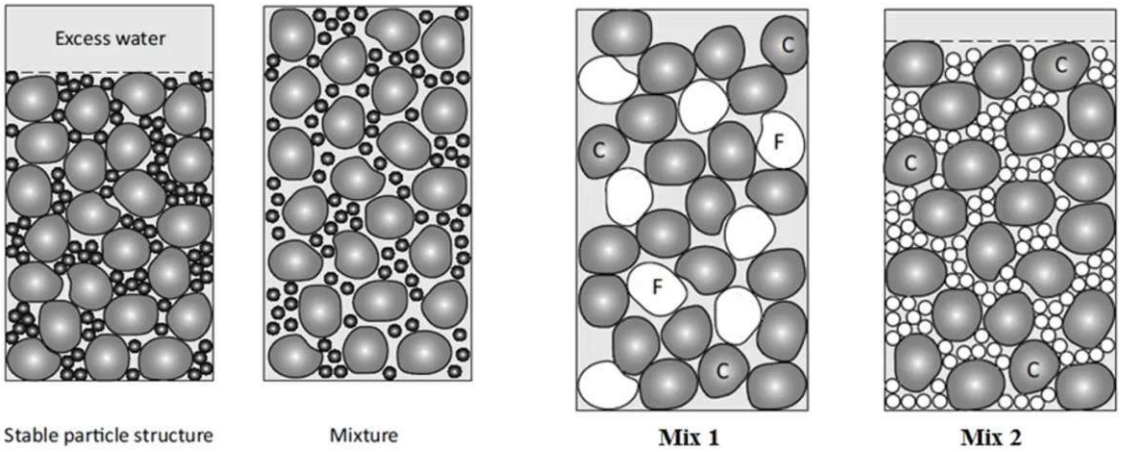

(a) Particle Packing Theory [52] **(b)** Usage of Fine Fillers [52]

Fig. 3.6: Packing Density and Composition

The following plot, Fig. 3.7 illustrates that not only the grain size difference between base grain and filler has a important impact on the workability.

The left figure depicts the theoretically highest packing density for a single grain size, where voids are minimized and excess water is available. This represents a stable condition with optimal packing density. However, when the mixture is set into movement, the right picture occurs, showing a less densely packed arrangement. In this state, the voids are significantly lager, and excess water is no longer available. The amount of water may be insufficient to fill these enlarged voids, leading to no excess water, and thus, a dry appearance and poor workability. Once the mixing process is stopped, the particles will gradually return to a more densely packed structure similar to that shown in Fig. 3.7a.

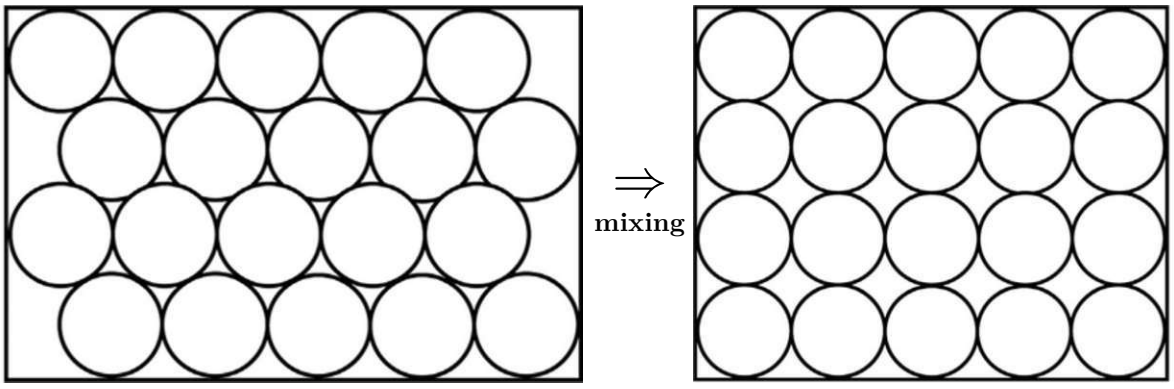

(a) Hexagonal Packing **(b)** Square Packing

Fig. 3.7: Packing Density of a Single Grain Mixture

The just described phenomenon is shown in Fig. 3.8 with a mixture of *0.25 CEM III LS30 MS10*. The left image Fig. 3.8a presents the mixture fresh out of the mixing bucket while kneading it. It has a dry appearance, almost solid, and crumbly, making it challenging to place into formwork. However, after just 3 seconds of relaxation, the mixture settles and adopts a more liquid appearance, allowing it to flow smoothly into the formwork. This transformation in workability highlights a significant issue: the mixture's initial dry state makes it impractical for use on a construction site or in precast concrete manufacturing, as it is difficult to pump.

Despite excellent self-compaction and ventilation of the mixture, the initial workability issues render it unsuitable for practical applications.

(a) Dry Appearance **(b)** Liquid Appearance

Fig. 3.8: Change of Condition or (=*Relaxation*) after 3s

3.2.8 Solution Approach

To address the workability issues identified, the mix proportion calculations were revised with a greater emphasis on packing density. The updated approach involved increasing the amount of microsilica in the mixture to improve flowability and workability. By focusing on packing density, the revised mix ensures that the voids between particles are adequately filled, while also providing sufficient excess water to maintain good flow characteristics. This adjustment aims to counteract problems with dry appearance and poor workability, making the mixture more suitable for practical applications such as construction and precast concrete manufacturing. The most important parameter added to the mixture calculation is the so called *surplus water*. It is defined as the difference between water demand (Eq. 3.7) and voids (Eq. 3.6) within the mix and should always be positive. A negative value signals, that the voids are bigger than the water demand, meaning more water than available is needed. This lack of water then leads to a dry, shear thickening mix. The calculation was done by using the Eq. 3.4-3.8

$$V_{\text{Solid}} = \sum_{i=1}^{n} V_{\text{Solids,i}} \tag{3.4}$$

$$V_{\text{Bulk}} = \frac{V_{\text{Solid}}}{PackingDensity} \tag{3.5}$$

$$V_{\text{Voids}} = V_{\text{Bulk}} - V_{\text{Solid}} \tag{3.6}$$

$$V_{\text{Water-demand}} = 1000 - V_{\text{Air-content}} - V_{\text{Solid}} - V_{\text{Solid-SP}} - V_{\text{Fibres}} \tag{3.7}$$

$$V_{\text{Surplus-water}} = V_{\text{Water-demand}} - V_{\text{Voids}} \tag{3.8}$$

The mix with the worst workability was identified as *0.25 CEM III LS30*, where the surplus water was *-38 litres*, meaning the void volume was already much higher than the amount of water available. To investigate whether this was the primary cause of shear thickening, the amount of microsilica in the mix was increased until the surplus water content became clearly positive. The chosen amount of silica fume was 40%, which allows the mixture of *0.25 CEM III LS30 MS40* to have *52 litres* of excess water. The revised mixture exhibited significantly improved behaviour during the mixing process, with shear thickening being no longer noticeable. This indicated a positive shift towards more manageable workability. The following table (Tab. 3.4) shows the before mentioned volumes, as well as the surplus water for all mixture designs discussed in this thesis.

Tab. 3.4: Surplus Water Depending on Mixture Design

Mix Design	V_{Solid} [dm^3]	V_{Bulk} [dm^3]	V_{Void} [dm^3]	Water Demand [dm^3]	Surplus [dm^3]
0.25 CEM III	714.99	956.04	241.05	262.80	21.75
0.25 CEM III MS10	732.20	935.05	202.85	244.56	41.71
0.25 CEM III MS10 no Sky	732.74	935.79	203.05	244.91	41.86
0.28 CEM III	698.04	930.98	232.94	280.66	47.72
0.28 CEM III MS10	716.10	913.22	197.12	262.37	65.25
0.37 CEM III	654.77	867.87	213.10	324.76	111.66
0.25 CEM III LS10	729.83	977.46	247.63	247.20	-0.43*
0.25 CEM III LS10 MS10	745.51	956.78	211.27	231.24	19.97
0.25 CEM III LS10 MS20	759.06	938.57	179.51	217.08	37.57
0.25 CEM III LS20	743.22	996.79	253.57	233.49	-20.08*
0.25 CEM III LS20 MS10	757.23	975.96	218.73	219.18	0.45
0.25 CEM III LS20 MS20	769.37	957.43	188.06	206.39	18.33
0.25 CEM III LS30	754.94	1,013.72	258.78	221.08	-37.70*
0.25 CEM III LS30 MS10	767.56	992.92	225.36	208.19	-17.17*
0.25 CEM III LS30 MS20	778.67	974.47	195.80	196.68	0.88
0.25 CEM III LS30 MS40	794.62	918.56	123.94	175.93	51.99

Values represent the contribution to 1m^3
Results marked with an asterisk (*) highlight negative values.

3.3 Mixing

The mixing process started in the *Eirich mixer* to break up the agglomerates, especially those from silica fume. Initially, all dry materials, including CEM III/B, QS, MS and LS were added and mixed for 4.5 minutes. The friction from the particles of different sizes broke up the agglomerates, leading to a evenly mixed powder. This stage is the so called *Pre-mix*. After that, the liquid ingredients, water and SP, were added and mixed for another 4.5 minutes, referred to as the *wet mix*. Figure 3.9 shows the mixers that have been used in this thesis. On the left hand side there is the Eirich mixer which features a turning pot and an eccentric spinning tool. On the right side, there is the *Mortar mixer*, a much simpler system where just the tool is spinning. Because most of the tested mixtures have shown a bad workability and flowability, the Eirich

mixer appeared to be more crushing through the mix then properly mixing it. Additionally, the distance between the spinning tool and the floor of the pot was slightly too high, probably because of wear, leaving unmixed cementitious powder on the floor. Therefore, in the end, the Eirich mixer was used only for the pre-mix with a high rotation speed, while the following wet mix was done in the Mortar mixer.

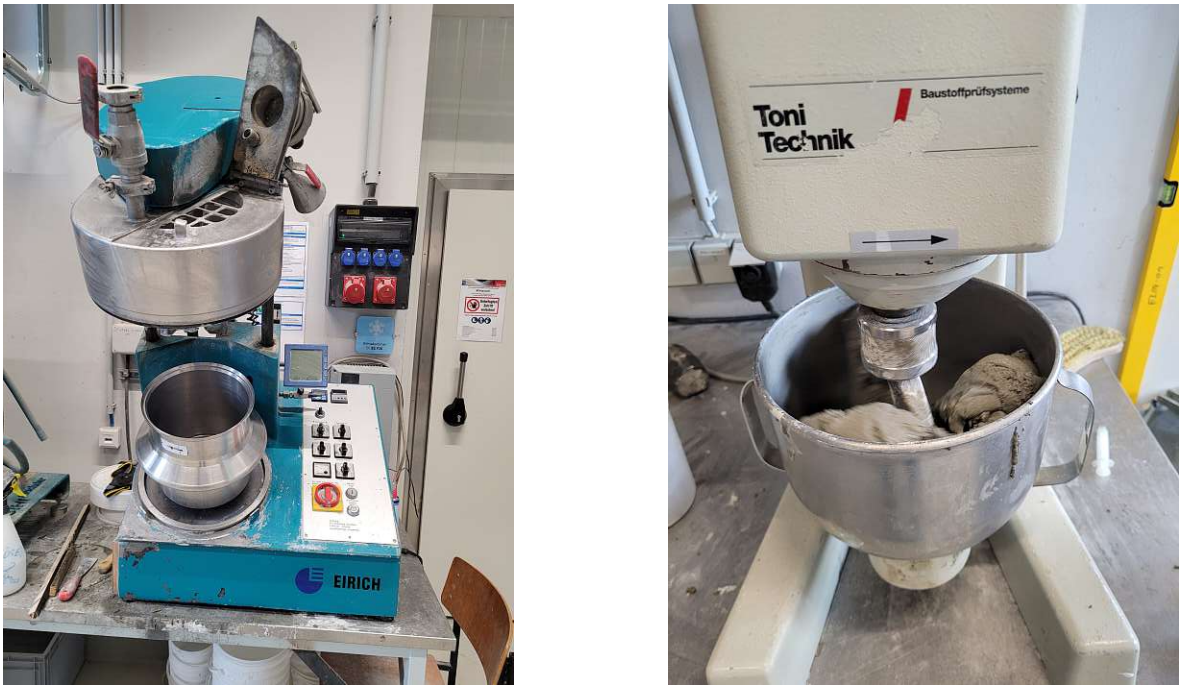

(a) Eirich Mixer **(b)** Mortar Mixer

Fig. 3.9: Mixers Used in This Thesis

In the very beginning, it was necessary to determine the optimal Revolutions per Minute (RPM) at which the concrete should be mixed. Therefore, a test mix was filled into the Eirich mixer and mixed for 4.5 minutes before water was added. The mixer power was documented for 300 (blue), 600 (purple) and 900 (yellow) RPM.

The following graph (Fig. 3.10) starts 90 seconds before water was added. After adding the water, an immediate increase in the mixing power is observed, meaning the mix is beginning to stiffen up. It takes 40 to 100 seconds to reach a peak value, depending on the RPM, before decreasing again until it stabilizes. At this point, continuous mixing is switched to interval mixing, where the mix is stirred for 1 minute and then allowed to rest for 1 minute. This process allows the concrete to rest, resulting in small peaks when mixing resumes. This is done to observe whether the mix stiffens further or liquefies, which was not the case. As the power stabilizes, the mix is considered homogeneous and ready to be molded. Higher RPMs reach the plateau faster, but not in direct proportion. The blue line (300 RPM) remains consistent, while the purple line (600 RPM) starts to increase slightly and the yellow one (900 RPM) clearly rising. Therefore, a low revolution of 300 RPM was chosen. This helped to keep the mixing temperature low and the mix homogeneous. Additionally, it prevented the mixer from crushing through more densely packed mixes, which occurred due to the bad workability of some mixtures.

However, because of the before mentioned problems that occurred, the final mixing process started with a 4.5 minutes pre-mix, in the Eirich mixer, followed by the addition of water and

another 4.5 minutes of wet mixing in the Mortar mixer. The mix quantity was approximately two litres, sufficient to fill two sets of formwork (2 times 3 prisms).

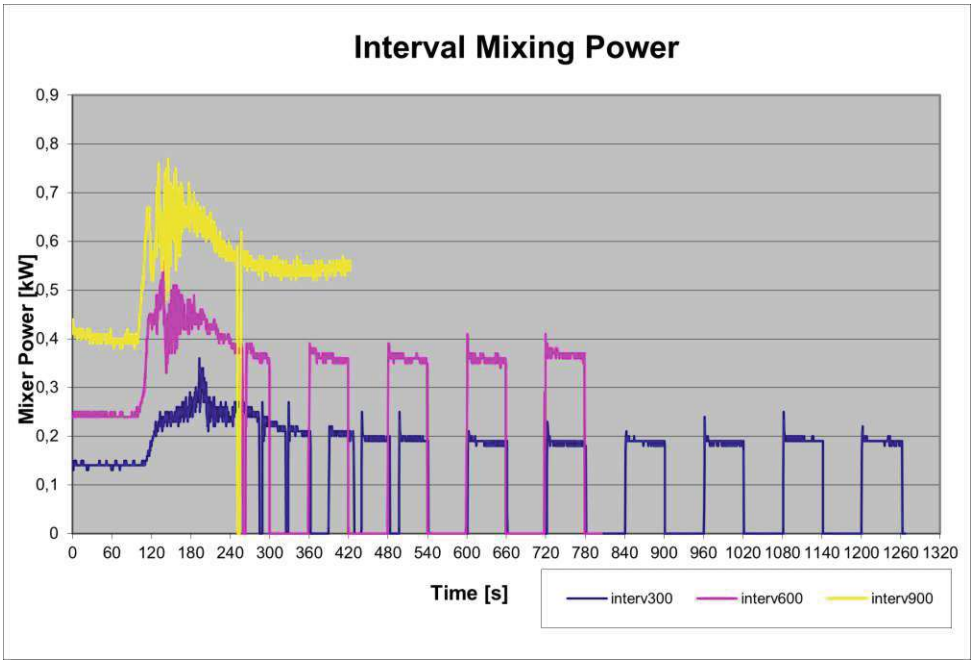

Fig. 3.10: Interval Mixing Energy

3.4 Slump-Flow Test

The slump-flow test provides information about the consistency of the fresh concrete. The test was carried out based on *ÖNORM B 4710-3* which is similar to *DIN EN 12350-5*. Before the test, the table and the cone need to be cleaned and moistened with a damp cloth, ensuring they are free from excessive water. The cone is then placed on the table with sufficient distance to the edges and filled with concrete from one single charge. The top surface is then smoothed with a trowel. After waiting for 10 to 30 seconds, the cone is lifted vertically in one motion within 1 to 3 seconds. For the UHPC mixes, the test was conducted without impacts and with a small slump cone (100mm base diameter; 70mm top diameter; 60mm height). After the concrete has completely spread, the largest diameter and the diameter perpendicular to it are measured. The average of these two measurements is then the result of the slump-flow test according to Eq. 3.9 [13]

$$f = \frac{d_1 + d_2}{2} \tag{3.9}$$

(a) Filled Slump-Flow Cone Just Before Lifting

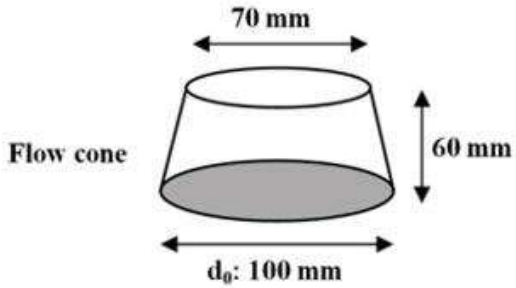

(b) Slump Cone-Mini Dimensions [67]

Fig. 3.11: Slump-Flow Test

In this test, you can also observe whether segregation occurs. Due to the small grain size and the dense matrix, this was not the case. Bleeding would also be recognizable in the test and could not be detected.

3.5 V-Funnel Test

The V-funnel test is used to get information about the viscosity of the fresh concrete. The test was conducted based on *ÖNORM B 4710-3* which is directly linked to the *DIN EN 12350-9*. Before the test, the flap and the inside of the funnel needs to be cleaned and moistened with a damp cloth. The flap is then closed and the funnel gets filled with concrete from one single charge without any compaction or vibration. The top surface is then smoothed with a trowel. The timing starts as soon as the flap is opened rapidly and stops at the very moment the observer can look vertically through the funnel for the first time. The flow must be continuous, if the funnel becomes clogged, the test needs to be restarted. If it clogs twice, the concrete is lacking viscosity. [14]

(a) V-Funnel During Test

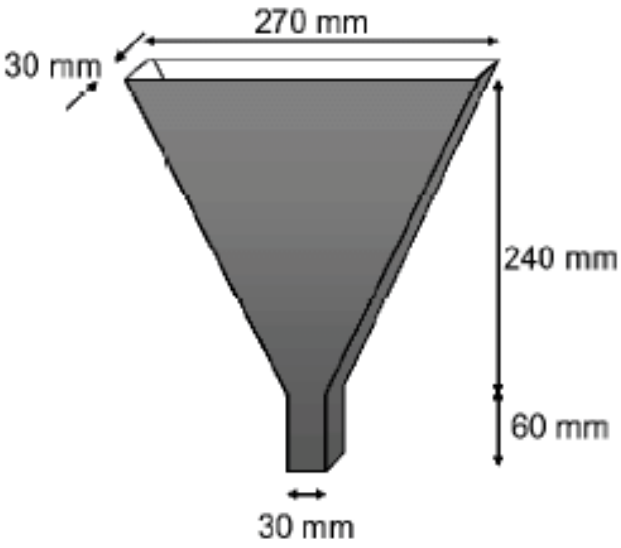

(b) V-Funnel-Mini Dimensions [30]

Fig. 3.12: V-Funnel Test

3.6 Prism Production

The ready-mixed concrete was taken out from the mixer and after the slump-flow and v-funnel test the mix was then filled into the pre-oiled prism formwork.

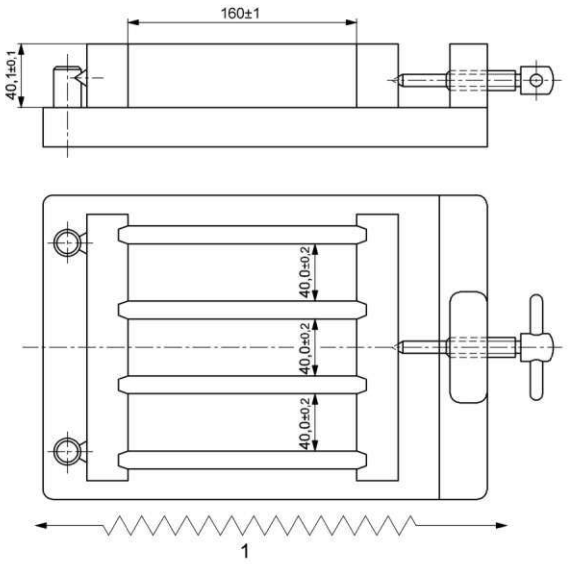

Legende
1 Abstreichrichtungen; mit sägenden Bewegungen abziehen.

Fig. 3.13: Prism Dimensions According to *DIN EN 196-1* [17]

To protect the samples from dehydration, they were immediately covered with a plastic wrap. In order to rule out inaccuracies, each prism consists of three samples as seen in Fig. 3.14a. Each mixture required 4 prism sets to perform all necessary tests after 1, 7, 28 and 56 days. One day after molding, the formwork was removed and the specimen were deburred and stored in water. The samples dimensions are 4x4x16cm.

It is worthwhile noting that, when mixing and especially when casting the concrete in the mold, a very strong effect of sheer thickening appeared for some mixtures. Fig. 3.14b shows, that the concrete appeared more granular than like a fluid while pouring it. As soon as it rested in the formwork for a couple of seconds, it liquefies again and spreads into the cast without the need of vibrations. The liquid properties were strongly dependent on the mixing composition. Limestone powder enhanced the shear thickening effect, while silica fume decreased it, as already mentioned earlier in this chapter.

(a) Prism Sets After 1 Day **(b)** Sheer Thickening While Pouring

Fig. 3.14: Prism Production

3.7 Storage Conditions

As specified in *DIN EN 12390-2* [16] the prisms were stored fully submerged in water at a constant room temperature around 25 degrees Celsius. This ensures a consistent supply of water throughout the curing period, supporting uninterrupted hydration of the cement. The strength of concrete samples is significantly influenced by their storage conditions [49]. When looking at the *Walz diagram* (Fig. 3.15), one can see that, for example, after 2 months (56 days) the strength can vary from 70% to 120% depending on the storage conditions. Additionally, since the tests were conducted for concrete without any rebars or fibres, it was important to keep the hydration temperature low to avoid micro-cracks, and therefore maintain a certain level of bending tensile strength [11][12][50][55].

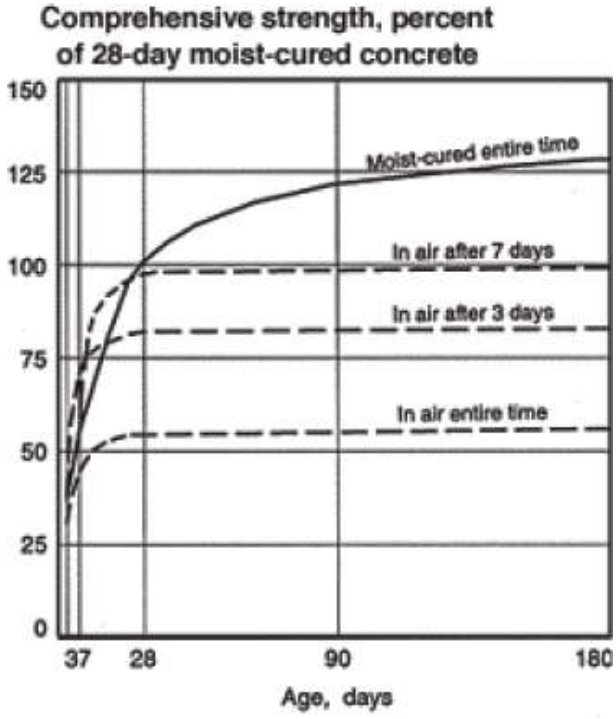

Fig. 3.15: Compressive Strength, Percent of 28-Day Moist Cured Concrete [48]

3.8 Prism Preparation for Mechanical Testing

Prism preparation for mechanical testing varied depending on the testing age of the samples. The most important results for this thesis have been the long time strength values, and therefore, these samples required more preparation.

1 day After stripping off the formwork and straightening the protruding edges, these specimen were wrapped in plastic foil to protect them from dehydration. Right before the bending tensile and compression tests, the samples were unwrapped, weighed and measured in order to be able to calculate the density later on. No further preparation was necessary.

7 days The samples have been taken out of the water storage approximately one hour before testing. The excessive water was wiped off and the samples have been stored in air at room temperature allowing the surface to dry a little, with no visible moisture being left. Right before the tests, the samples were weighed and measured in order to enable density calculation later on.

28 and 56 days The preparation for 28 and 56 days was similar to that for 7 days, but additional steps were required. After taking the samples out of the water curing, the front ends needed to be grinded to achieve parallel surfaces. The longitudinal sides needed to be sanded to even out small notches. The reasons for these additional steps are:

1. The Modulus of Elasticity (E-mod) is tested, which requires plain surfaces in order to obtain reliable results.
2. To avoid any notch effect, due to small imperfections in the formwork, as much as possible.

3. To have comparable results for the 28 & 56 days strengths to the standard, the samples should have a similar form and surface.

3.9 Prism Tests

After the fresh concrete tests for consistency and viscosity were done immediately subsequent to the mixing process, the tests on the hardened prisms have been done after 1, 7, 28 and 56 days. As mentioned above the preparation for the different testing ages of the samples varied. Table 3.5 provides an overview of the tests conducted at each specimen age.

Tab. 3.5: Tests Done Depending on Sample Age

	1 Day	7 Days	28 Days	56 Days
Density	✓	✓	✓	✓
Bending Tensile Strength	✓	✓	✓	✓
Compression Strength	✓	✓	✓	✓
Modulus of Elasticity	-	-	✓	✓
Carbonation	-	-	✓	✓

3.9.1 Density

At the beginning of each sample testing, the specimen were removed from water curing. After excessive water was wiped away, the prisms were allowed to rest at room temperature for approximately one hour, for the surface water to evaporate. The prisms were then measured to determine the volume and weighed to calculate their density. Due to minor imperfections in the formwork and the fact that samples for 28 and 56 days were scratched, the dimensions of the prisms will be slightly different to 4x4x16cm.

3.9.2 Bending Tensile Strength Test

The bending tensile strength is only of secondary importance in this thesis, because steel fibres have not been considered in the mixing design and will significantly enhance the bending tensile strength. As previously mentioned, the protruding edges of the samples have been straightened to minimize any potential notch effect and to ensure a stable support for the full specimen width in the testing apparatus. The bending tensile strength test is a three-point bending test. It represents a single-span girder with two supports on the two ends and a central point (line) load. The distance between the supports is 100mm. One of the supports and the load application point are equipped with a flexible joint to accommodate any deviations from perfectly parallel surfaces. The test starts with a pre-load of 50N, for two reasons:

1. The pre-load stabilizes the prism and ensures accurate seating.
2. Due to the slightly different heights of the specimen, the pre-load compensates for these differences by closing any gap, while applying a consistent force. This leads to an uniform origin of coordinates from the testing software and allows to overlay and compare the results.

Following the pre-load, the software initiates the main testing process. The load is continuously increased by a rate of 50 (+/-10) N/s until the prism finally breaks. During this test, the machine

records the load and displacement data. With this information and the given dimensions the software can create a stress-strain diagram (σ - ϵ - diagram)

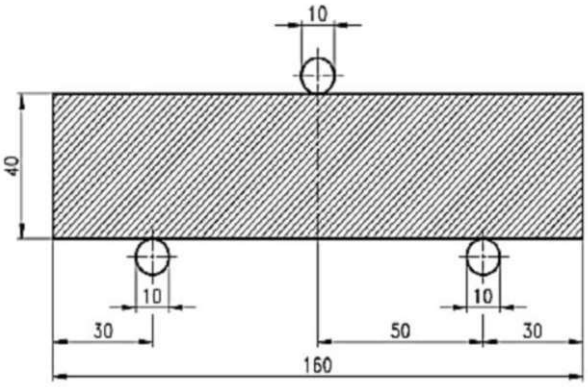

(a) Static Sketch [10]

(b) Bending Test

Fig. 3.16: 3-Point Bending Test

3.9.3 Compression Strength Test

The compression strength is the most important parameter in this thesis. The very dense matrix and the small PSD are responsible for the very high compression strength of UHPC. In upcoming thesis the influence of added steel fibres will be observed. It is expected that it doesn't influence the compression strength as much as the bending tensile strength. The test is done between two steel plates with an area of 40x40mm. Similar to the bending tensile strength test, the support is rigid, while the load application has a flexible joint to accommodate slight deviations from parallel surfaces.

The test also begins with a pre-load of 50N to stabilize the sample and the testing tool and to ensure a uniform origin of coordinates for comparison. Then the software starts the actual testing process. The load is incrementally increased at a rate of 1kN/s until the prism fails. During the test the machine records the loads and displacements data. The software uses then these measurements, along with the given dimensions, to create a stress-strain diagram (σ - ϵ - diagram)

Fig. 3.17: Compression Strength Test

3.9.4 E-mod

The E-mod is an important property for understanding the long-term behaviour of the samples. The 28 day value was important for the comparison with other types of concrete, as this is the age used in the standards. Further, the 56 day value provides insight into whether the E-mod already reached its maximum after 28 days, or if it continues to increase. To accurately measure the E-mod it is necessary that the two front ends are as perfectly parallel as possible. Before testing, the sample got cleaned and the displacement sensor was attached. It is important to ensure that the sensor does not rest on any air pockets within the sample to obtain reliable results. The prism is then placed upright into the testing press according to Fig. 3.18a. After applying the *pre-load*, the load is gradually increased until it reaches around 1/3 of its compression strength. The load is then reduced over time until it is nearly zero again. This process is repeated for a total of 3 cycles as shown in Fig. 3.18b. The software measures the applied load and corresponding displacement. With the known cross-section area (40x40mm in this thesis), the stress can be calculated, and therefore also the E-mod from the commonly known *Hooke's law*:

$$E = \frac{\sigma}{\epsilon} \tag{3.10}$$

(a) Modulus of Elasticity Test

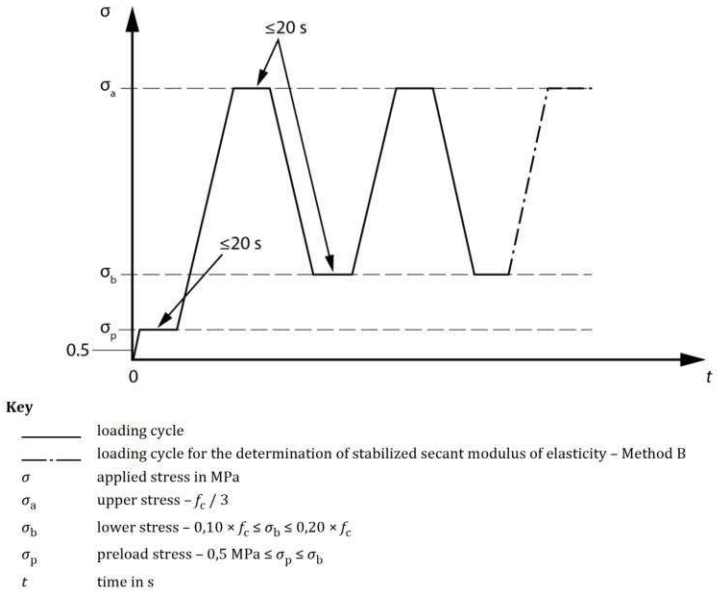

(b) Load Cycles According to *DIN EN 12390-13* [15]

Fig. 3.18: Testing Process to Validate the Modulus of Elasticity

3.9.5 Carbonation

Concrete is generally very alkaline with a typical high Potential of Hydrogen (pH)-value around 13. This alkaline environment protects the rebars from corrosion. Over time, however, CO_2 from the surrounding air reacts with calcium hydroxide ($Ca(OH)_2$) in the cement to form calcium carbonate ($CaCO_3$) with the byproduct of water, according to Eq. 3.11.

$$Ca(OH)_2 + CO_2 \longrightarrow CaCO_3 + H_2O \tag{3.11}$$

Luckily, the process slows down the deeper it reaches because concrete usually gets less permeable in carbonation reaction. Carbonation leads to a significantly reduced pH-value, since $CaCO_3$ is much less alkaline (pH∼9) then $Ca(OH)_2$ (pH∼13). The protection of the rebars in the carbonated depth is no longer given and they start to corrode. Recent studies estimate that rebar corrosion starts already at around pH 11. Rust has a much higher surface area than the original steel, which ultimately leads to surface flaking, thereby destroying the concrete from the inside. As an structural engineer, the aim is to try to avoid these types of damage by placing the rebar outside this carbonation zone, leaving a safety margin known as the *concrete cover*. This refers to the minimum clear distance from the outer surface to the surface of the first rebar layer. In the *Eurocode 2*, this safety margin varies depending on the acidity of the environment [43][53][70][73].

To determine the carbonation depth, Phenolphthalein is used to colour areas with pH of 9 or higher in its typical pink tone. It is very important to use a freshly broken sample to avoid a distortion of the results with early-stage carbonation of the fractured surface.

In the following comparison (Fig. 3.19) the difference between conventional concrete with CEM I and UHPC with CEM III/B gets obvious. Picture 3.19a shows some of the analyzed CEM III/B UHPC samples from this thesis. Clearly, no carbonation is observable, which aligns

with various studies indicating that the carbonation depth is limited to less than one millimeter for UHPC [6][18][47], depending on the mixture composition. Carbonation has little to no effect to UHPC due to its densely packed matrix, low porosity and therefore high air-tightness [63]. CEM III/B has a high amount of slag, which forms calcium silicate hydrate (C-S-H) and therefore further densifies the matrix. The method of curing also indirectly influences the resistance against carbonation. A water-cured UHPC has reduced porosity due to an enhanced hydration process, resulting in a denser matrix, compared to a dry-cured sample [2][35]. This resistance to carbonation in UHPC allows for the use of steel fibres to increase the strength, which would not be feasible with conventional concrete as the fibres would simply corrode inside the carbonation area. Fig. 3.19b shows a reference sample of conventional concrete (with w/c=0.6 CEM I, approximately 1 year of carbonation), where the carbonation depth is clearly visible.

(a) Carbonation CEM III/B UHPC **(b)** Carbonation Conventional Concrete

Fig. 3.19: Carbonation Comparison

Chapter 4

Results and Discussion

For all results, the subsequent graphs follow the same idea: the grey block or line always represents the reference mixture with w/c of 0.25 and no additives. The red dashed line indicates the height of the reference value to make it easier to compare it with the other values. For the bar charts, the red symbol on top of each bar indicates a qualitative representation of the standard deviation in scale. Yellow colour tones show varied superplasticizers, red tones indicate different w/c values. Green indicates the influence of LS and blue shows the combined influence of LS and MS.

4.1 Fresh Concrete Properties

Fresh concrete properties are measured directly after mixing, as already mentioned above. These properties give an direct indication about the usability of the mixture. It might be possible to work with a dry, stiff concrete in the laboratory or even in the precast factory, but it is almost impossible to use such concrete on the construction site if it can't be conveyed or pumped. Most of the results have been in an acceptable area, though some mixtures exhibited a better and some a worse workability, depending on the amount of surplus water described earlier. No mixture showed signs of bleeding or segregation when being molded into the formwork or during the slump flow or v-funnel test. The samples showed a good self-leveling and self compaction, with air bubbles rising immediately after pouring without the use of vibrations. This is not due to a high w/c, but rather the result of a high proportion of fine aggregates and superplasticizers.

4.1.1 Slump-Flow Test

This test provides a reference for the consistency of the concrete. The higher the spread value, the lower is the consistency and the better the workability. Ideally, the spread from the slump flow should be between 25 and 35 cm. A spread less than 25cm indicates a high stiffness and therefore probably a poor workability for the mix. When the spread exceeds 35cm, the mix shows excessive flowability, implying the risk of bleeding or segregation. The plot Fig. 4.1 illustrates that, in general, mixes with only limestone have shown a higher spread compared to mixes where both limestone and microsilica was added, although the workability appeared vice versa. The reference mix *0.25 CEM III*, shown in grey, is between these two groups with a spread of 23.5cm. These values heavily correlate with the amount of superplasticizers, where even a single gram can significantly affect the spread. The mixture *0.25 CEM III LS30 MS10* is shown with the spread of "0". Due to the poor flow properties of this paste, a proper test was not possible. The results for all mixtures can also be seen in Tab. 4.1

4.1.2 V-Funnel Test

This test give a reference for the viscosity. The higher the run-out time, the higher is the viscosity i.e., thicker the paste. Ideally, the run-out time should be between 10 and 20 s. The maximum

testing time was set to 60 seconds, meaning mixes that took 60s or longer to leave the v-funnel have been declared as *non-measurable*. In general, an increased amount of limestone powder shows a negative impact on the viscosity, as can be seen in the mixes in the green tones in Fig. 4.2. While the run-out time for *0.25 CEM III LS10* is at 29 seconds, it rises with an increasing amount of limestone powder, reaching 55 seconds and therefore almost doubles the run-out time for *0.25 CEM III LS30*. The mixes with only limestone have approximately the same run-out time like the mixes with 10 percent microsilica. However, the mixes with 20 percent microsilica have been very sticky and not been measurable. These values heavily correlate with the amount of superplasticizers again, where even a single gram can affect the the run-out time significantly. The reference mix, *0.25 CEM III*, shown in grey, has a run-out time of 45s. Silica fume seemed to enhance the workability. It reduces consistency while increasing viscosity leading to an sticky appearance like fresh dough. Tab. 4.1 presents the results of the slump-flow test and v-funnel test in context.

Tab. 4.1: Fresh Concrete Test Results

Mix Design	Slump-Flow Test [cm]	V-Funnel Test [s]
0.25 CEM III	23.5	45
0.25 CEM III MS10	26	16.5
0.25 CEM III MS10 no Sky	20	28
0.28 CEM III	-	-
0.28 CEM III MS10	-	-
0.37 CEM III	-	-
0.25 CEM III LS10	34	29
0.25 CEM III LS10 MS10	22.5	32
0.25 CEM III LS10 MS20	16	>60[(2)]
0.25 CEM III LS20	31.5	42
0.25 CEM III LS20 MS10	21	43
0.25 CEM III LS20 MS20	16	>60[(2)]
0.25 CEM III LS30	33	55
0.25 CEM III LS30 MS10	0[(1)]	>60[(2)]
0.25 CEM III LS30 MS20	16	>60[(2)]
0.25 CEM III LS30 MS40	-	-

[(1)] Mixture was too stiff to be tested
[(2)] Test was aborted after 60 seconds

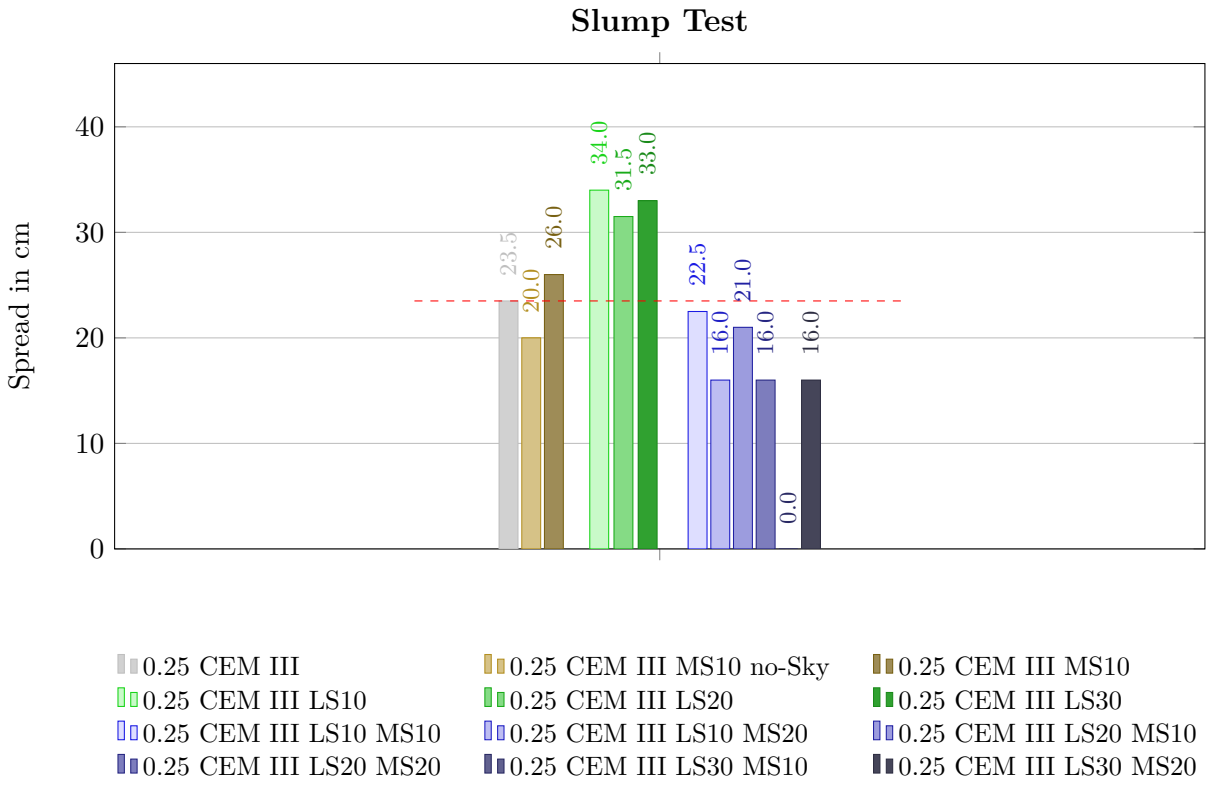

Fig. 4.1: Slump-Flow Test

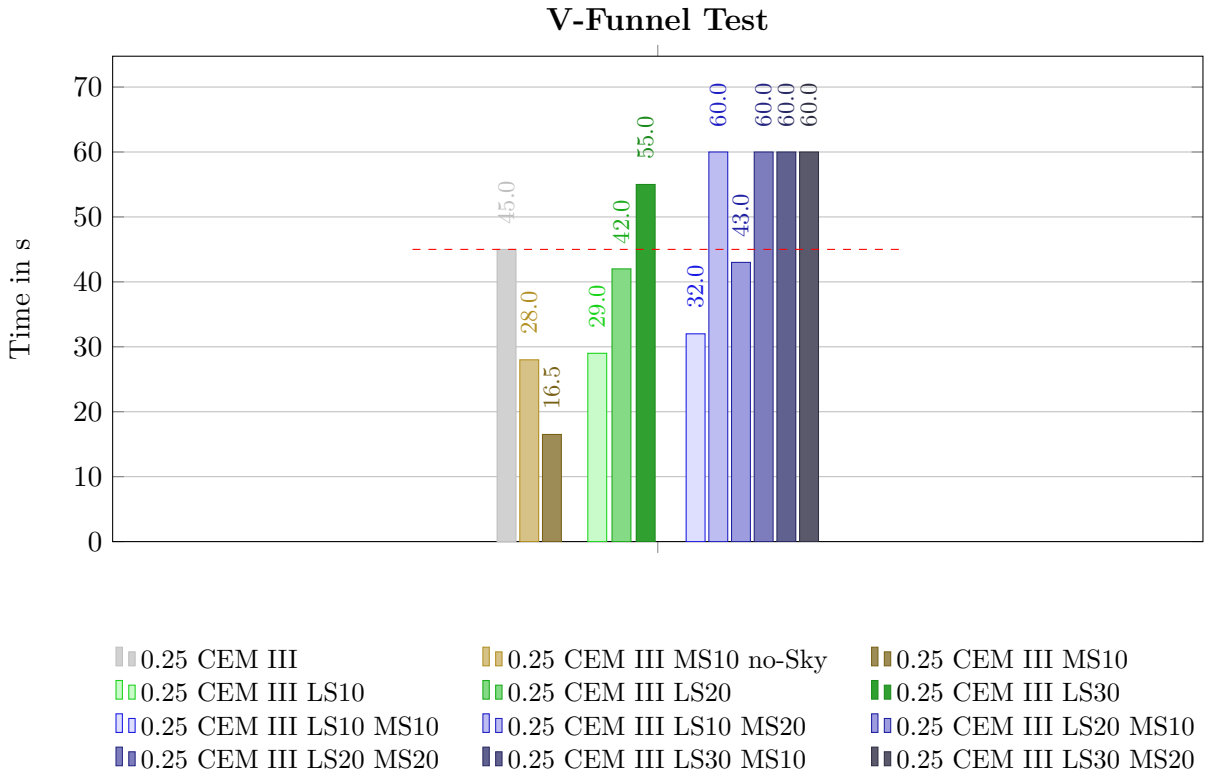

Fig. 4.2: V-Funnel Test

As previously mentioned, even small amounts of superplasticizers can significantly affect the workability of concrete, particularly in terms of consistency and viscosity, where even a single gram difference can lead to notable variations in performance. This sensitivity, combined with the influence of only LS or its combination with MS, contributes to the zigzag pattern observed in the results, as depicted in in Fig. 4.3. The graph illustrates the spread on the primary ordinate and the run-out time on the secondary ordinate as a function of the CEM III/B content on the abscissa. For readability, results with a value of "0" have been left out. The data shows that the spread increases with a higher cement content, while the run-out time decreases as cement content rises. Consequently, as the amount of cement increases, the proportion of additives decreases, resulting in a smaller solid volume fraction and a higher total amount of water in the mix. This leads to reduced consistency and viscosity, ultimately enhancing the flowability of the concrete mixture.

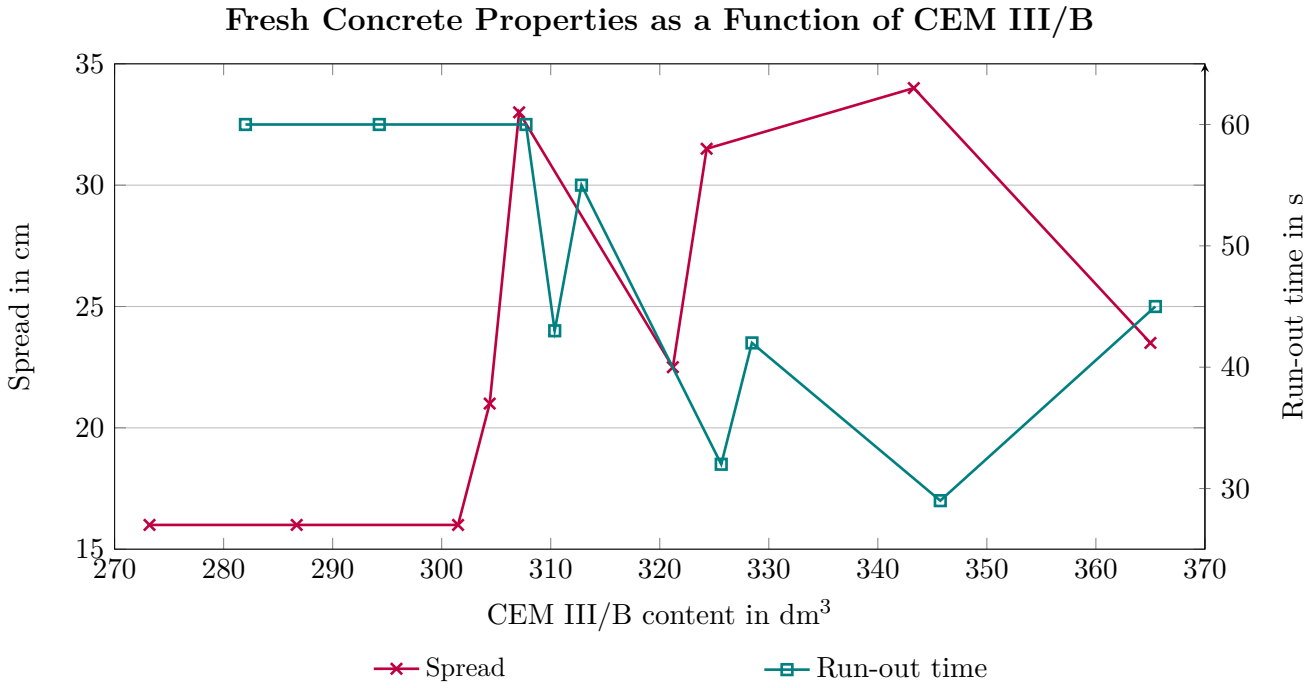

Fig. 4.3: Fresh Concrete Properties as a Function of CEM III/B

4.2 Hardened Concrete Properties

While the standard typically compares values at 28 days, this study also examines the properties at 1, 7 and 56 days to understand the evolution of strength over time. There was only one test conducted after 42 days for the *0.25 CEM III LS30 MS40* mix. Since this sample considered surplus water in the mixture design, the results of the other mixes for 28 and 56 days were linearly interpolated in order to make them comparable. The hardened concrete properties provide information about the durability, strength and the long term behaviour, such as creep.

4.2.1 Density

The density of concrete provides indirect information about the packing density of the matrix. This is particularly important in harsh environments, such as those affected by chloride ion penetration. Ideally, the density should be consistent within a sample series, with a low standard

deviation. This allows the conclusion that the concrete mixture is well mixed and all components are evenly distributed. However, due to the uneven surface of the top side in the formwork (which was not scratched), performing accurate density measurement is challenging. The following Fig. 4.4 shows an average value over all samples and all tested ages. It further illustrates a very small standard deviation, which implies, that the density is more or less constant over time. It can be observed that mixtures including LS show a slightly higher density compared to the reference mix, while microsilica, quite surprisingly, seem to reduce the density a little bit.

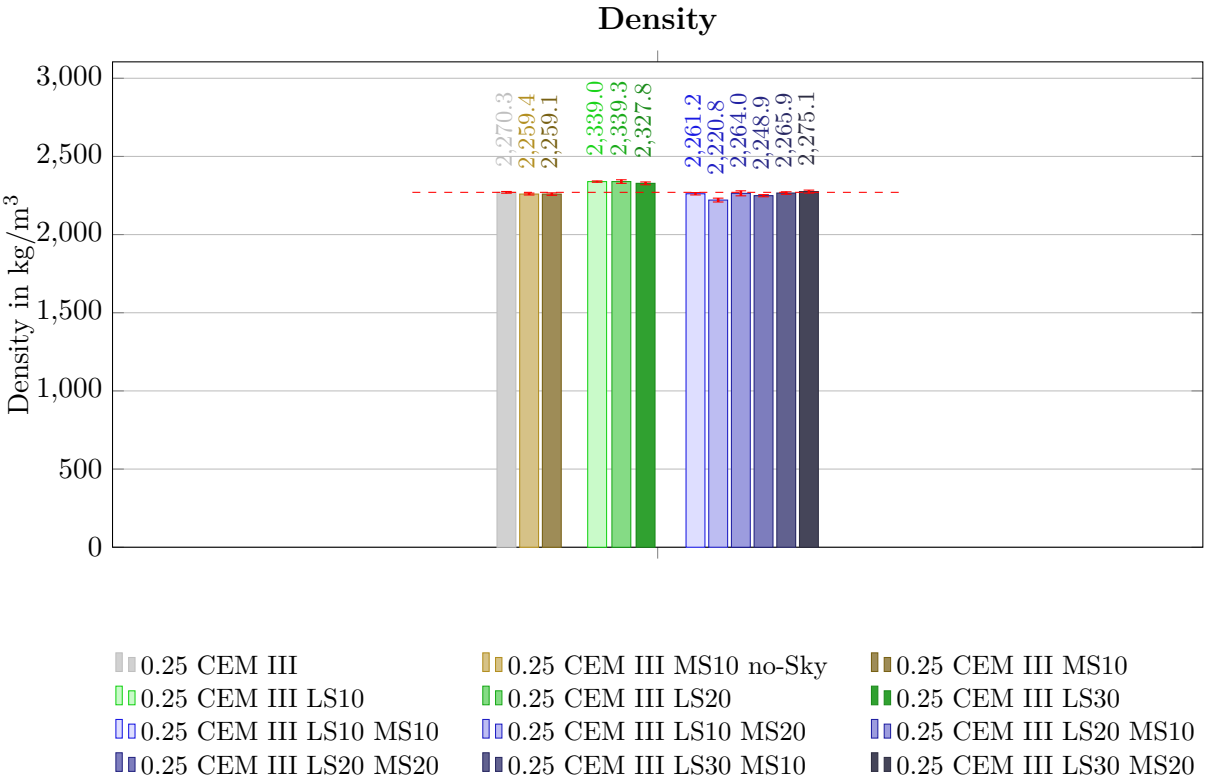

Fig. 4.4: Density

4.2.2 Compression Strength

The most important properties of UHPC are its superior strength and durability, which allows it to support high-load-bearing structures and the application in environments with aggressive exposure conditions. The compression strength is the primary indicator of the concretes ability to withstand a high load without failure. All results for compression strengths are shown in Tab. 4.2 and will be further discussed and interpreted in this chapter.

Tab. 4.2: Compression Test Results

Mix Design	$\sigma_{c,1d}$ [MPa]	$\sigma_{c,7d}$ [MPa]	$\sigma_{c,28d}$ [MPa]	$\sigma_{c,42d}$ [MPa]	$\sigma_{c,56d}$ [MPa]
0.25 CEM III	32.1	77.3	111.0	114.3*	117.5
0.25 CEM III MS10	33.5	90.5	118.8	123.8*	128.7
0.25 CEM III MS10 no Sky	37.0	96.5	123.8	124.8*	125.8
0.28 CEM III	-	-	-	-	-
0.28 CEM III MS10	-	-	-	-	-
0.37 CEM III	-	-	-	-	-
0.25 CEM III LS10	32.0	86.9	126.9	131.7*	136.5
0.25 CEM III LS10 MS10	31.1	95.4	115.5	115.5*	115.5
0.25 CEM III LS10 MS20	34.9	94.5	116.6	122.4*	128.2
0.25 CEM III LS20	32.9	90.4	125.2	130.4*	135.6
0.25 CEM III LS20 MS10	31.7	97.7	120.3	123.7*	127.2
0.25 CEM III LS20 MS20	31.8	97.7	131.6	132.8*	133.9
0.25 CEM III LS30	33.2	84.0	129.8	133.8*	137.9
0.25 CEM III LS30 MS10	32.3	97.1	121.1	123.2*	125.4
0.25 CEM III LS30 MS20	34.3	103.2	132.8	135.8*	138.8
0.25 CEM III LS30 MS40	-	-	-	134.3	-

Results marked with an asterisk (*) are linearly interpolated.

Influence w/c-Ratio and MS

The chart Fig. 4.5 illustrates the impact of the w/c ratio on compression strength. As shown, the strength increased by more than 20% when reducing the w/c-ratio from 0.37 to 0.28. Additionally, incorporating 10% MS further enhanced the strength by approximately 10%. To achieve optimal strength results, it is crucial to maintain the w/c-ratio as low as workability allows. Initially, the w/c-ratio was set at 0.28, but it was soon reduced to 0.25. This adjustment led to some problems with workability, that had been already discussed in **Chapter 3: Methods and Early Stage Results**.

Influence Sky

Superplasticizers play a crucial role in determining the workability of the concrete mixture. ACE acts as a flow agent, enhancing the liquidity of the mix, while Sky serves as a consistency holder, delaying the chemical reactions of the concrete. This leads to the phenomenon, that early age strengths are higher for the mixtures without Sky, compared to the samples where both, ACE and Sky are added, as can be seen in Fig. 4.6. However, after approximately two months, the strength values of mixtures with the different superplasticizers leveled out. This observation indicates, that the choice of superplasticizers should primarily focus on optimizing workability. Based on that information, the composition was set to a mix of approximately 2/3 ACE and 1/3 Sky. The amount of superplasticizer was chosen based on experience with CEM I UHPC mixes, showing that roughly the same amount of superplasticizer was necessary, with 2-4% of flow agent (ACE) and 1-2% consistency holder (Sky).

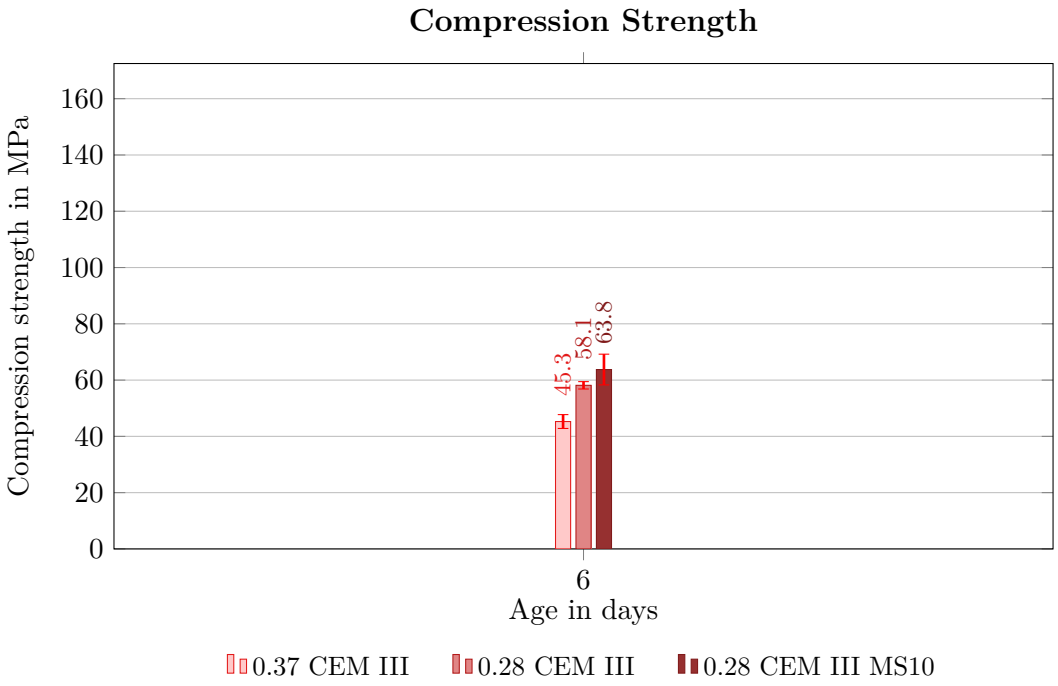

Fig. 4.5: Compression Strength - Influence w/c-Ratio

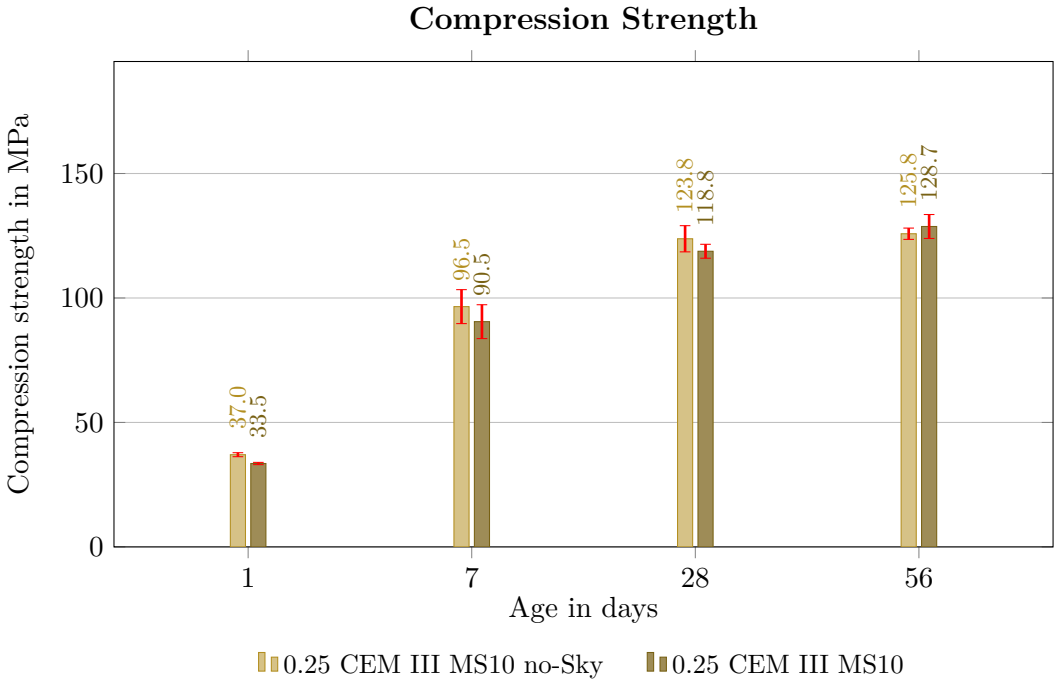

Fig. 4.6: Compression Strength - Influence Sky

Influence Limestone Powder

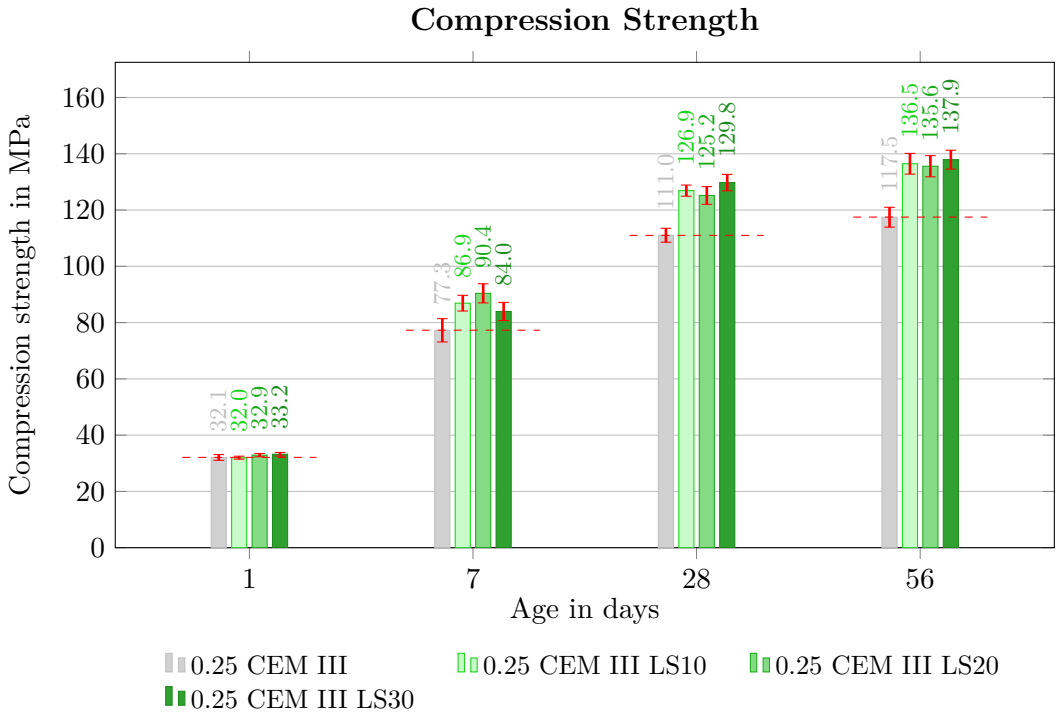

Fig. 4.7: Compression Strength - Influence LS

Limestone powder typically reduces the compression strength of UHPC mixtures [60]. However, on UHPC mixes utilizing CEM III/B, it positively influences the compression strength, as can be seen in Fig. 4.7. It further shows, that the amount of limestone powder has a minimal effect on strength, with 10, 20 and 30 percent of it delivering almost the same result. However, all three mixtures have a significantly higher value than the reference mix, *0.25 CEM III*. With a rising ratio of LS, a drastically dropping workability was clearly noticeable. Although LS also increased the early age strength, the biggest advantage compared to the reference mix can be seen in the long term strength (28 and 56 days).

The influence of LS content is further illustrated in the following Figures (Fig. 4.8-4.10). These plots show the compression strength as a function of LS content, categorized by different MS percentages.

It is clearly visible that MS has a positive effect on the compressive strength after 7 days. Additionally, an increase in LS content generally leads to an increase in compression strength, up to a certain point. The effect of LS on the compression strength also depends on the MS content. At lower SF percentages, between 10% and 20%, the strength decreases as the LS content increases, after reaching a peak value between 60 and 70 dm^3. With 20% of MS added, the strength continues to increase even further from this point.

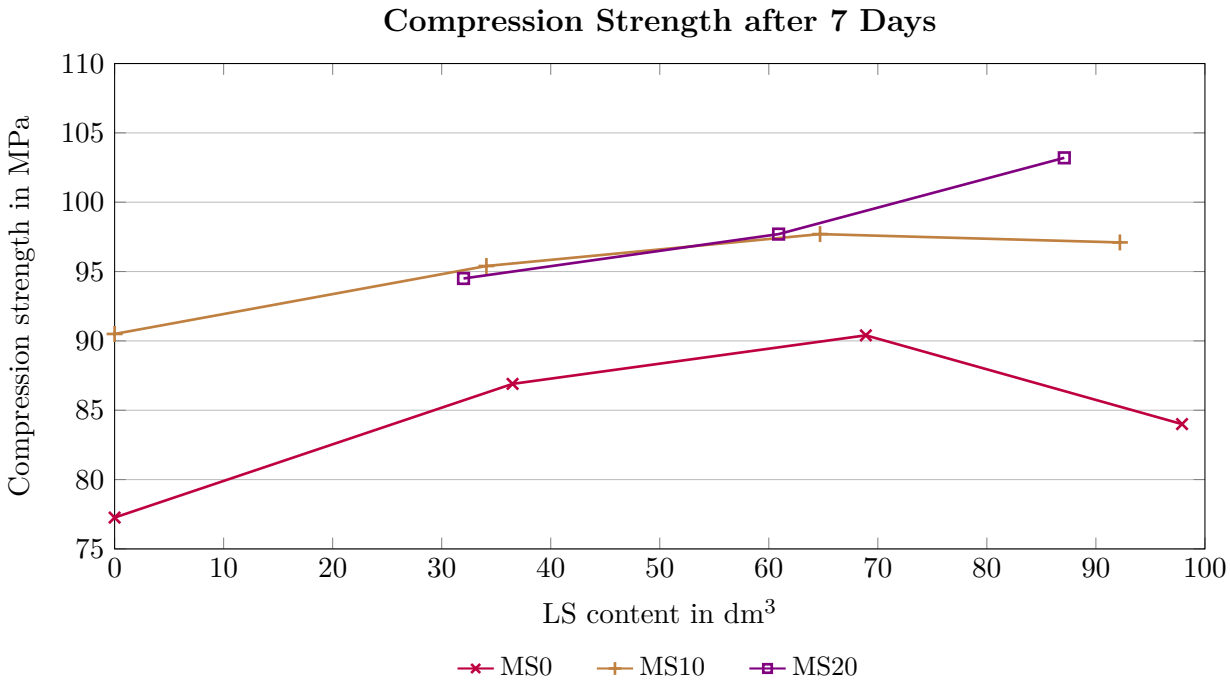

Fig. 4.8: Compression Strength after 7d as a Function of LS

After 28 days, an increase in LS content clearly enhances the compression strength. However, with only 10% of MS, the strength is reduced compared to the results without any added MS. As with the 7-day results, this graph also shows, that the highest results are achieved with a combination of high LS and MS contents.

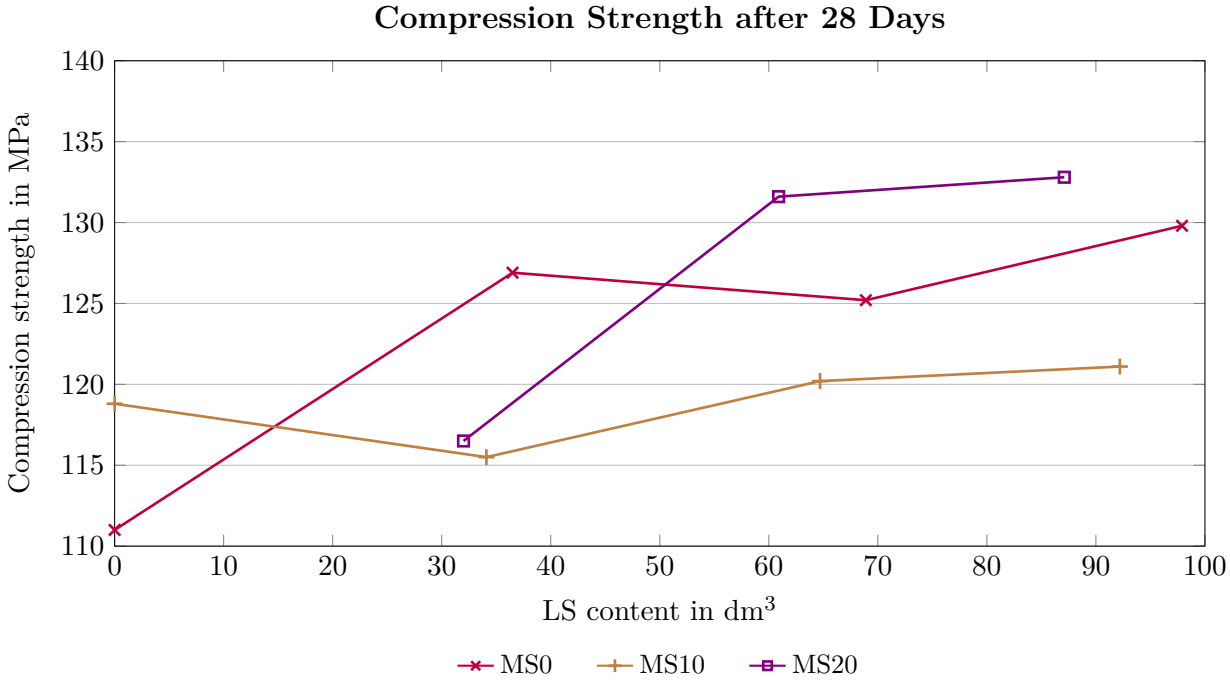

Fig. 4.9: Compression Strength after 28d as a Function of LS

The 42 day results show again that, increasing LS content leads to an increase in compressive strength, and small amount amount of MS has a negative impact on strength. Comparing it with the 7 and 28 days, it can be seen, that the influence of MS is reduced with time. Although there was insufficient data for MS40 to draw a definitive conclusion, the measured values at 42 days were among the highest results in this thesis.

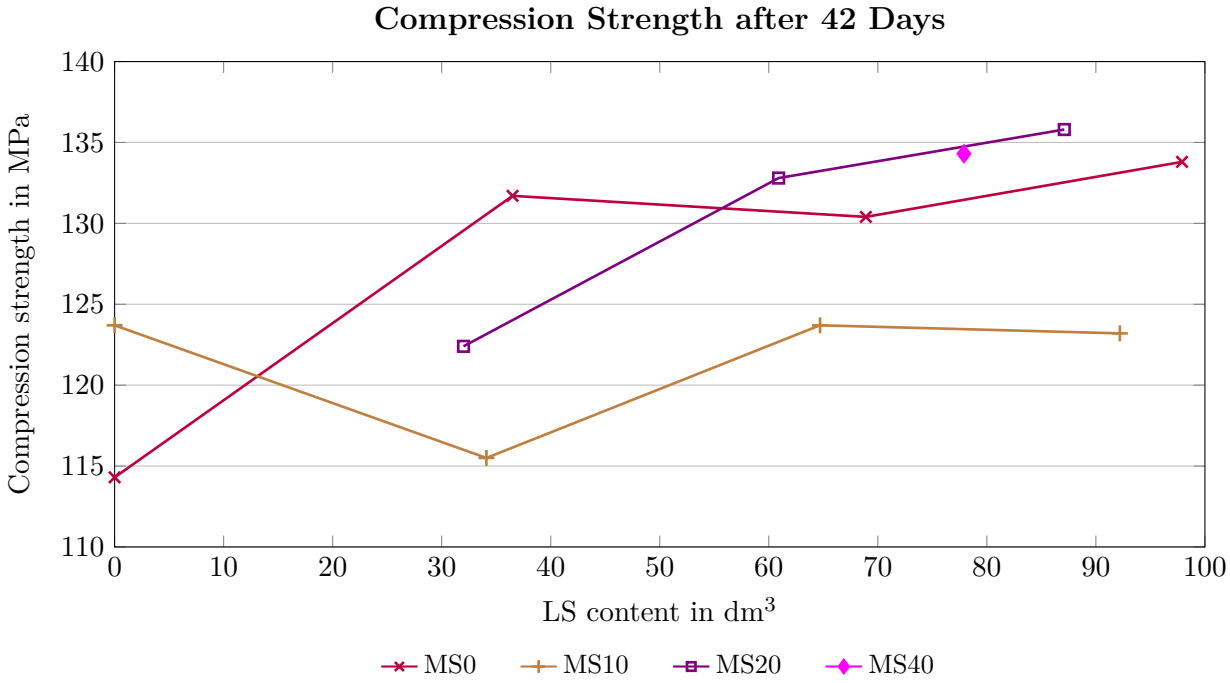

Fig. 4.10: Compression Strength after 42d as a Function of LS

Influence Silica Fume

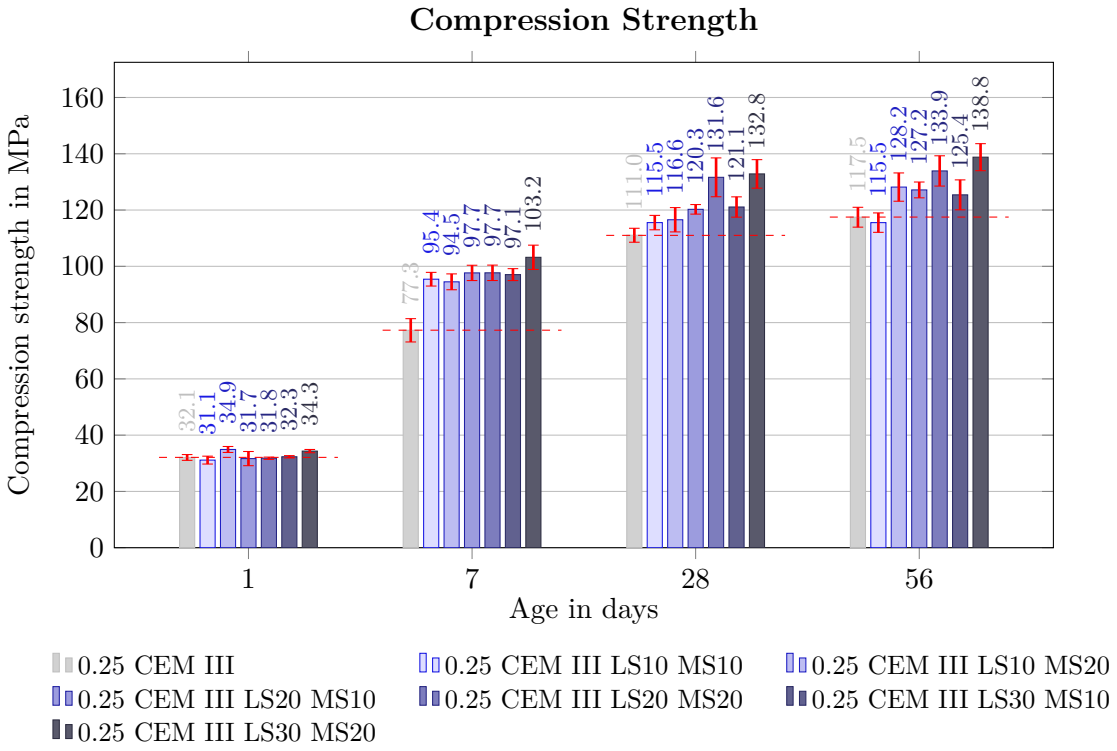

Fig. 4.11: Compression Strength - Influence LS and MS Combined

Silica fume, or microsilica, is primarily used to improve the workability of the concrete mixture by facilitating the creation of an apollonian packing. This enhances the packing density, resulting in increased compression strength, particularly in early stages. This improvement is due to the pozzolanic reaction of silica fume, which forms C-S-H. The positive effects of silica fume on long-term strength are also evident. This is illustrated in Fig. 4.11, where the compression strength at 28 and 56 days is significantly higher for mixtures with 20% silica fume (e.g. 0.25 CEM III LS30 MS20). Similar trends are observed for mixtures with different limestone powder contents. Although silica fume helps to reduce CO_2 emissions because it is a by-product of silicon production, it is relatively expensive - approximately 20 times more costly than limestone powder or cement. Considering this ecological and economic aspect, the percentage should be kept as low as possible, between 10% and 20%, as long as workability allows.

The influence of MS content is further illustrated in the following Figures (Fig. 4.12-4.14).These plots show the compression strength as a function of MS content, categorized by different LS percentages.

With an increasing amount of MS, the early compression strength after 7 days increases consistently. Higher percentages of LS also result in higher strengths, with LS30 delivering the highest results at high MS content.

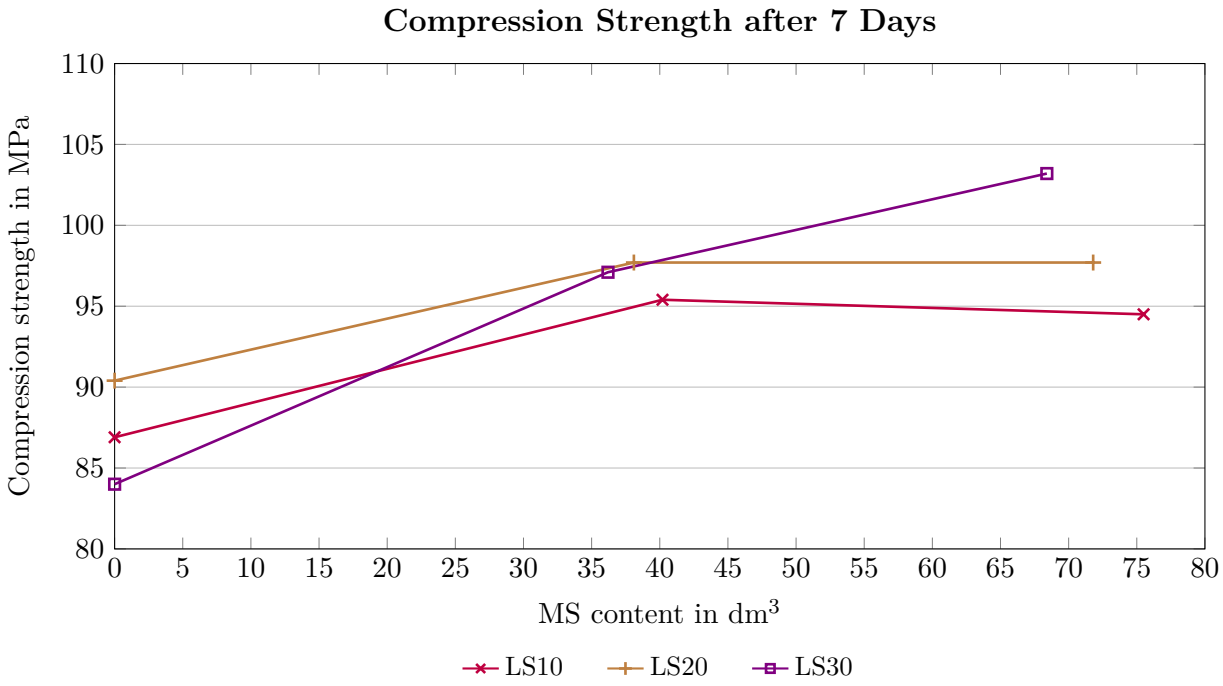

Fig. 4.12: Compression Strength after 7d as a Function of MS

After 28 days, it is observed that increasing MS content initially leads to a decrease in strength, reaching a low point around 35-40dm^3 (10% MS). After this low point, the strength increases again, reaching the highest results at high MS and LS percentages.

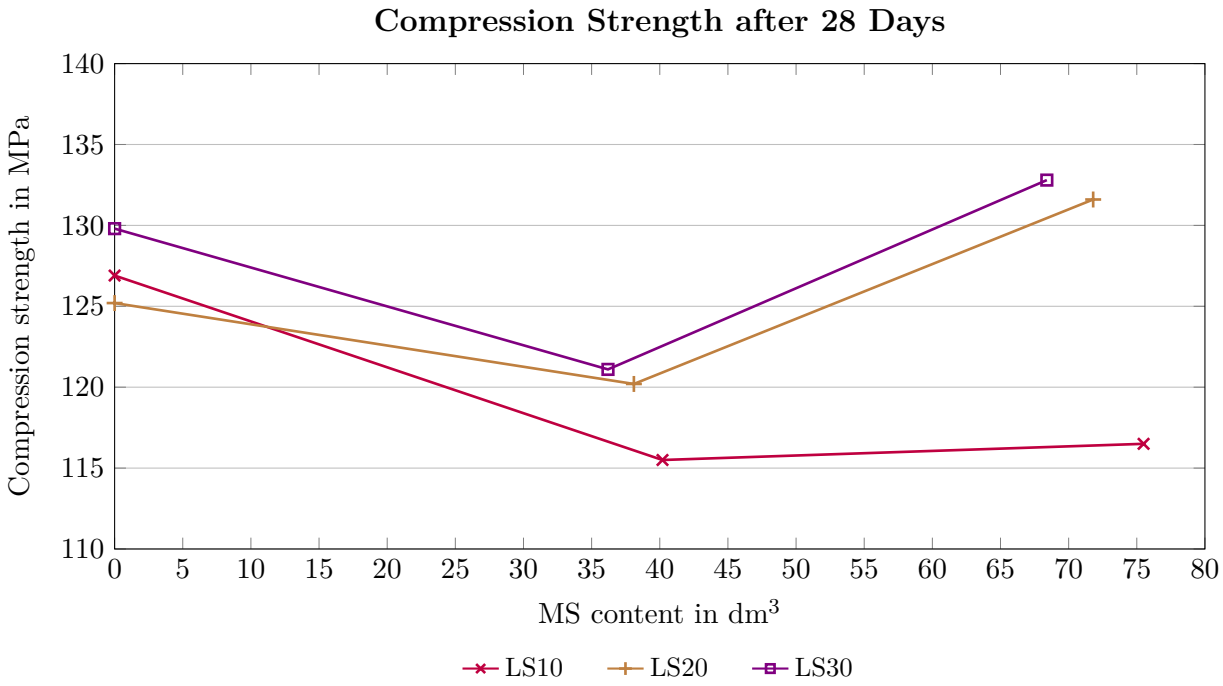

Fig. 4.13: Compression Strength after 28d as a Function of MS

The graph after 42 days follows a similar pattern to the 28 day result at first, with an additional sample containing a much higher amount of MS. As mentioned earlier, the long term compression strength decreases when a small amount of SF is added, before rising again. After reaching a maximum at roughly 70dm^3 (20% MS), the strength begins to slowly decrease with a further increasing amount of SF. Therefore, it can be conducted, that the amount of MS should be carefully selected, with particular attention on workability. While it has a significant influence on compressive strength, the effect becomes negligible once the lowest point is surpassed, while it further increases the workability clearly, by filling the voids and thus, generating surplus water.

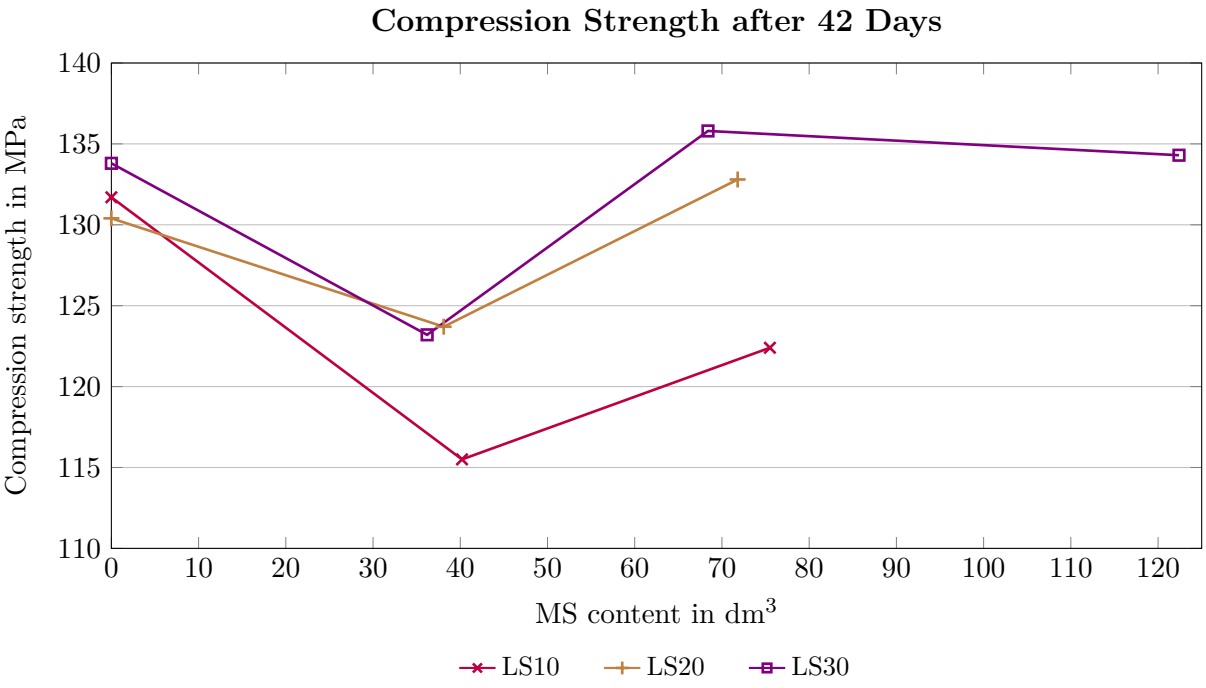

Fig. 4.14: Compression Strength after 42d as a Function of MS

Influences of Additives Compared

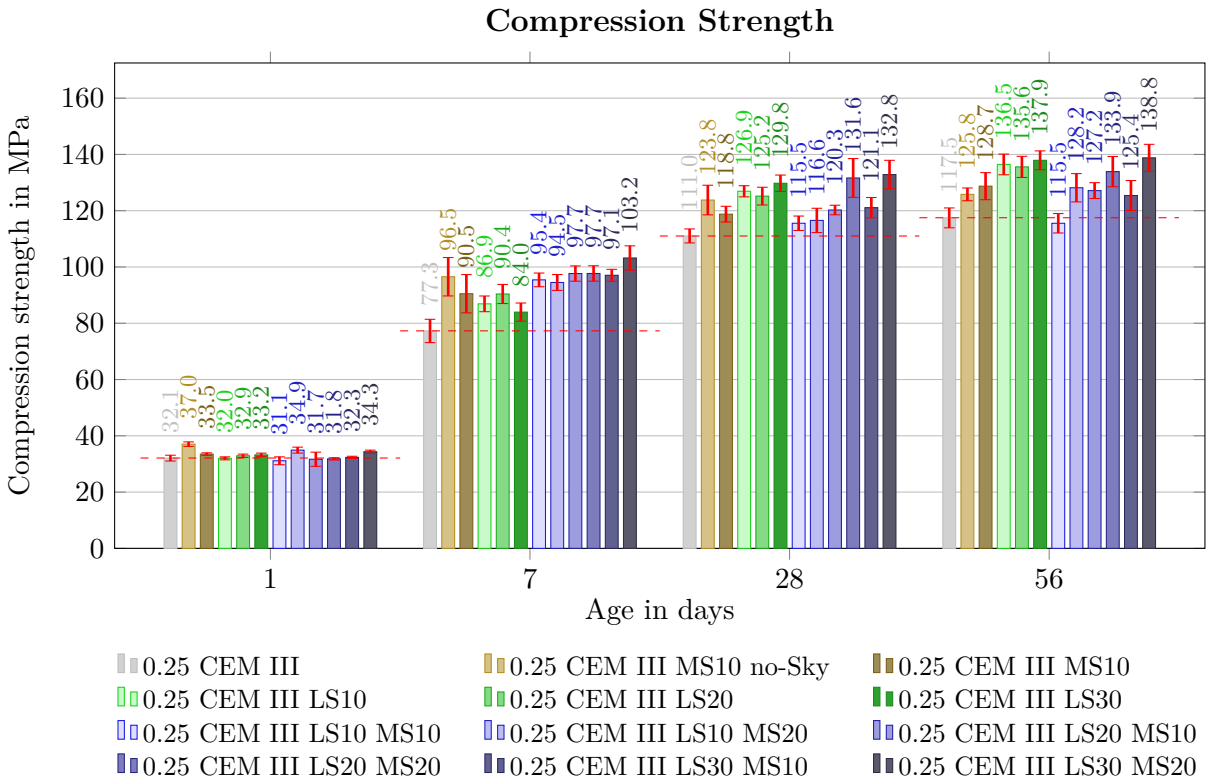

Fig. 4.15: Compression Strength - Influences of Additives Compared

The plot Fig. 4.15 may initially appear cluttered but it effectively combines the before discussed influences of the different additives into a single visual representation. It is evident that, at least for compression strength, every mixture including LS or MS achieves higher values compared to the reference mix *0.25 CEM III*, which contains no additives. As noted earlier, mixtures with MS generally exhibit higher early-age strength at 7 days. In contrast, the long-term strength increases proportionally with the amount of LS added. The long term strength of mixes containing LS is slightly reduced when 10% of MS is included, compared to the mixes without MS. Increasing the MS content to 20% compensates for this reduction, resulting in a compression strength comparable to that of mixtures containing only the same amount of LS.

Comparison of Mixtures Including 10% LS

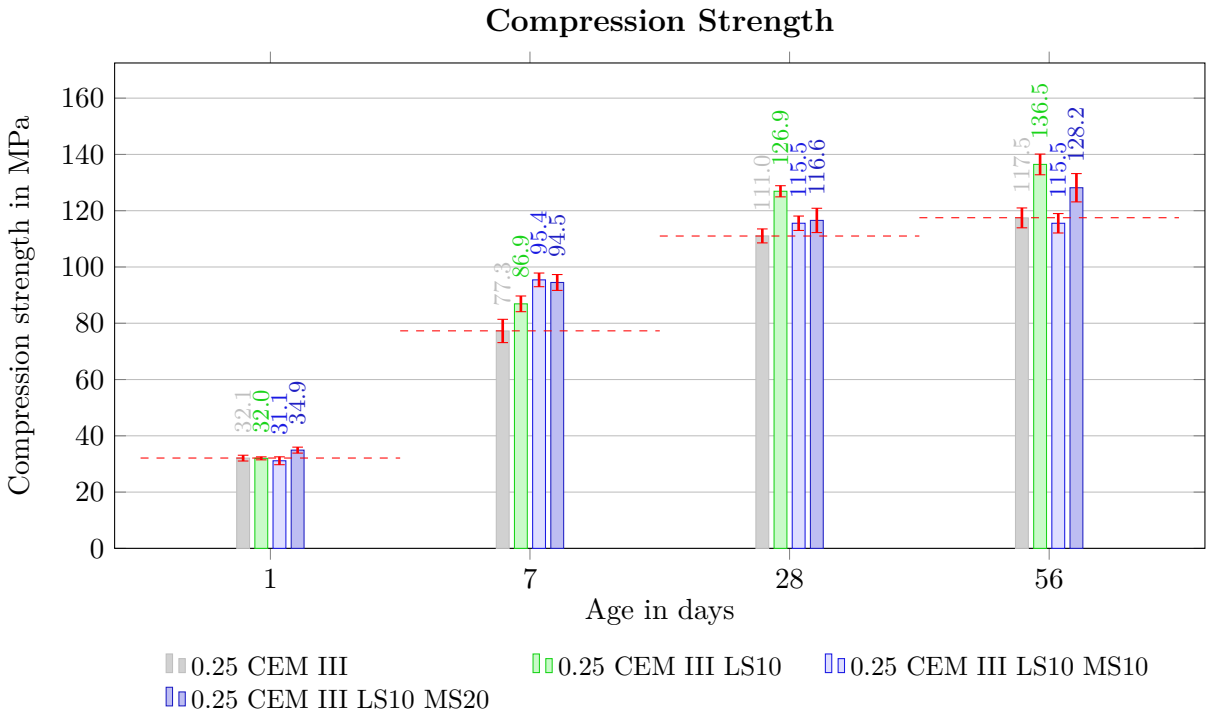

Fig. 4.16: Compression Strength - Comparison of Mixes with 10% LS

Using the same raw data, all the mixes including 10% LS can now be analyzed and compared to the reference mix. As shown in Fig. 4.16, it is evident, that MS tends to enhance early-age strengths. This can be seen at the 7 days value, where the mixes containing MS have a higher value than the reference mix or the pure LS mixture. Limestone has a more substantial effect on long-term compression strength, as can be seen after 28 and 56 days, where it clearly surpasses the mixtures with SF added. The data reveals, that adding a small amount (10%) of MS reduces the long-term compression strength compared to the same mix without MS. Further, increasing the amount to 20% will then increase the compression strength again.

Comparison of Mixtures Including 20% LS

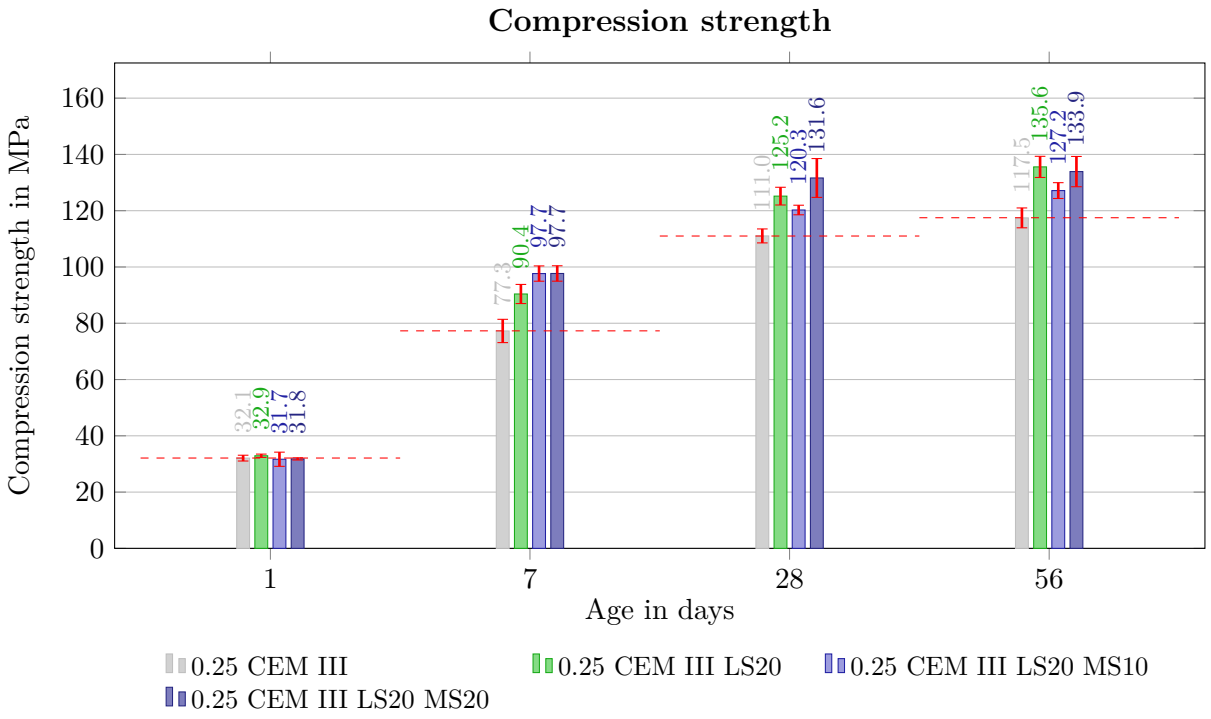

Fig. 4.17: Compression Strength - Comparison of Mixes with 20% LS

With the same raw data, all the mixes including 20% LS are analyzed and compared to the reference mix. As illustrated in Fig. 4.17, MS primarily enhances early-age strengths, while limestone significantly improves long-term compression strength. The data shows that adding a small amount (10%) of MS decreases the compression strength compared to the mix without MS. Further, increasing the amount to 20% will then increase the compression strength again.

Comparison of Mixtures Including 30% LS

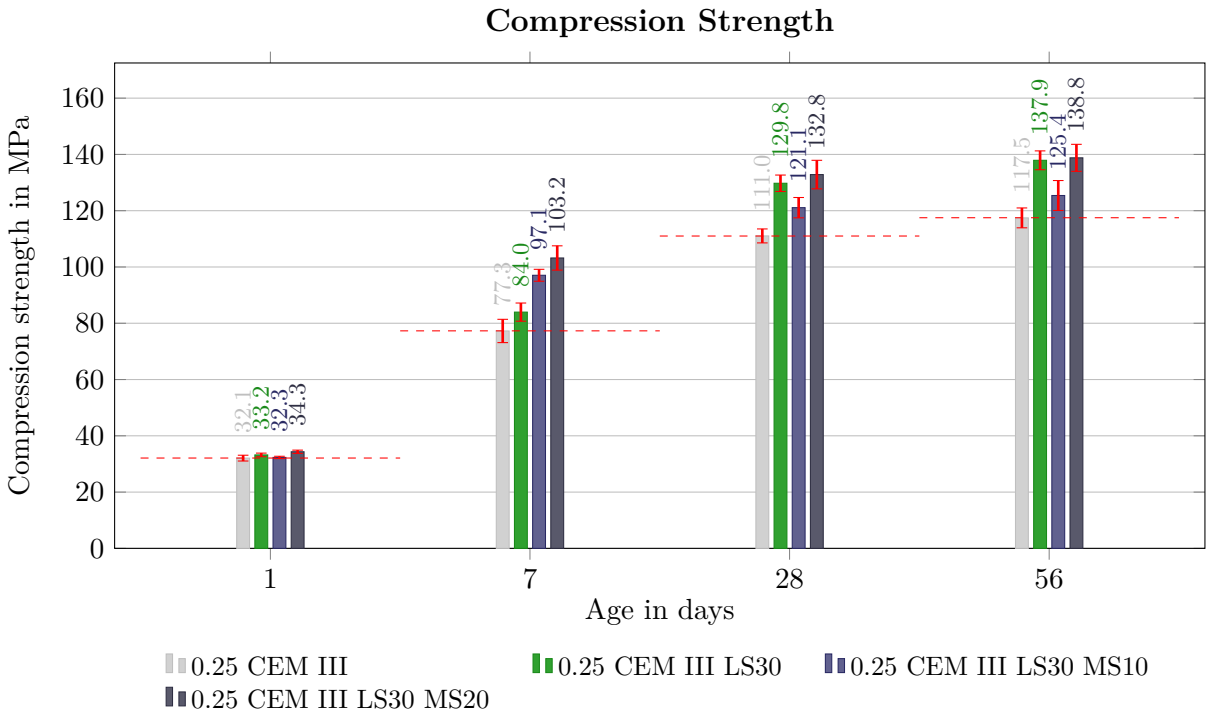

Fig. 4.18: Compression Strength - Comparison of Mixes with 30% LS

Using the same raw data, all the mixes including 30% LS are analyzed and compared to the reference mix. Fig. 4.18 shows that MS has a significant impact on the early-age strengths, where mixtures containing SF are clearly better than those without. Limestone mainly improves the long-term compression strength. The plot also illustrates, that adding a small amount (10%) of MS decreases the compression strength compared to the same mix without MS. Increasing the amount to 20% will then increase the compression strength again.

42d Compression Strength with Surplus Water Considered

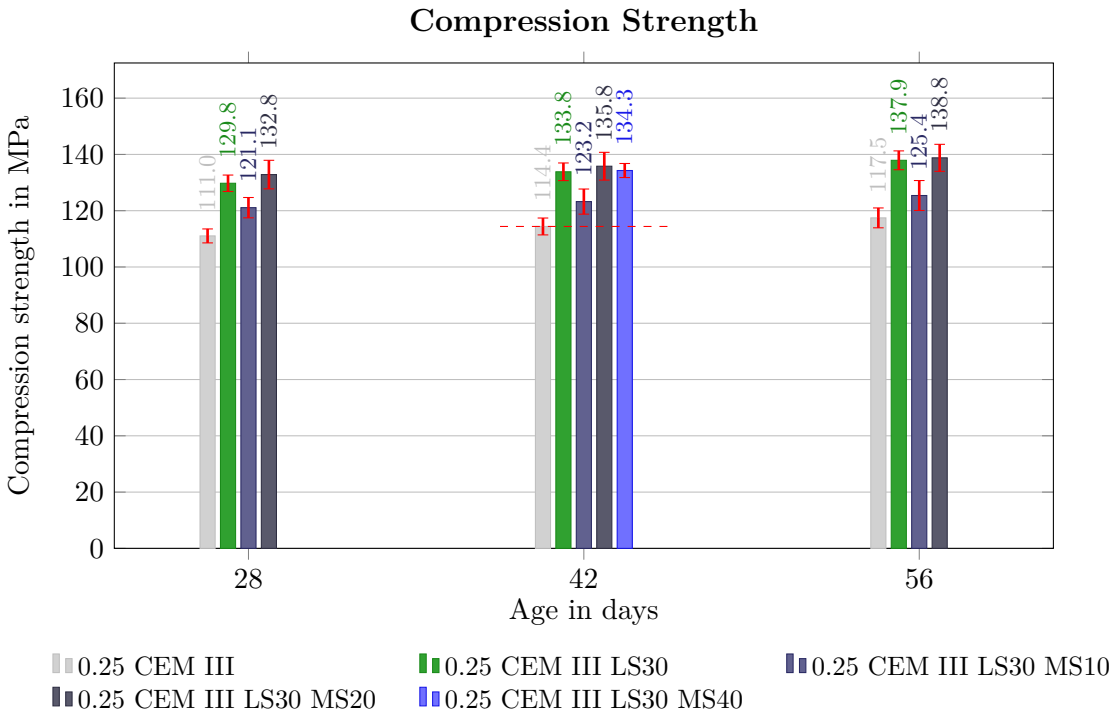

Fig. 4.19: Compression Strength - with Considered Packing Density

To assess the direction of the mix with the significantly increased microsilica (*0.25 CEM III LS30 MS40*, a test was conducted after 42 days. While the other tests were performed after 1, 7, 28 and 56 days, this was not perfectly comparable. However, the 42-day data was approximated by linearly interpolating the values between 28 and 56 days. This approximation provides a reasonably accurate estimation. The chart shows, that the compression strength of the mix with increased microsilica surpasses that of the reference mix of *0.25 CEM III*. This supports the earlier observation, where microsilica or limestone powder in certain proportions enhance compression strength. Although the strength did not improve any further compared to the mixture with 20% microsilica, it remained stable, and much more important, increasing the workability significantly. Further, the standard deviation is noticeable smaller than that of the other tested mixes. This might be due to the high amount of microsilica causing a better flowability and therefore more evenly distributed ingredients and properties within the mixture. While precise prediction about strength evolution are difficult to make, the trends observed in the mixes with both, MS and LS suggest that the mixture is likely to achieve high early-age strength and finding a pretty stable level at 134.3 MPa, most likely not to increase much more.

Compression Strength Evolution - Influence Sky

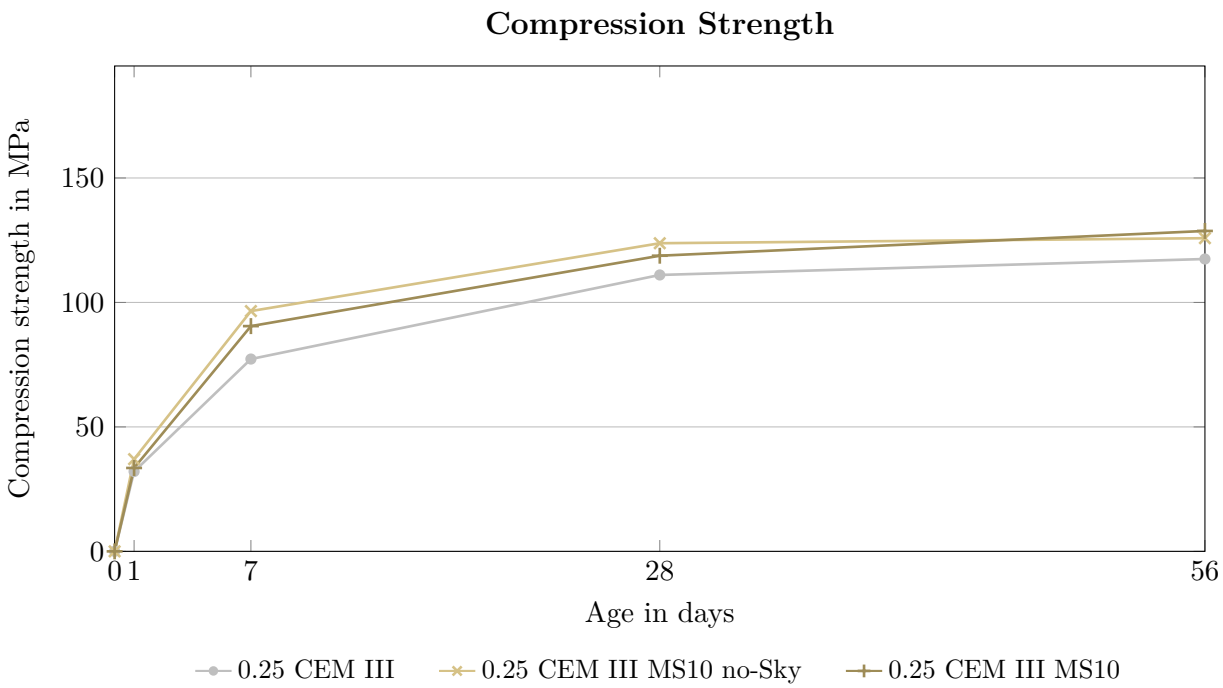

Fig. 4.20: Compression Strength Evolution - Comparison with and without Sky

These graphs visualize the evolution of compression strength over time. The presented line charts always refer to the grey line, that shows the reference mixture *0.25 CEM III*, similar to the grey bar in the bar charts. The bigger the gap between the colored lines and the grey line, the bigger the advantage of the mixture over the reference mix is. Both mixes containing superplasticizers show improved strength compared to the reference mixture. While the consistency holder, Sky, is responsible for lower early-age compression strength, it exaggerates the compression strength of the samples with no Sky between 28 and 56 days.

Compression Strength Evolution - Influence of Limestone Powder

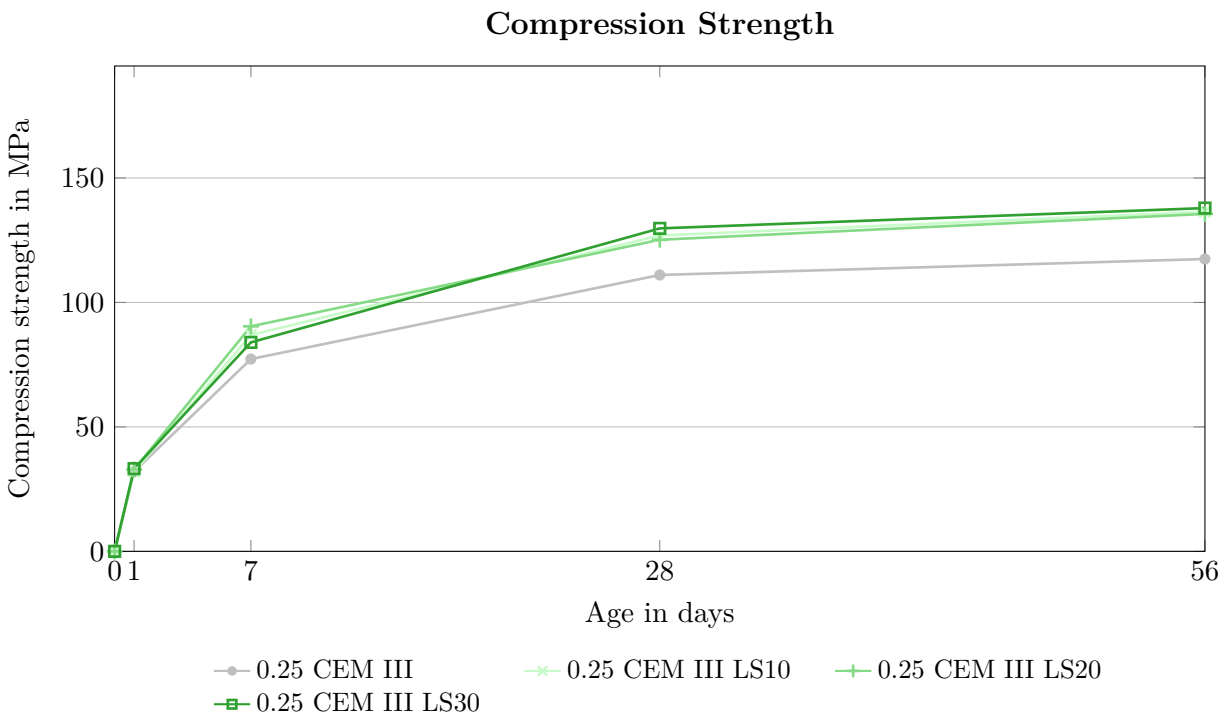

Fig. 4.21: Compression Strength Evolution - Comparison LS

Adding just 10% of limestone powder to the mix increases the compression strength significantly and consistently throughout the testing period. Increasing the LS content to 20% or 30% does not show a notable impact on the compression strength, as illustrated in Fig. 4.21. This observation suggests that a chemical reaction starts when a small amount of limestone powder is added and can't be further accelerated by increasing the amount of LS. The decision on the LS percentage in the mix should therefore be made on other properties, such as shrinkage behaviour, durability, workability and more.

Compression Strength Evolution - Influence of Silica Fume

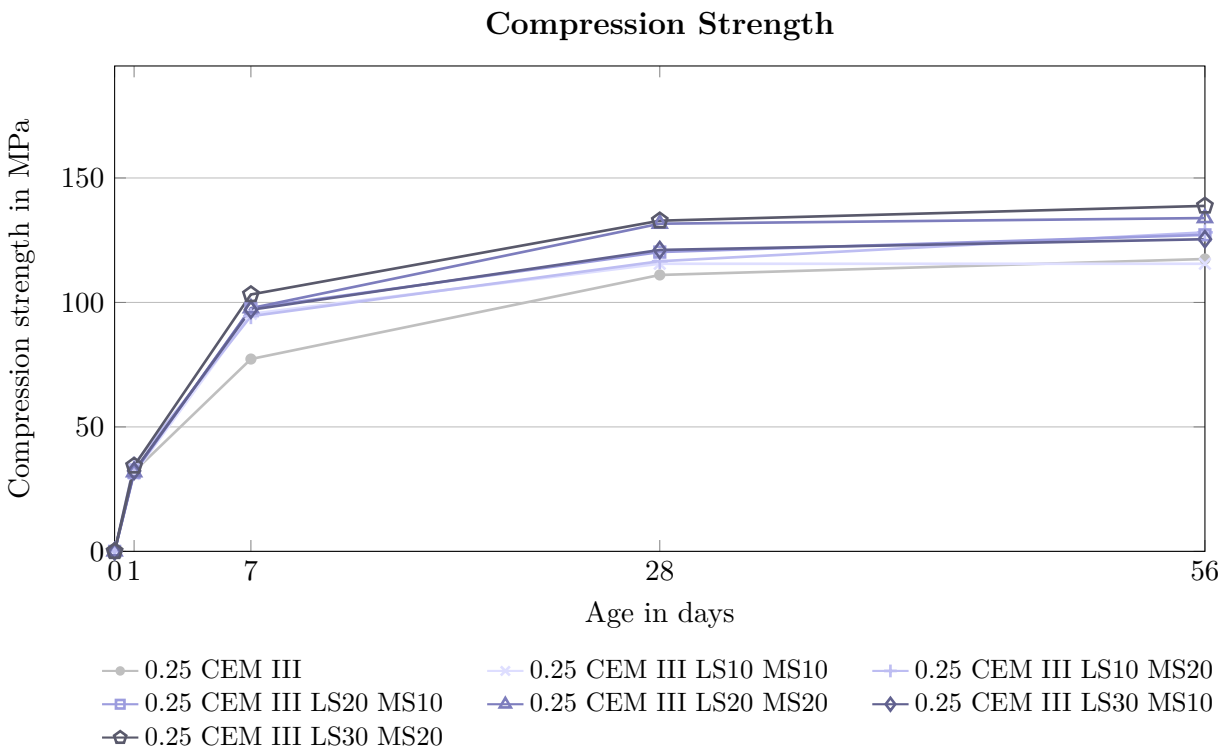

Fig. 4.22: Compression Strength Evolution - Comparison LS and MS Combined

Adding microsilica to the mix notably enhances the early-age compression strength but becomes more or less irrelevant towards 56 days. As shown in Graph 4.22, the early-age strength after just 7 days is impressively high, with already around 80% of its end value. This results in only a clear increase in early strength compared to other mixtures. It is known that CEM III/B has significantly reduced hydration heat compared to conventional concrete [38]. However, the use of microsilica as additive in heavy-mass applications, such as large foundations, remains to be elevated. Typically, higher early-age strength is associated with increased hydration temperatures, which may impact the feasibility of MS in such applications.

Compression Strength Evolution - Influences of additives compared

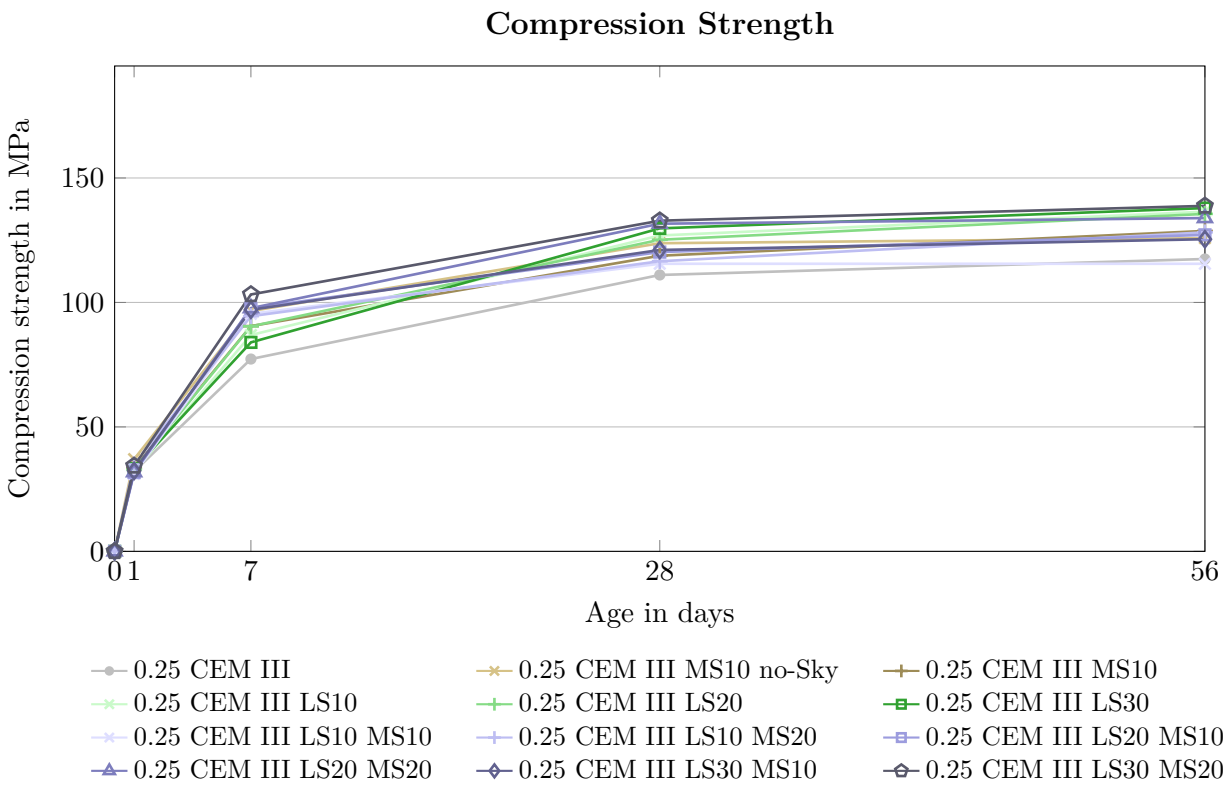

Fig. 4.23: Compression Strength Evolution - Influences of Additives Compared

This line graph overlays the compression strength evolution data from the previous graphs. Although the chart may appear overloaded, it effectively highlights several key points:

1. All mixes exhibit a higher compression strength than the reference mix, *0.25 CEM III*, throughout the observation period. Only one mixture (*0.25 CEM III LS10 MS10*) achieved comparable (low) long-term results, but none showed lower strengths.

2. While microsilica enhances early-age compression strength, it tends to level out over time. Limestone consistently increases the strength throughout the entire observation period.

Compression Strength as a Function of LS+MS

The following graph (Fig. 4.24) displays the compression strength after 42 days on the primary ordinate and the solid volume fraction (ϕ) on the secondary ordinate, as a function of LS+MS content plotted on the abscissa. While the data may initially appear zigzagged, there is still a clear trend towards increasing strength with rising percentages of additives, up to a certain point. This trend can be explained by the increasing solid volume fraction with rising percentage of additives. As more cement mass being replaced with LS and MS, and with the w/c ratio fixed at 0.25, the total amount of cement and thus the water in the mixture, is reduced. This reduction leads to a higher solid volume fraction, resulting in an increased compression strength due to a more densely packed mixture.

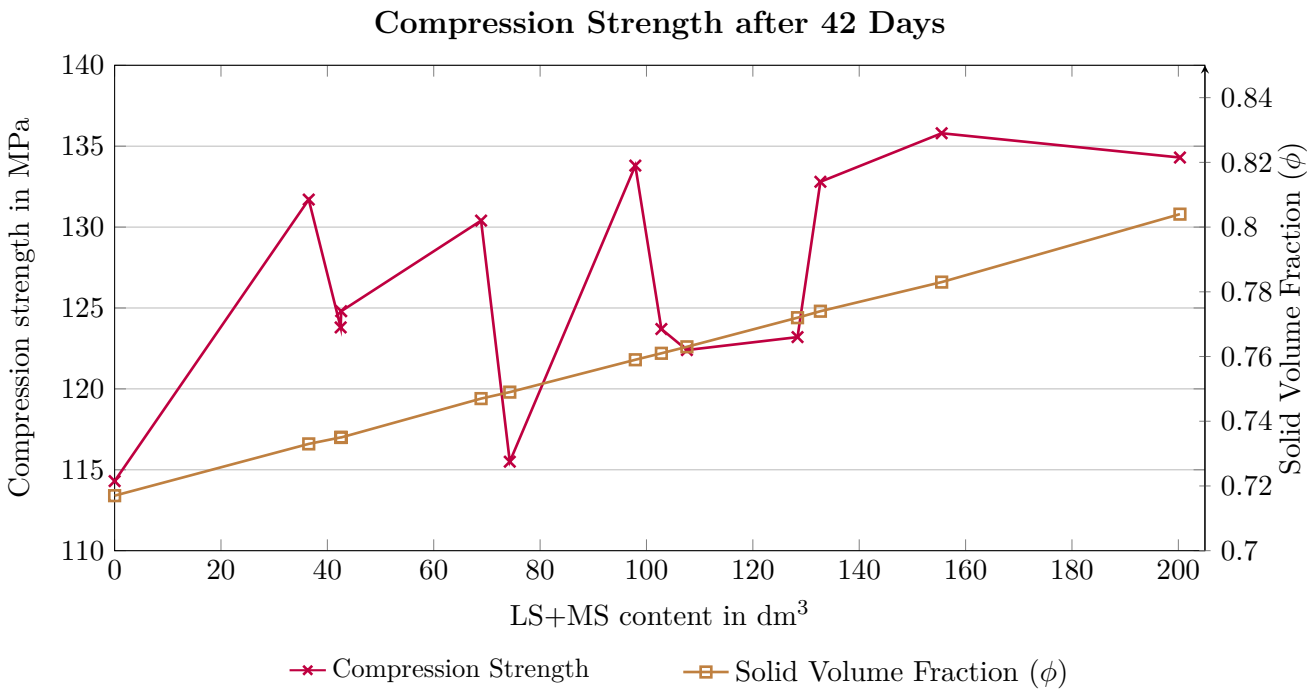

Fig. 4.24: Compression Strength after 42d as a Function of LS+MS

Compression Strength as a Function of CEM III/B

As shown in Fig. 4.25, despite slight zigzag pattern, the compressive strength trends to decrease with an increasing amount of CEM III/B, which might seem paradox at first. A higher cement content generally means a lower percentage of additives. With a constant w/c ratio of 0.25, the amount of water in the mixture is directly proportional to the cement content. In other words, the amount of water and cement is directly correlated. Less water results in a more densely packed matrix and therefore to higher strengths.

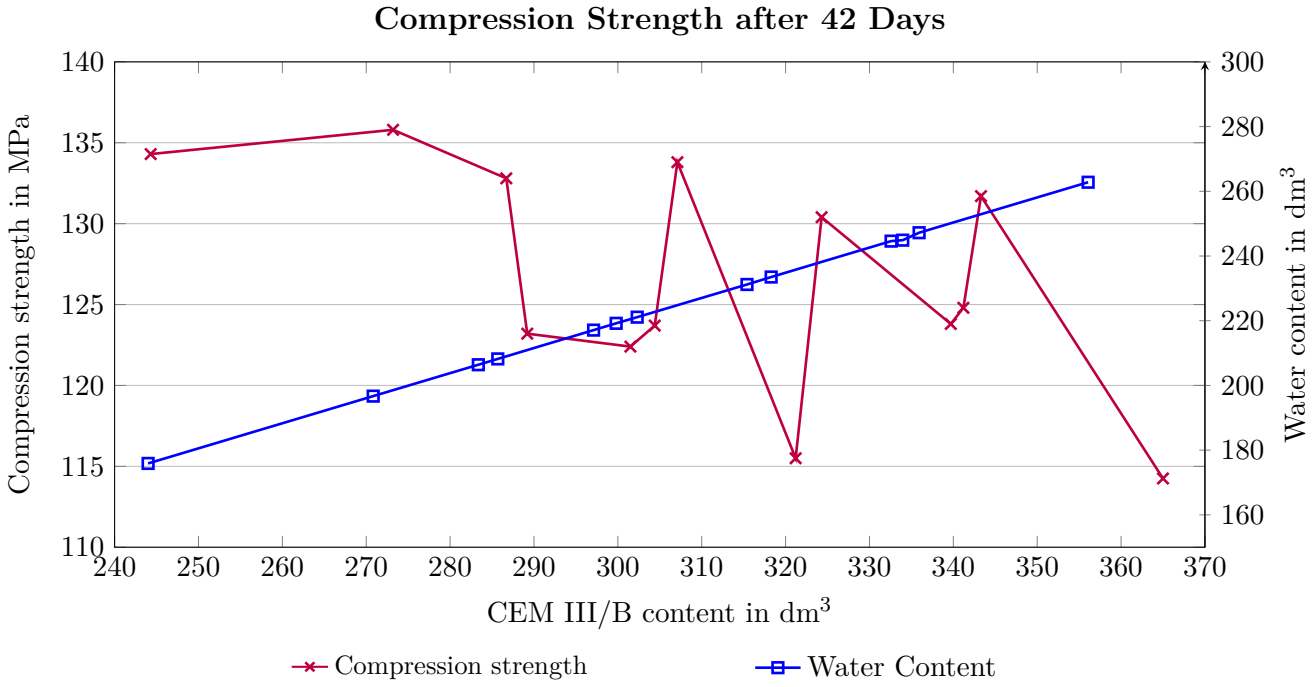

Fig. 4.25: Compression Strength after 42d as a Function of CEM III/B

4.2.3 Bending Tensile Strength

In reinforced concrete, the loads are typically divided between compression and tension. Concrete primarily takes compression loads, while reinforcement, usually in form of steel bars, takes the tensions loads. This principle also applies to UHPC, where steel fibres are usually added to improve the tensile strength. Although concrete is primarily designed for compression, it still possesses some capacity to resist tension. Typically, concretes tensile strength is roughly one-tenth of its compression strength, which corresponds to what was observed in this thesis. In real-world applications, it is often challenging to clearly distinguish between areas under pure compression and those under tension. Many structural elements, such as beams, slabs, columns, or walls with eccentric loads, experience both, compression and tension. In tension zones, concrete tends to crack because the tensile strength is exceeded and the steel fibres, which have much higher ductility, have not yet contributed to the load-bearing, before the crack occurred. For applications where cracking is undesirable, such as in waterproof basements, it is crucial to keep the tensile strength low. The bending tensile strength results are shown in **Appendix A**.

4.2.4 E-mod

As previously noted, the E-mod is an important value to understand deformations. It has a significant influence on the instant deformation and also on the long-term behaviours such as creep. It only makes sense to apply the load, when the concrete has reached a high percentage of its final strength already, which is why the E-mod was only evaluated at 28 and 56 days. Typically, the E-mod mirrors the pattern observed in the compression strength of the concrete. All results for E-mod are shown in Tab. 4.3 and will be further discussed and interpreted in this chapter.

Tab. 4.3: Modulus of Elasticity Test Results

Mix Design	E-mod$_{28d}$ [MPa]	E-mod$_{42d}$ [MPa]	E-mod$_{56d}$ [MPa]
0.25 CEM III	39,471.3	39,546.3*	39,621.3
0.25 CEM III MS10	-	-	39,555.3
0.25 CEM III MS10 no Sky	-	-	39,118.0
0.28 CEM III	-	-	-
0.28 CEM III MS10	-	-	-
0.37 CEM III	-	-	-
0.25 CEM III LS10	41,896.3	42,754.0*	43,611.7
0.25 CEM III LS10 MS10	40,063.0	39,296.1*	38,529.2
0.25 CEM III LS10 MS20	38,641.0	39,196.3*	39,751.7
0.25 CEM III LS20	42,515.7	43,213.5*	43,911.3
0.25 CEM III LS20 MS10	40,541.7	41,051.1*	41,560.5
0.25 CEM III LS20 MS20	41,636.3	41,670.1*	41,703.8
0.25 CEM III LS30	43,675.7	44,262.8*	44,849.9
0.25 CEM III LS30 MS10	41,049.3	41,418.1*	41,786.9
0.25 CEM III LS30 MS20	42,959.0	43,145.8*	43,332.6
0.25 CEM III LS30 MS40	-	44,669.7	-

Results marked with an asterisk (*) are linearly interpolated.

Influence Sky

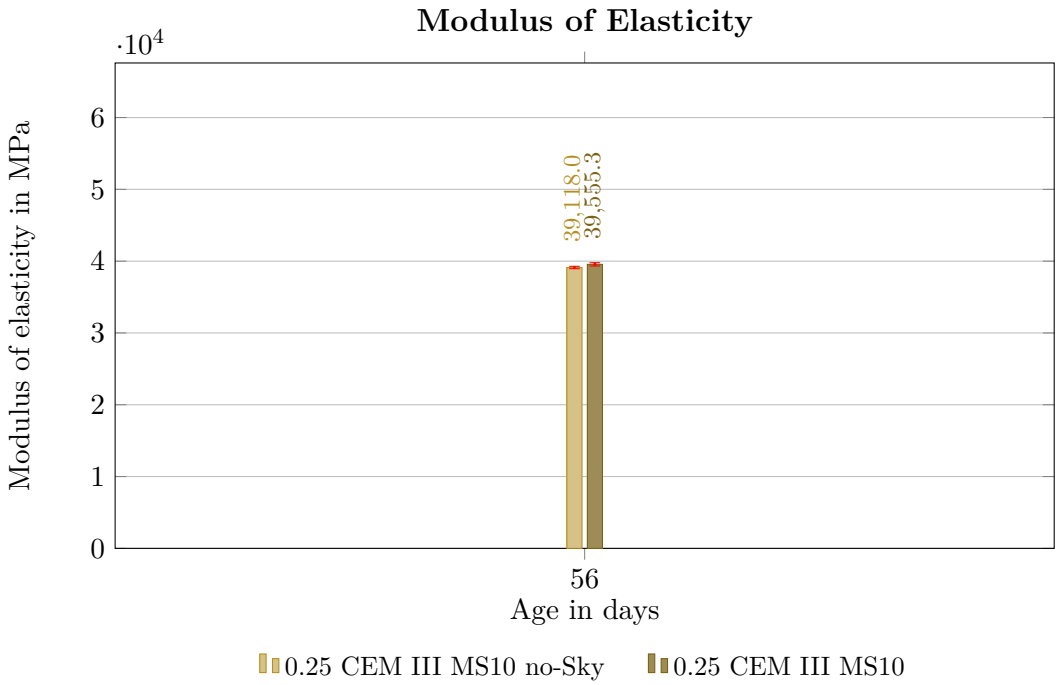

Fig. 4.26: Modulus of Elasticity - Influence Sky

As the superplasticizer only has a minor influence on strength and consistency, it was decided that the modulus of elasticity here is only measured after 56 days. The results indicate that the modulus of elasticity follows a pattern similar to the compression strength. The mix without Sky and the mix of ACE and Sky combined, deliver almost the same value, with a little advantage of the combined use of consistency holder and flow agent.

Influence Limestone Powder

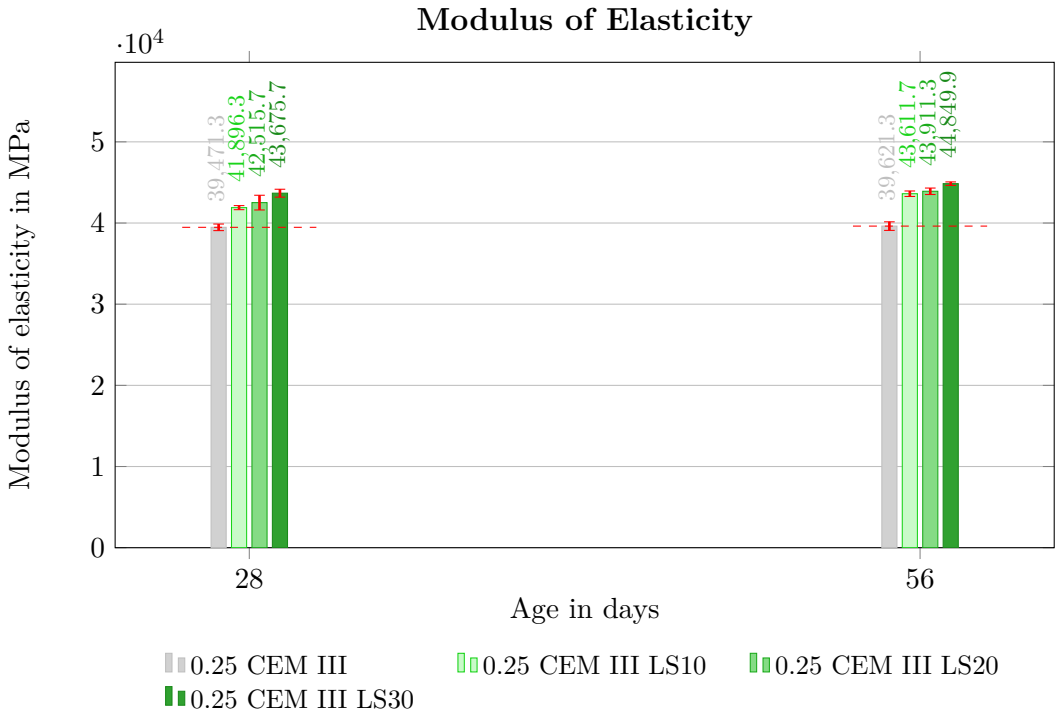

Fig. 4.27: Modulus of Elasticity - Influence LS

As expected through the results of the compression strength, limestone powder has a significant influence on the modulus of elasticity, increasing the result by 6%-10.5% at 28 days and about 10-14 % after 56 days. It also shows, that the reference mix stays at an almost constant plateau between 28 and 56 days, while the mixes including limestone powder further increase their value.

The influence of the LS content is further illustrated in the following Figures (Fig. 4.28 and Fig. 4.29). These plots show the E-mod as a function of LS content, categorized by different MS percentages.

For 28 days, it clearly shows that the E-mod is increasing, with a rising LS content. A similar pattern to that observed for compression strength can be seen, where a small amount of MS is decreasing the E-mod. However, as the MS percentage increases further, the E-mod is rising again.

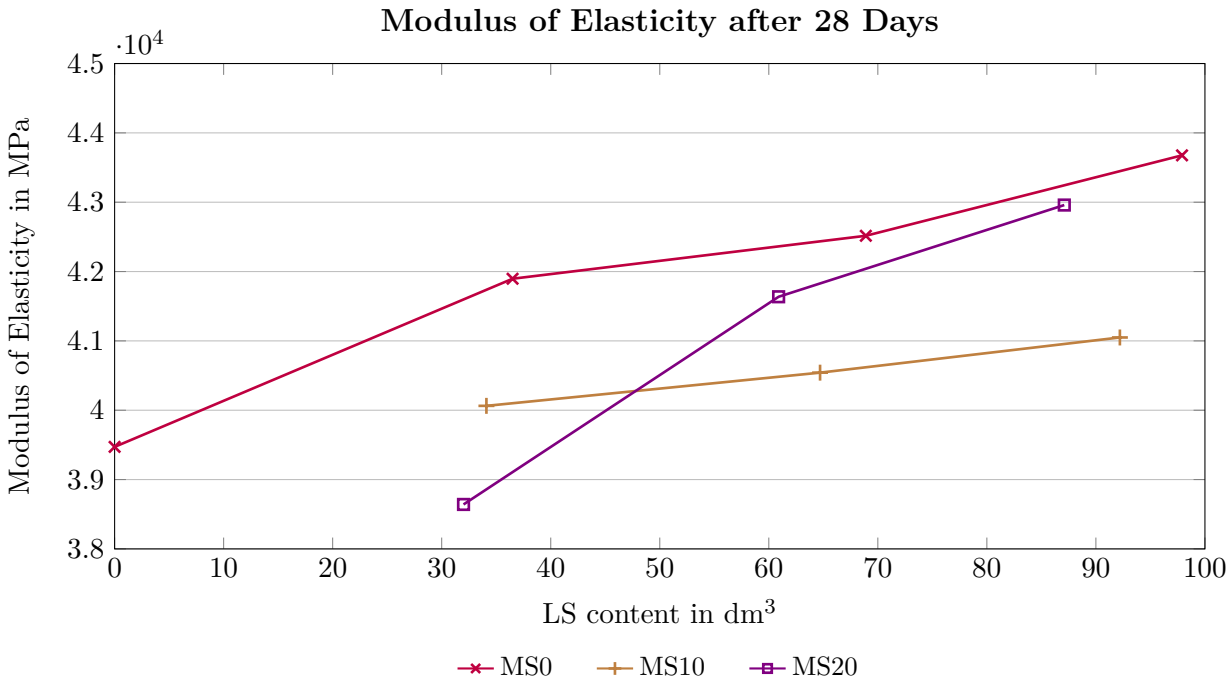

Fig. 4.28: Modulus of Elasticity after 28d as a Function of LS

The results after 42 days follow the same trend, where LS increases the E-mod, while a small amount of MS initially decreasing it, before higher amounts of MS lead to an increase in E-mod again.

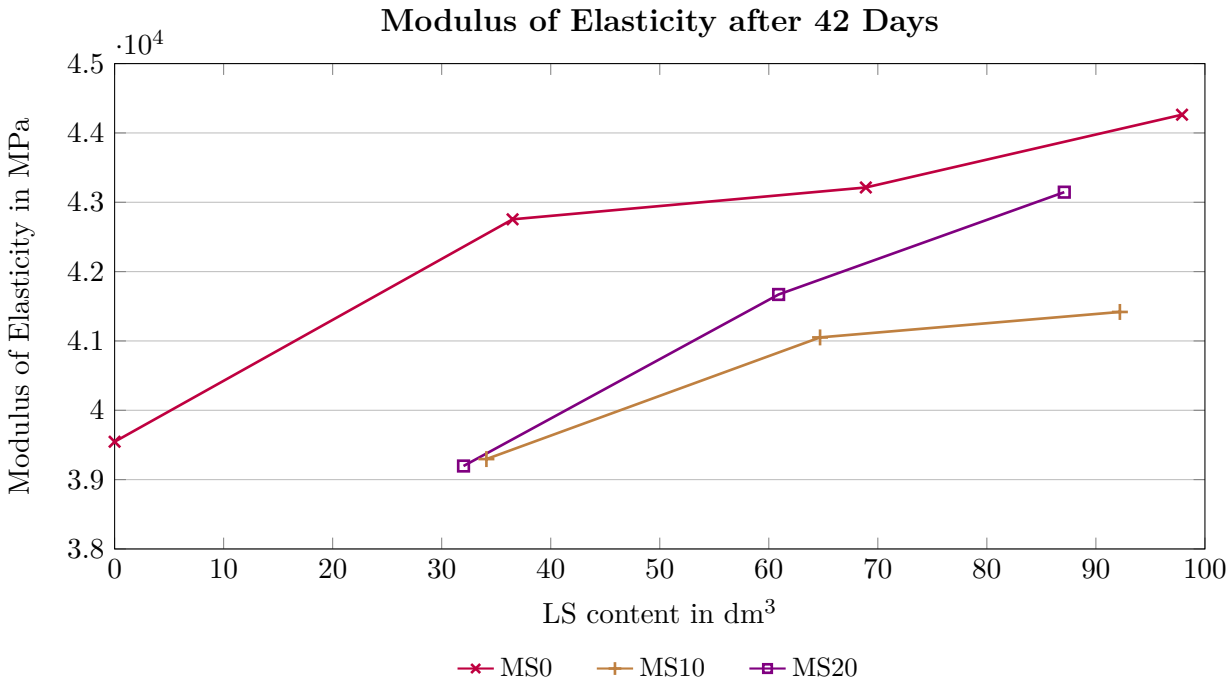

Fig. 4.29: Modulus of Elasticity after 42d as a Function of LS

Influence Silica Fume

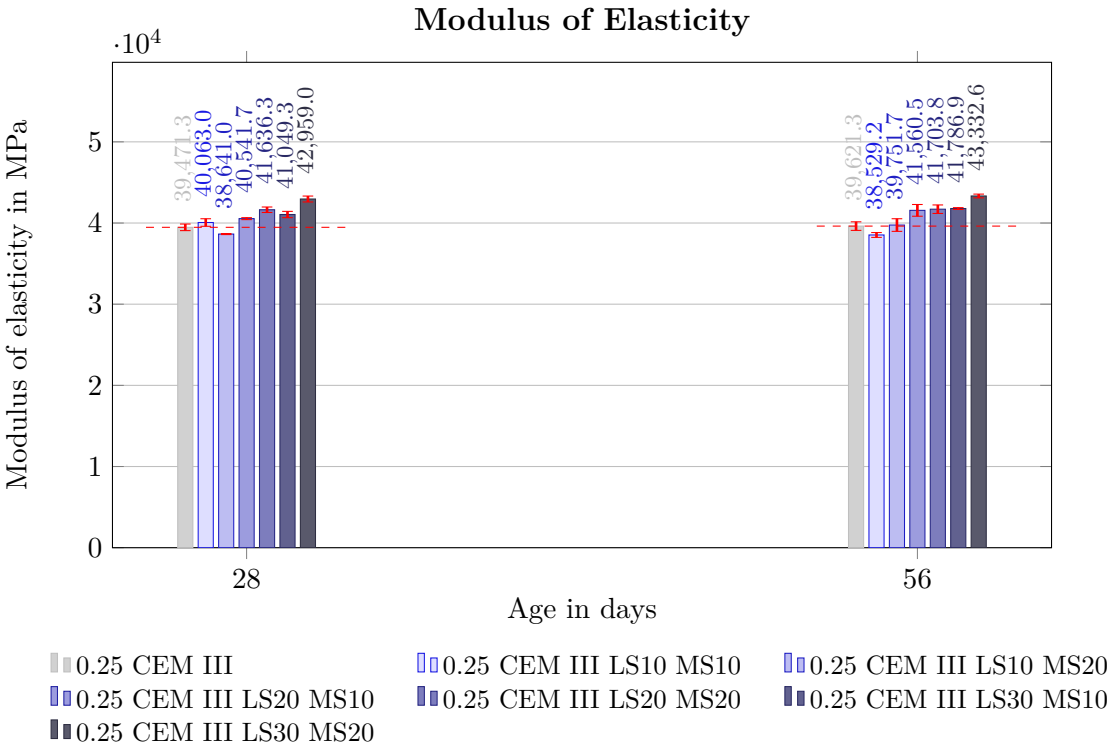

Fig. 4.30: Modulus of Elasticity - Influence LS and MS Combined

Also microsilica delivered the expected results, with most of them being slightly higher then the reference mix. Further, it shows that a small amount of SF reduces the E-mod. When the amount of SF is then increased, it also shows an increasing modulus of elasticity. This leads to the conclusion that MS to a certain amount tends to reduced the E-mod but probably has the potential to increase with a higher percentage added.

The influence of MS content is visualized in the following Figures (Fig. 4.31-4.32). These figures show the E-mod as a function of MS content, categorized by different LS percentages.

As previously mentioned for the 28 day results, an increasing amount of MS is decreasing the E-mod at first. In mixes containing 10% and 20% LS, the E-mod rises again after reaching a low point at MS10. However, with LS30 the E-mod continues to decrease. The results also demonstrate that the E-mod increases proportionally with the amount of LS added.

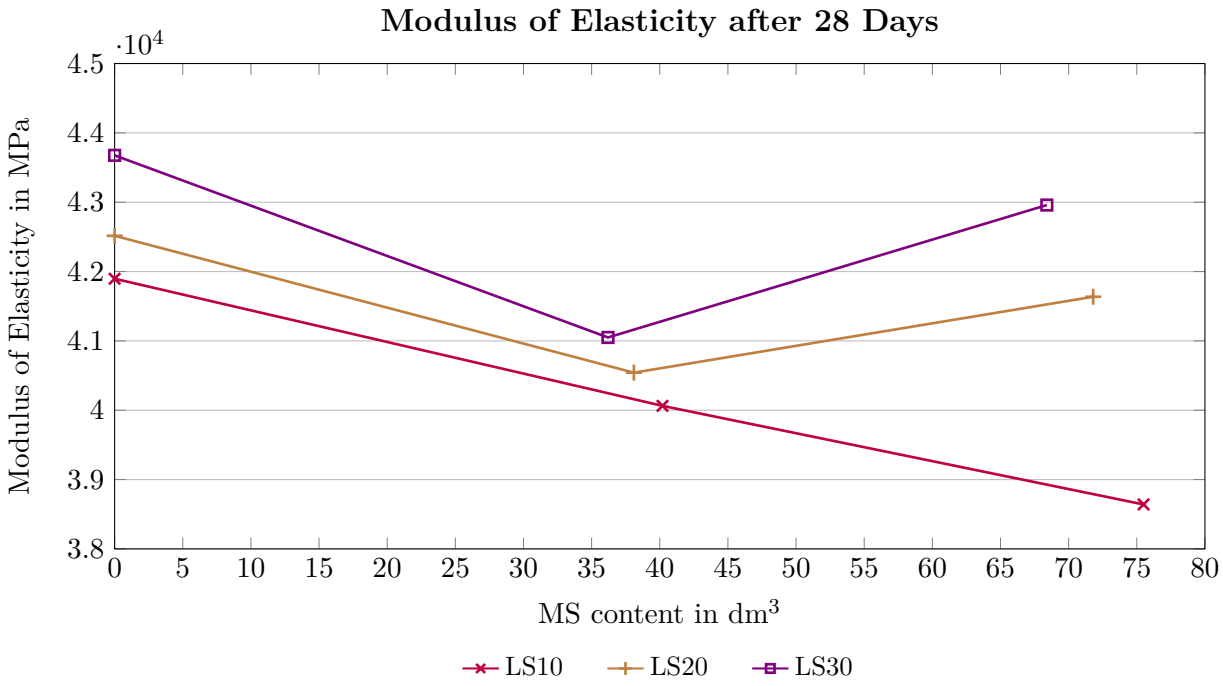

Fig. 4.31: Modulus of Elasticity after 28d as a Function of MS

Fig. 4.32 shows exactly the same pattern for 42 day results as it was with 28 days. While a small amount of MS initially leads to a decrease in E-mod, increasing the percentage of MS further will then lead to an increased E-mod. Additionally, it is clear that the E-mod directly correlates with the amount of LS added to the mixture.

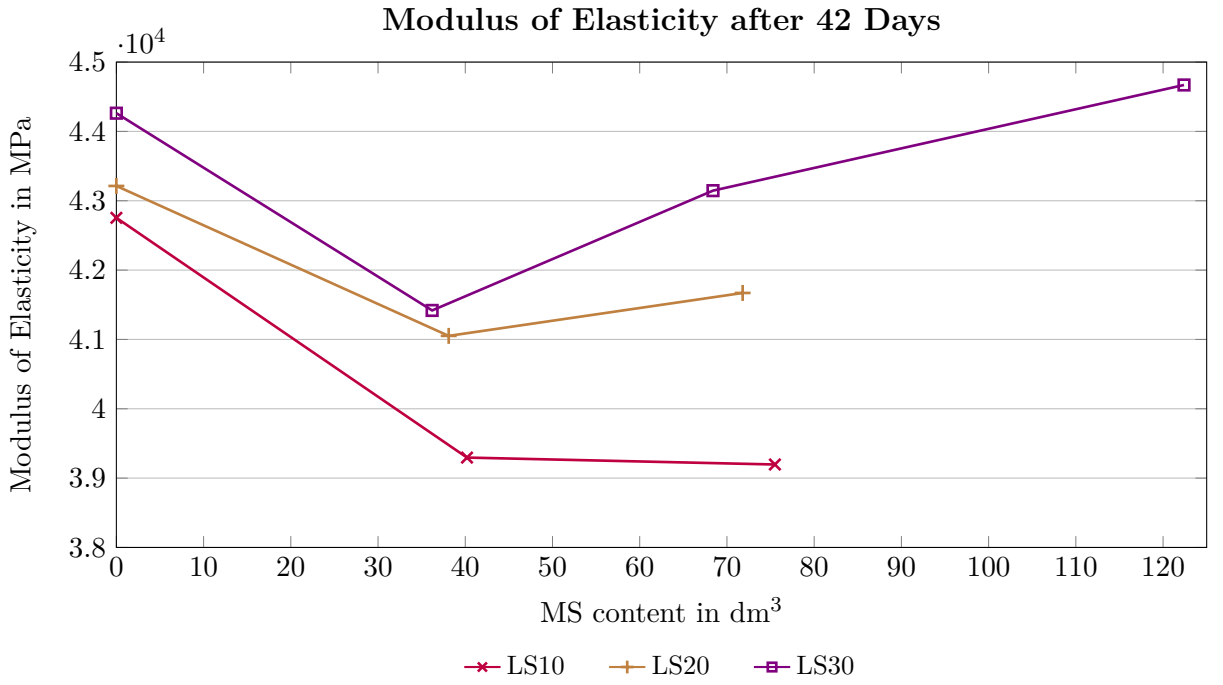

Fig. 4.32: Modulus of Elasticity after 42d as a Function of MS

Influences of Additives Compared

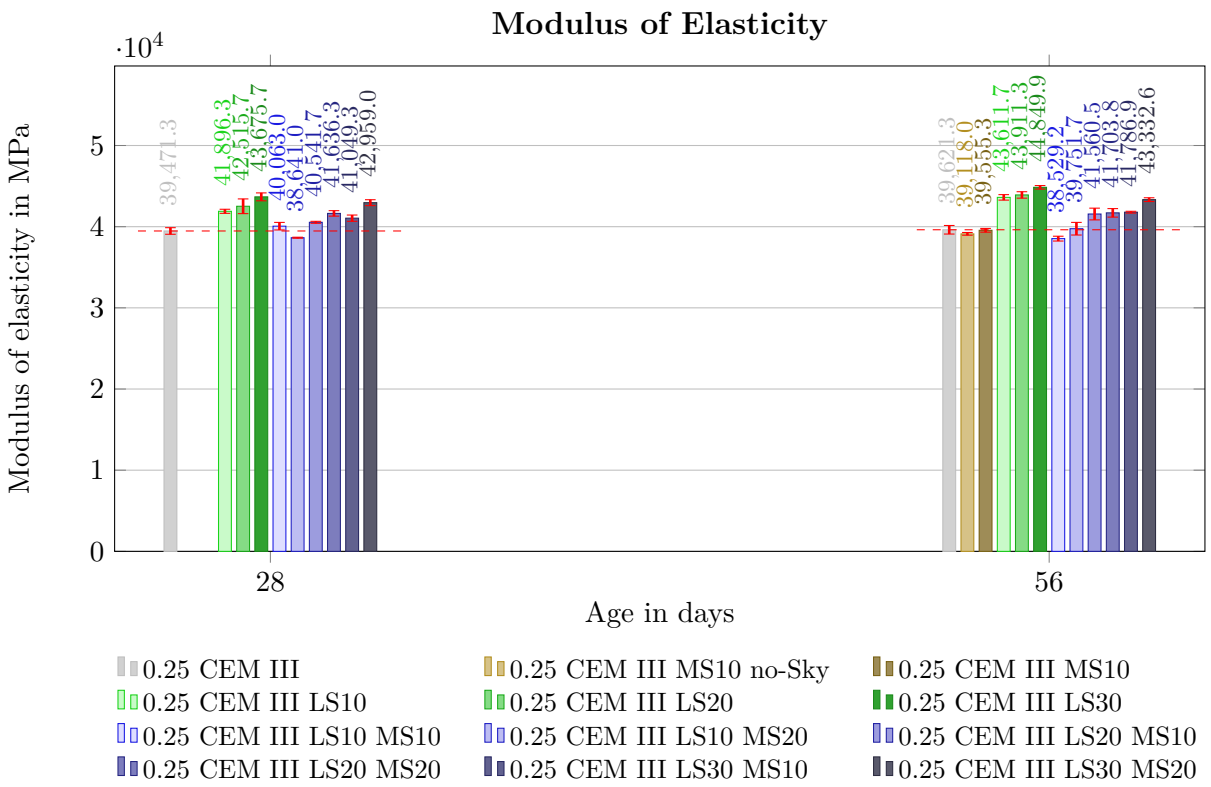

Fig. 4.33: Modulus of Elasticity - Influences of Additives Compared

This chart appears, as the combination charts above, overloaded at first glance, but it represents the relations of the influences. It can be observed, that all of the mixes are at least around the same value as the reference mix, with almost all mixes being clearly higher. The biggest impact can be observed with the mixes containing limestone powder, where the E-mod is significantly higher compared to the reference mix or the mixes containing both, LS and MS.

Comparison of Mixtures Including 10% LS

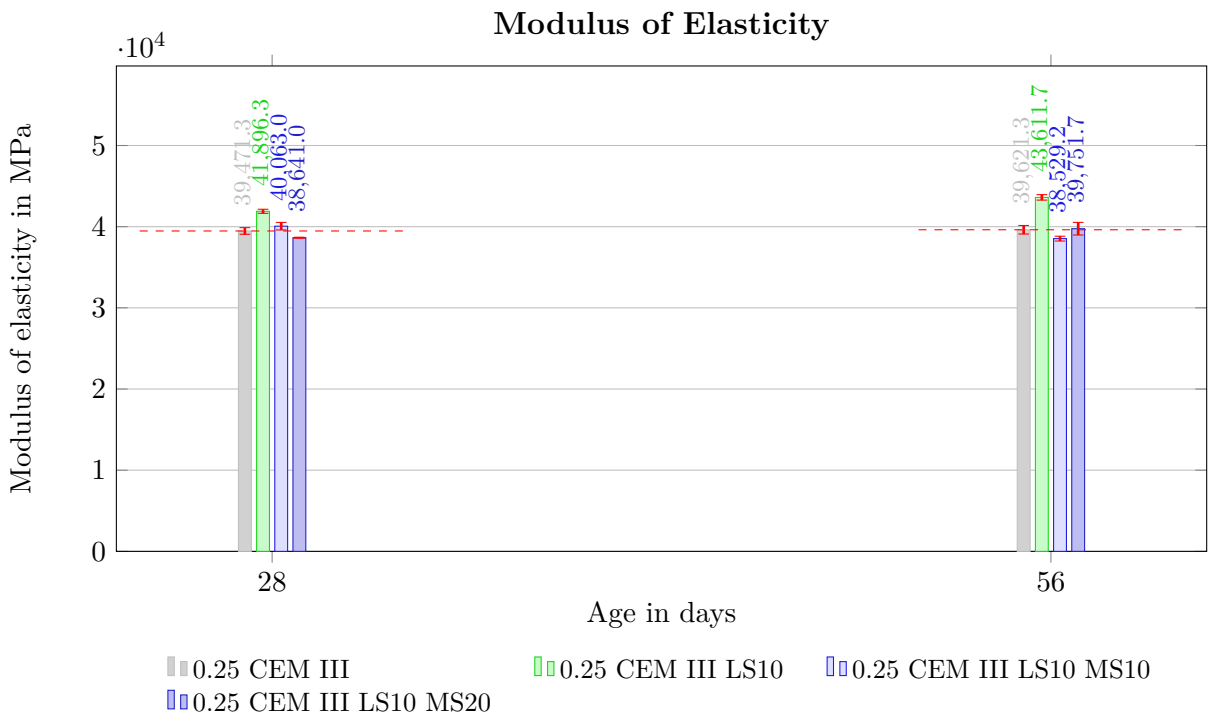

Fig. 4.34: Modulus of Elasticity - Influence LS10

Figure 4.34 compares all mixtures including 10% LS. It is evident, that limestone has a positive effect on the modulus of elasticity and microsilica reducing it. The combination of both additives results in a E-mod similar to that of the reference mix, *0.25 CEM III*. This applies to both, 28 and 56 days.

Comparison of Mixtures Including 20% LS

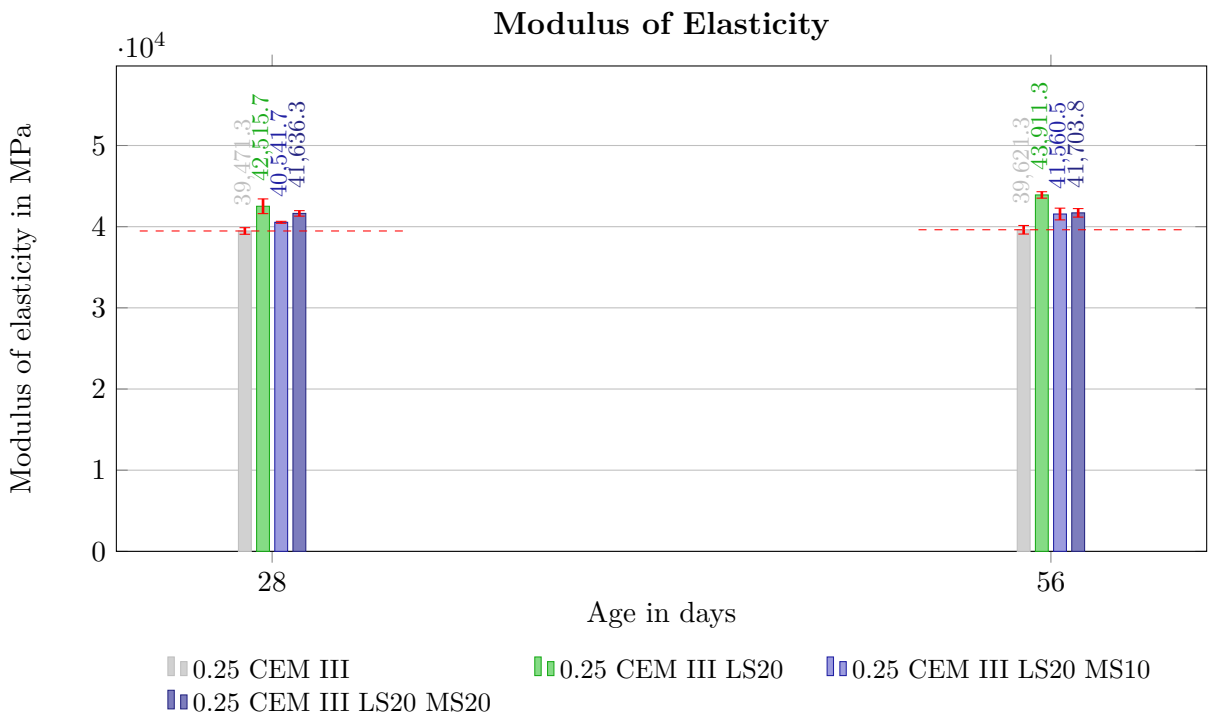

Fig. 4.35: Modulus of Elasticity - Influence LS20

The mixes including 20% LS show a more significant improvement compared to the reference mixture. Although small amounts of MS is reducing the E-mod, the limestone amount is high enough for the mixture ending up to be higher then the reference mix for 28 and 56 days.

Comparison of Mixtures Including 30% LS

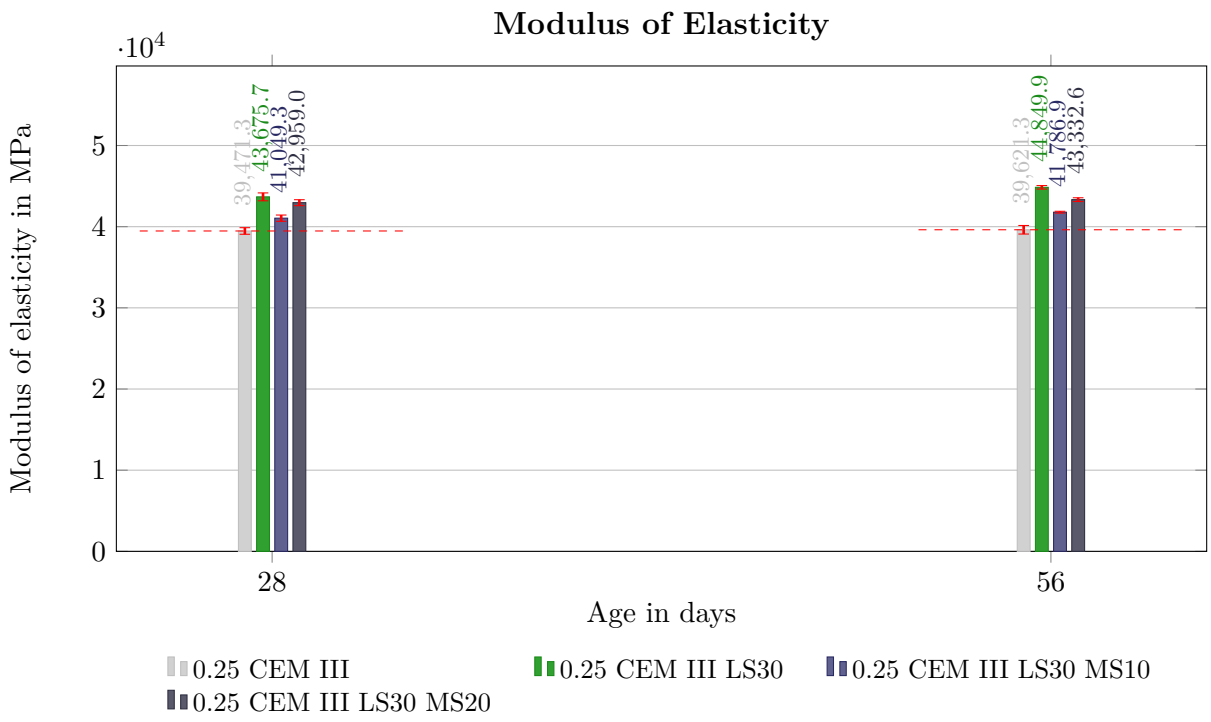

Fig. 4.36: Modulus of Elasticity - Influence LS30

The same pattern, even more pronounced is showing for the mixes with 30% limestone powder included. This applies to both, 28 and 56 days.

Modulus of Elasticity with Surplus Water Considered

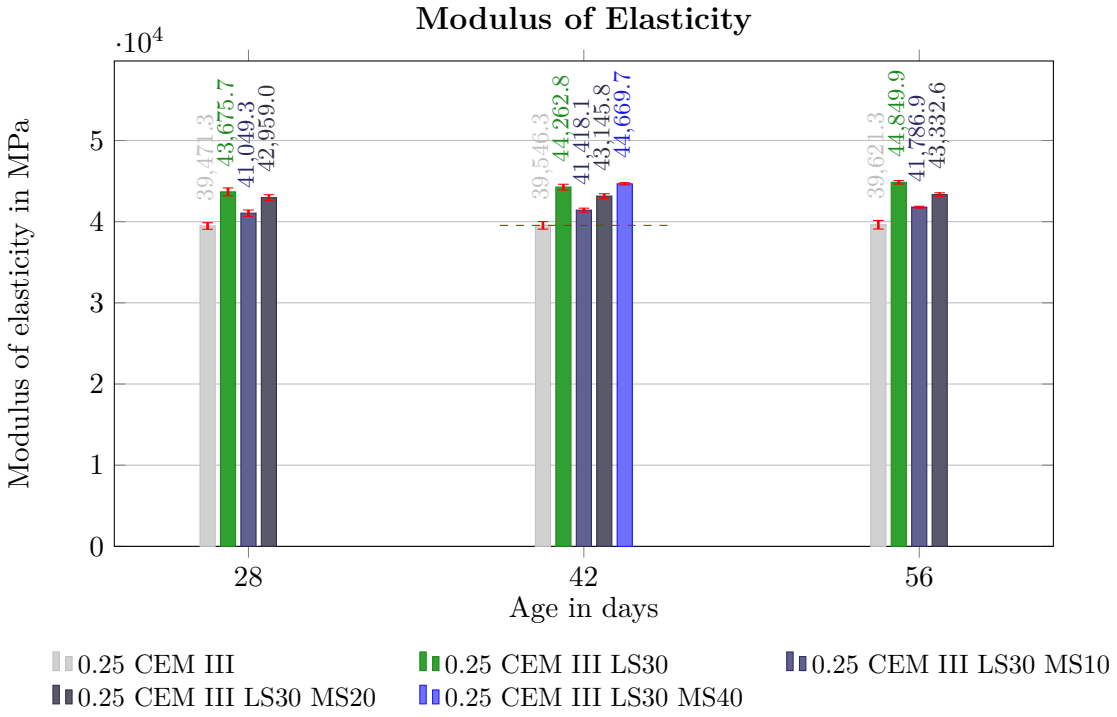

Fig. 4.37: Modulus of Elasticity - with Considered Packing Density

As with compression and bending tensile strength, the E-mod was also elevated after 42 days. To enable comparison with the other test data, the results for 28 and 56 days were linearly interpolated, providing a reasonable estimation. As expected, the modulus of elasticity was rising equivalently with the compression strength. At 42 days of age it shows a much higher modulus of elasticity compared to the reference mix. The value is slightly higher than the one of 30% limestone powder only without microsilica added to the mix. Interestingly, when a little bit of silica fume is added, the modulus of elasticity reduces clearly with almost 10%. Then, when more and more silica fume is added, it will increase again. The value of *0.25 CEM III LS30* is then exceeded.

Chapter 5

Conclusion

With this thesis, it was shown that it is possible to create UHPC using *CEM III/B* in similar ways as with conventional cement. Since the building sector, and cement in particular, is a major source of CO_2 emissions world wide [66], the usage of *CEM III/B* could be a step into the right direction, although it has not the potential to change the industry, simply because most of the slag from steel production is already used [56]. It will need much more than just one alternative to conventional cement to have a significant impact on the emissions. Fortunately, a lot of research is done lately and promising alternatives are being tested. After spending the last decades to increase the strengths of concrete more and more, the main focus may now shift towards research to achieve these values with more environmentally friendly alternatives.

The results for strengths of the discussed mixes have been excellent, with compression strengths exceeding 135 MPa and bending tensile strengths reaching up to 20 MPa. The addition of steel-fibre reinforcement is expected to significantly increase these strengths further and should be studied in a following thesis. Additives in general had a positive effect on the strengths, although a rising amount of LS led to problems with the workability and flowability, with a strong shear thickening effect occurring proportionally with the amount of LS added.

After some trial and error, the primary cause for that was identified as packing density. Considerations have been made and the mixture calculation was updated to avoid this issue. The mixture design was revised, supplemented with the important parameter *surplus water*, which indicates the difference between the water demand and void volume. This value needs to be positive for every mixture and was initially negative for some mixes. The packing density has an important role in the mixture calculation, directly influencing the bulk volume and therefore also the void volume and ultimately, the surplus water. With an increased amount of silica fume, the voids between cement and limestone particles have been filled up. The water there was displaced and now acted as excess water or surplus water to increase the flowability.

Although the main issue was identified, there are still some questions left. Why is this problem more pronounced with CEM III/B compared to CEM I or even Portland Composite Cement (CEM II)? Is it due to chemical or physical factors? Could it be related to the particle shape or size distribution? These questions should be observed in future research or thesis.

Personally, as a structural engineer with at least some experience with large projects, I think the goal has to be to find cost-effective environmentally friendly alternatives – the economy will always decide on the best price to value ratio, unless there are government restrictions. I hope there will be more alternatives to be developed and I hope to encounter them in my career and maybe have a pioneer project with some sustainable cement alternative.

List of Tables

List of Figures

Bibliography

[1] S. Adu-Amankwah, M. Zajac, C. Stabler, B. Lothenbach, and L. Black. "Influence of limestone on the hydration of ternary slag cements". In: *Cement and Concrete Research* 100 (2017), pp. 96–109. ISSN: 0008-8846. DOI: https://doi.org/10.1016/j.cemconres.2017.05.013. URL: https://www.sciencedirect.com/science/article/pii/S0008884616304914.

[2] T. Ahmed, D. M. Elchalakani, A. Karrech, M. Ali, and L. Guo. "Development of ECO-UHPC with very-low-C3A cement and ground granulated blast-furnace slag". In: *Construction and Building Materials* 284 (May 2021), p. 15. DOI: 10.1016/j.conbuildmat.2021.122787.

[3] A. K. Akhnoukh and C. Buckhalter. "Ultra-high-performance concrete: Constituents, mechanical properties, applications and current challenges". In: *Case Studies in Construction Materials* (2021), p. 10. ISSN: 2214-5095. DOI: https://doi.org/10.1016/j.cscm.2021.e00559. URL: https://www.sciencedirect.com/science/article/pii/S2214509521000747.

[4] M. Amran, S.-S. Huang, A. M. Onaizi, N. Makul, H. S. Abdelgader, and T. Ozbakkaloglu. "Recent trends in ultra-high performance concrete (UHPC): Current status, challenges, and future prospects". In: *Construction and Building Materials* (2022), p. 34. ISSN: 0950-0618. DOI: https://doi.org/10.1016/j.conbuildmat.2022.129029. URL: https://www.sciencedirect.com/science/article/pii/S0950061822026848.

[5] M. Amran, S.-S. Huang, A. M. Onaizi, N. Makul, H. S. Abdelgader, and T. Ozbakkaloglu. "Recent trends in ultra-high performance concrete (UHPC): Current status, challenges, and future prospects". In: *Construction and Building Materials* 352 (2022), p. 129029. ISSN: 0950-0618. DOI: https://doi.org/10.1016/j.conbuildmat.2022.129029. URL: https://www.sciencedirect.com/science/article/pii/S0950061822026848.

[6] C. Andrade and J. Torres. "Long term carbonation of UHPC". In: *Proceedings of International Symposium on Ultra-High Performance Fiber-Reinforced Concrete. Marseille, France.* Vol. 256. 2013.

[7] P. Astle. *How can we reduce the embodied carbon of structural concrete?* 2021. DOI: https://doi.org/10.56330/NWSR6863. URL: https://www.istructe.org/journal/volumes/volume-99-(2021)/issue-2/how-can-we-reduce-the-embodied-carbon-of-concrete/ (visited on 05/09/2024).

[8] N. Azmee and N. Shafiq. "Ultra-high performance concrete: From fundamental to applications". In: *Case Studies in Construction Materials* (2018), p. 15. ISSN: 2214-5095. DOI: https://doi.org/10.1016/j.cscm.2018.e00197. URL: https://www.sciencedirect.com/science/article/pii/S2214509518301360.

[9] M. Bajaber and I. Hakeem. "UHPC evolution, development, and utilization in construction: a review". In: *Journal of Materials Research and Technology* 10 (2021), pp. 1058–1074. ISSN: 2238-7854. DOI: https://doi.org/10.1016/j.jmrt.2020.12.051. URL: https://www.sciencedirect.com/science/article/pii/S223878542032127X.

[10] F. Binici, M. Akcan, E. Mustafaraj, M. Corradi, and Y. Yardim. "Physical–Mechanical and Mineralogical Properties of Fired Bricks of the Archaeological Site of Harran, Turkey". In: *Heritage* (Sept. 2020), pp. 1018–1035. DOI: 10.3390/heritage3030055.

[11] M. C. Block. *The Most Effective Concrete Curing Methods: Know Before Curing*. 2022. URL: https://mirconcreteblock.com/blog/the-most-effective-concrete-curing-methods-know-before-curing/ (visited on 09/12/2024).

[12] X. Dai. "Experimental Study on Compressive Strength of Concrete Under Simple Curing and Encased in Steel Mould". In: *Journal of Civil Engineering and Construction* 13 (June 2024), pp. 67–75. DOI: 10.32732/jcec.2024.13.2.67.

[13] *DIN EN 12350-5:2019: Prüfung von Frischbeton - Teil 5: Ausbreitmaß*. Deutsch. Berlin: DIN Deutsches Institut für Normung e. V., Sept. 2019.

[14] *DIN EN 12350-9:2010: Prüfung von Frischbeton - Teil 9: Selbstverdichtender Beton - Auslauftrichterversichen*. Deutsch. Berlin: DIN Deutsches Institut für Normung e. V., Sept. 2010.

[15] *DIN EN 12390-13:2021: Prüfung von Festbeton – Teil 13: Bestimmung des Elastizitätsmoduls unter Druckbelastung (Sekantenmodul)*. Deutsch. Berlin: DIN Deutsches Institut für Normung e. V., Nov. 2021.

[16] *DIN EN 12390-2:2019: Prüfung von Festbeton - Teil 2: Herstellung und Lagerung von Probekörpern für Festigkeitsprüfungen*. Deutsch. Berlin: DIN Deutsches Institut für Normung e. V., Oct. 2019.

[17] *DIN EN 196-1:2016: Methods of testing cement – Part 1: Determination of strength*. Deutsch. Berlin: DIN Deutsches Institut für Normung e. V., Nov. 2016.

[18] E. Dr.-Ing, M. Habil, J. Walraven, T. Leutbecher, and S. Fröhlich. *Ultra-High Performance Concrete UHPC: Fundamentals, Design, Examples*. Wilhelm Ernst & Sohn, Aug. 2014, p. 192. ISBN: 978-3-433-03087-5. DOI: 10.1002/9783433604076.

[19] circular ecology. *ICE V3.0 Beta 2019*. 2019. URL: https://circularecology.com/embodied-carbon-footprint-database.html (visited on 08/01/2024).

[20] W. Eden. "Einfluss der Verdichtung von Kalk-Sand-Rohmassen auf die Scherbenrohdichte von Kalksandsteinen". PhD thesis. Universität Kassel, Jan. 2011.

[21] Y. Elakneswaran, T. Nawa, and K. Kurumisawa. "Zeta potential study of paste blends with slag". In: *Cement and Concrete Composites* 31.1 (2009), pp. 72–76. ISSN: 0958-9465. DOI: https://doi.org/10.1016/j.cemconcomp.2008.09.007. URL: https://www.sciencedirect.com/science/article/pii/S0958946508001200.

[22] I. Ferroglobe USA Silica Fume Sales. *Ferroglobe Silica Fume: An Environmental Product Declaration*. 2024. URL: https://pcr-epd.s3.us-east-2.amazonaws.com/1107.EPD_Ferroglobe_Silica_Fume.pdf (visited on 09/29/2024).

[23] D. Gastaldi, F. Bertola, S. Irico, G. Paul, and F. Canonico. "Hydration behavior of cements with reduced clinker factor in mixture with sulfoaluminate binder". In: *Cement and Concrete Research* 139 (Jan. 2021), p. 106261. DOI: 10.1016/j.cemconres.2020.106261.

[24] B. Gates. *How to avoid a climate disaster: The solutions we have and the breakthroughs we need*. Harlow, England: Penguin Books, 2022. ISBN: 978-0-141-99301-0.

[25] O. P. Gibbons and J. J. Orr. *How to calculate embodied carbon (Second edition)*. England: IStructE Ltd, 2022. ISBN: 978-1-906335-56-4.

[26] G. Heirman, L. Vandewalle, D. Van Gemert, and Ó. Wallevik. "Integration approach of the Couette inverse problem of powder type self-compacting concrete in a wide-gap concentric cylinder rheometer". In: *Journal of Non-Newtonian Fluid Mechanics* 150.2 (2008), p. 11. ISSN: 0377-0257. DOI: https://doi.org/10.1016/j.jnnfm.2007.10.003. URL: https://www.sciencedirect.com/science/article/pii/S0377025707002108.

[27] Holcim (Österreich) GmbH. *Produktdatenblatt "DER BLAUE"*. 2023. URL: https://www.holcim.at/fileadmin/Bibliothek/2_Zement/PDBL2023/PDBL_Der_Blaue_Mannersdorf.pdf (visited on 05/23/2024).

[28] Holcim (Österreich) GmbH. *Produktdatenblatt "ECO Planet VIOLETT"*. 2023. URL: https://www.holcim.at/fileadmin/Bibliothek/2_Zement/PDBL2023/PDBL_ECOPlanet_Violett_Retznei.pdf (visited on 05/23/2024).

[29] Housing News Desk. *UHPC: Everything you Need to Know*. 2023. URL: https://housing.com/news/all-about-uhpc/ (visited on 05/12/2024).

[30] A. Jaafer and S. Resan. "Punching Shear Strength of Self Compacted Ferrocement Slabs". In: *Journal of Engineering* 21 (Feb. 2015). DOI: 10.31026/j.eng.2015.02.04.

[31] A. Kashani, J. L. Provis, G. G. Qiao, and J. S. van Deventer. "The interrelationship between surface chemistry and rheology in alkali activated slag paste". In: *Construction and Building Materials* 65 (2014), pp. 583–591. ISSN: 0950-0618. DOI: https://doi.org/10.1016/j.conbuildmat.2014.04.127. URL: https://www.sciencedirect.com/science/article/pii/S0950061814004607.

[32] H. Kemer, R. Bouras, N. Mesboua, M. Sonebi, and O. Kinnane. "Shear-thickening behavior of sustainable cement paste — Controlling physical parameters of new sources of supplementary cementitious materials". In: *Construction and Building Materials* 310 (2021), p. 11. ISSN: 0950-0618. DOI: https://doi.org/10.1016/j.conbuildmat.2021.125277. URL: https://www.sciencedirect.com/science/article/pii/S095006182103018X.

[33] M. Kępniak, P. Woyciechowski, and W. Franus. "Transition Zone Enhancement with Waste Limestone Powder as a Reason for Concrete Compressive Strength Increase". In: *Materials* 14 (Nov. 2021), p. 7254. DOI: 10.3390/ma14237254.

[34] M. H. Lai and J. Ho. "Cause and mitigation of dilatancy in cement powder paste". In: *Construction and Building Materials* 236 (Jan. 2020), p. 12. DOI: 10.1016/j.conbuildmat.2019.117595.

[35] J. Li, Z. Wu, C. Shi, Q. Yuan, and Z. Zhang. "Durability of ultra-high performance concrete – A review". In: *Construction and Building Materials* 255 (Sept. 2020), p. 13. DOI: 10.1016/j.conbuildmat.2020.119296.

[36] T. Lysett. *Ultra-High Performance Concrete (UHPC): Fundamentals & Applications*. 2018. URL: https://cor-tuf.com/ultra-high-performance-concrete-uhpc-fundamentals-applications/ (visited on 05/13/2024).

[37] K. Ma, J. Feng, G. Long, and Y. Xie. "Effects of mineral admixtures on shear thickening of cement paste". In: *Construction and Building Materials* 126 (2016), pp. 609–616. ISSN: 0950-0618. DOI: https://doi.org/10.1016/j.conbuildmat.2016.09.075. URL: https://www.sciencedirect.com/science/article/pii/S0950061816315161.

[38] W. Matthes, A. Vollpracht, Y. Villagran Zaccardi, S. Kamali-Bernard, D. Hooton, E. Gruyaert, M. Soutsos, and N. De Belie. *Ground granulated blast-furnace slag*. eng. Ed. by N. De Belie, M. Soutsos, and E. Gruyaert. Vol. 25. RILEM STATE-OF-THE-ART REPORTS. Springer Nature, 2018. ISBN: 9783319706054. URL: http://doi.org/10.1007/978-3-319-70606-1_1.

[39] J. Maybury, J. Ho, and S. Binhowimal. "Fillers to lessen shear thickening of cement powder paste". In: *Construction and Building Materials* 142 (July 2017), pp. 268–279. DOI: 10.1016/j.conbuildmat.2017.03.076.

[40] B. Mercado-Borrayo, R. Schouwenaars, J. González-Chávez, and R. M. Zamora. "Multi-analytical assessment of iron and steel slag characteristics to estimate the removal of metalloids from contaminated water". In: *Journal of environmental science and health. Part A, Toxic/hazardous substances & environmental engineering* 48 (July 2013), pp. 887–95. DOI: 10.1080/10934529.2013.761492.

[41] T. G. Mezger. *Angewandte Rheologie: Mit Joe Flow auf der Rheologie-Strasse*. 3. Auflage. Österreich: Anton Paar GmbH, 2017. ISBN: 978-3-200-03652-9.

[42] S. Moula, A. Ben Fraj, T. Wattez, M. Bouasker, and N. B. Hadj Ali. "Mechanical properties, carbon footprint and cost of ultra-high performance concrete containing ground granulated blast furnace slag". In: *Journal of Building Engineering* 79 (2023), p. 107796. ISSN: 2352-7102. DOI: https://doi.org/10.1016/j.jobe.2023.107796. URL: https://www.sciencedirect.com/science/article/pii/S2352710223019769.

[43] mpa: The Concrete Centre. *Concrete carbonation*. [Online; accessed 13-June-2024]. URL: https://www.concretecentre.com/Performance-Sustainability/Whole-life-carbon/Carbonation-of-concrete.aspx.

[44] M. Nehdi. "Why some carbonate fillers cause rapid increases of viscosity in dispersed cement-based materials". In: *Cement and Concrete Research* 30 (Oct. 2000), p. 8. DOI: 10.1016/S0008-8846(00)00353-7.

[45] J. Orr, O. Gibbons, and W. Arnold. "A brief guide to calculating embodied carbon". In: *The Structural Engineer* 98 (July 2020), pp. 22–27. DOI: 10.56330/JZNX5709.

[46] A. Ostadfar. "Chapter 1 - Fluid Mechanics and Biofluids Principles". In: *Biofluid Mechanics*. Academic Press, 2016, pp. 1–60. ISBN: 978-0-12-802408-9. DOI: https://doi.org/10.1016/B978-0-12-802408-9.00001-6. URL: https://www.sciencedirect.com/science/article/pii/B9780128024089000016.

[47] J. Piérard, B. Dooms, and N. Cauberg. "Evaluation of durability parameters of UHPC using accelerated lab tests". In: *Proceedings of the 3rd International Symposium on UHPC and Nanotechnology for High Performance Construction Materials, Kassel, Germany*. 2012, pp. 371–376.

[48] Portland Cement Association. *Concrete Curing*. 2021. URL: https://jaybird-mfg.com/applications/concrete/concrete-curing/ (visited on 01/03/2024).

[49] P. Prem, B. Bharatkumar, and N. Iyer. "Influence of curing regimes on compressive strength of ultra high performance concrete". In: *Sadhana* 38 (Dec. 2013). DOI: 10.1007/s12046-013-0159-8.

[50] S. Ram, A. Dengri, and R. Kumar. "Assessment of Compressive Strength in Ordinary Portland Cement Concrete: A Study of Curing Methods and Duration". In: *Evergreen* 11 (Apr. 2024), pp. 640–651. DOI: 10.5109/7183321.

[51] H. Ritchie. "What share of global CO2 emissions come from aviation?" In: *Our World in Data* (2024). https://ourworldindata.org/global-aviation-emissions.

[52] R. Romjon. *Concrete: The movement towards a phase of sustainability*. 2014. URL: https://concrete-limestone.wixsite.com/sustainable-concrete/particle-packing (visited on 07/23/2024).

[53] Rooflock. *What is Concrete Carbonation and how is it treated?* [Online; accessed 13-June-2024]. July 2019. URL: https://www.rooflock.com/concrete-carbonation/.

[54] R. Rostami, A. Klemm, and F. Almeida. "The Effect of SCMs in Blended Cements on Sorption Characteristics of Superabsorbent Polymers". In: *Materials* 14 (Mar. 2021), p. 21. DOI: 10.3390/ma14071609.

[55] A. Sand. *The importance of curing in construction*. 2024. URL: https://www.alphasand.in/blog/importance-of-curing-in-construction (visited on 09/12/2024).

[56] M. Schneider. *Buildings & Infrastructure Priority Actions for Sustainability: Embodied Carbon: Concrete*. London, England, 2023. URL: https://www.istructe.org/IStructE/media/Public/Resources/ARUP-Embodied-carbon-concrete_1.pdf.

[57] M. Schneider. "The cement industry on the way to a low-carbon future". In: *Cement and Concrete Research* 124 (2019), p. 19. ISSN: 0008-8846. DOI: https://doi.org/10.1016/j.cemconres.2019.105792. URL: https://www.sciencedirect.com/science/article/pii/S0008884619301632.

[58] F. Schwanda. "Der Hohlraumgehalt von Korngemischen". In: *Beton 9* (1959), H.1.

[59] F. Schwanda. "Der Hohlraumgehalt von Korngemischen - Ein Vergleich rechnerisch gewonnener Werte mit Versuchsmäßig ertmittelten". In: *Beton 9* (1959), H.12.

[60] P. Singniao, M. Sappakittipakorn, and P. Sukontasukkul. "Effect of silica fume and limestone powder on mechanical properties of ultra-high performance concrete". In: *IOP Conference Series: Materials Science and Engineering* 897.1 (July 2020), p. 012009. DOI: 10.1088/1757-899X/897/1/012009. URL: https://dx.doi.org/10.1088/1757-899X/897/1/012009.

[61] P. Singniao, M. Sappakittipakorn, and P. Sukontasukkul. "Effect of silica fume and limestone powder on mechanical properties of ultra-high performance concrete". In: *IOP Conference Series: Materials Science and Engineering* 897 (Aug. 2020). DOI: 10.1088/1757-899X/897/1/012009.

[62] R. Snellings, G. Mertens, and J. Elsen. "Supplementary Cementitious Materials". In: *Reviews in Mineralogy and Geochemistry* 74 (May 2012), pp. 211–278. DOI: 10.2138/rmg.2012.74.6.

[63] M. G. Sohail, R. Kahraman, N. Al Nuaimi, B. Gencturk, and W. Alnahhal. "Durability characteristics of high and ultra-high performance concretes". In: *Journal of Building Engineering* 33 (2021), p. 101669. ISSN: 2352-7102. DOI: https://doi.org/10.1016/j.jobe.2020.101669. URL: https://www.sciencedirect.com/science/article/pii/S2352710220311797.

[64] A. Spasojevic. "Structural implications of ultra-high performance fibre-reinforced concrete in bridge design". PhD thesis. École Polytechnique Fédérale de Lausanne, Jan. 2008. DOI: 10.5075/epfl-thesis-4051.

[65] A. Stangl. "Optimierung der Packungsdichte und Bestimmung der minimal erforderlichen Wasserfilmdiche zur Herstellung von Ultra-Hochleistungsbeton". PhD thesis. Technische Universität Wien, Mar. 2011.

[66] Z. Technologies. *Embodied Carbon: Why Your Clients will be Asking About it (if they aren't already)*. 2021. URL: https://zs2technologies.com/embodied-carbon-why-your-clients-will-be-asking-about-it-if-they-arent-already/ (visited on 05/09/2024).

[67] G. Türedi, Ö. Keskin, and S. Keskin. "Self-Compacting Mortar Production by using Calcium Aluminate Cement". In: *Mugla Journal of Science and Technology* 6 (Sept. 2020). DOI: 10.22531/muglajsci.686144.

[68] United Nations Environment and International Energy Agency. *Towards a zero-emission, efficient, and resilient buildings and construction sector - Global Status Report 2017*. 2017. URL: https://worldgbc.org/wp-content/uploads/2022/03/UNEP-188_GABC_en-web.pdf (visited on 08/02/2024).

[69] United Nations Framework Convention on Climate Change (UNFCCC). *Paris Agreement*. UN Doc. FCCC/CP/2015/L.9/Rev.1. Adopted on 12 December 2015, entered into force on 4 November 2016. URL: https://unfccc.int/sites/default/files/english_paris_agreement.pdf (visited on 04/15/2024).

[70] Wikipedia contributors. *Carbonatation — Wikipedia, The Free Encyclopedia*. [Online; accessed 13-June-2024]. 2023. URL: https://en.wikipedia.org/w/index.php?title=Carbonatation&oldid=1187967249.

[71] M. Yang, Z. He, X. Chen, M. Li, and Z. Peng. "Comparative Study on the Macroscopic and Microscopic Properties of UHPC Mixed with Limestone Powder and Slag Powder". In: *Geofluids* 2021 (Apr. 2021). DOI: 10.1155/2021/5510490.

[72] J. Zhang, H. Ye, X. Gao, and W. Wu. "Adsorption and desorption of polycarboxylate ether superplasticizer in fresh cementitious materials blended with mineral admixtures". In: *Journal of Materials Research and Technology* 17 (Mar. 2022), pp. 1740–1751. DOI: 10.1016/j.jmrt.2022.01.145.

[73] Y.-F. Zhu, R. G. Du, H. Xu, Y. Li, F.-M. Tang, W. Chen, and C.-J. Lin. "Effect of pH on the Corrosion Behavior of Reinforcing Steel in Simulated Concrete Pore Solutions". In: *ECS Transactions* 33.35 (Apr. 2011), p. 77. DOI: 10.1149/1.3577755. URL: https://dx.doi.org/10.1149/1.3577755.

Appendix A

Bending Tensile Strength

The following table Tab. A.1 shows the bending tensile strength results and will be further discussed and interpreted in this appendix.

Tab. A.1: Bending Tensile Test Results

Mix Design	$\sigma_{c,1d}$ [MPa]	$\sigma_{b,7d}$ [MPa]	$\sigma_{b,28d}$ [MPa]	$\sigma_{b,42d}$ [MPa]	$\sigma_{b,56d}$ [MPa]
0.25 CEM III	6.6	8.9	16.4	15.1*	13.9
0.25 CEM III MS10	6.4	12.4	19.0	18.3*	17.5
0.25 CEM III MS10 no Sky	6.0	13.8	18.3	18.5*	18.8
0.28 CEM III	-	-	-	-	-
0.28 CEM III MS10	-	-	-	-	-
0.37 CEM III	-	-	-	-	-
0.25 CEM III LS10	6.7	8.8	17.7	16.6*	15.4
0.25 CEM III LS10 MS10	6.4	10.5	17.5	17.3*	17.1
0.25 CEM III LS10 MS20	6.8	11.8	17.4	18.7*	19.9
0.25 CEM III LS20	6.4	9.2	17.6	16.6*	15.6
0.25 CEM III LS20 MS10	6.0	11.9	16.2	17.0*	17.8
0.25 CEM III LS20 MS20	6.1	12.5	16.3	18.3*	20.3
0.25 CEM III LS30	6.9	11.4	15.4	16.1*	16.8
0.25 CEM III LS30 MS10	6.6	11.4	16.2	17.3*	18.3
0.25 CEM III LS30 MS20	6.5	13.7	18.0	19.8*	21.6
0.25 CEM III LS30 MS40	-	-	-	13.9	-

Results marked with an asterisk (*) are linearly interpolated.

Influence w/c-Ratio and MS

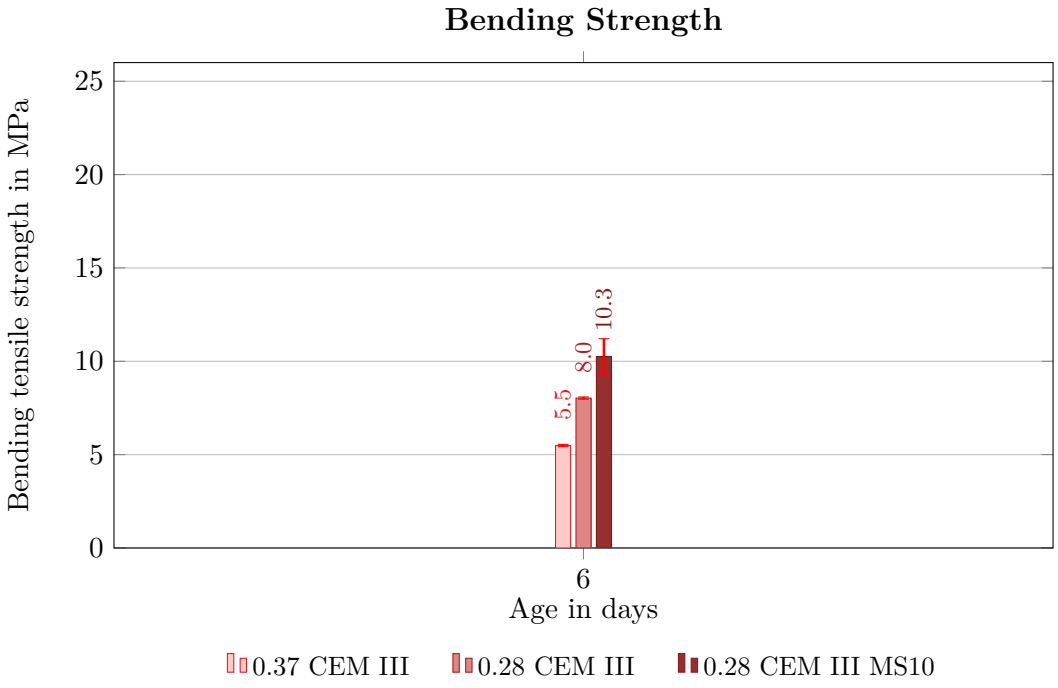

Fig. A.1: Bending Tensile Strength - Influence w/c-Ratio

This chart shows the influence of the w/c ratio on the bending tensile strength. A significant increase in strength of over 50% is observed when reducing the w/c ratio from 0.37 to 0.28. Adding 10% of MS further enhances the tensile strength by approximately 30%. To achieve optimal strength, it is inevitable to keep the w/c ratio as low as workability permits. Initially, a w/c ratio of 0.28 was used, which was later reduced to 0.25. This reduction, while beneficial for strength, introduced some challenges that will be discussed later in this chapter.

Influence Sky

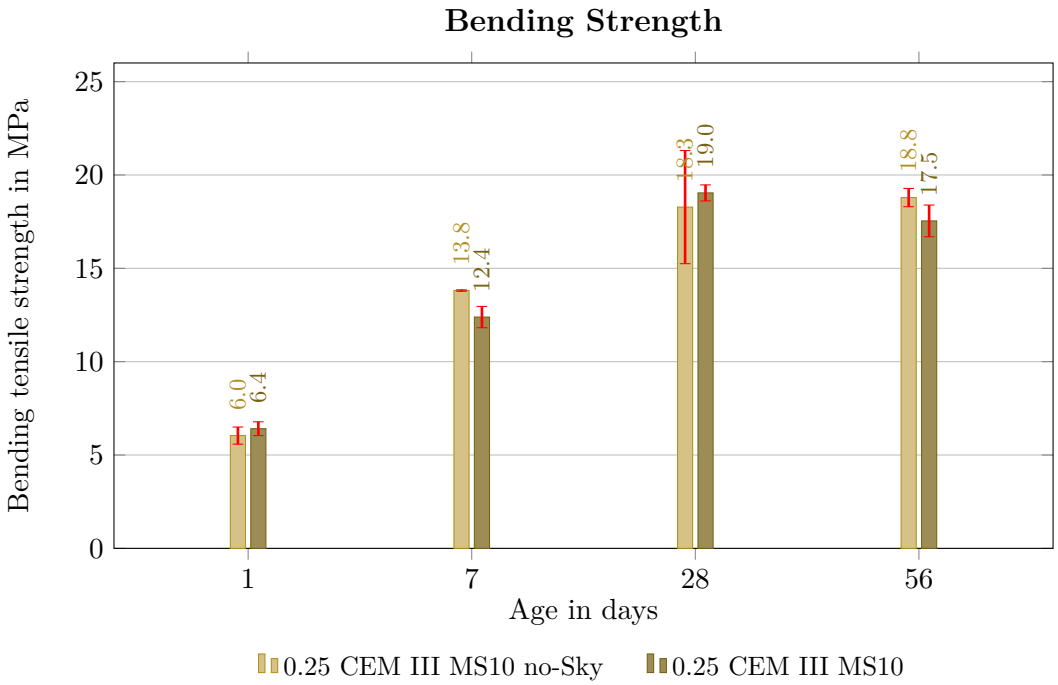

Fig. A.2: Bending Tensile Strength - Influence Sky

While ACE acts as a flow agent, causing the mixture to liquefy, Sky is a consistency holder, delaying the chemical reactions of the mix. While the effect of superplasticizers on compression strength was relatively clear, their impact on bending tensile strength is less obvious. The 28 day value for the mixture without Sky appears to be an outlier due to the high value of the standard deviation. Aside from the first day, the bending tensile strength for mixes without Sky is consistently slightly higher than those with both, ACE and Sky combined, as can be seen in Fig. A.2. In conclusion, neither compression strength nor bending tensile strength is significantly affected by the type of superplasticizer used. Therefore, the choice of superplasticizer should prioritize workability. As already mentioned, the chosen mix consists of approximately 2/3 of ACE and 1/3 of Sky.

Influence Limestone Powder

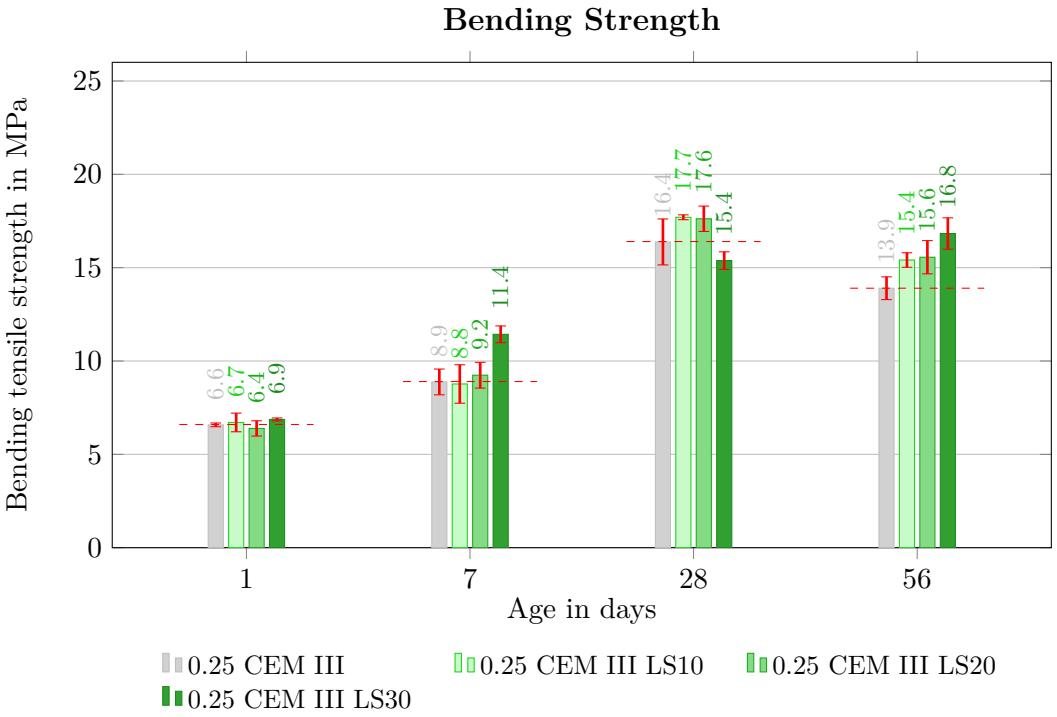

Fig. A.3: Bending Tensile Strength - Influence LS

Limestone powder generally has a positive effect on bending tensile strength, as shown in Fig. A.3. The graph indicates that, with the exception of one test, all mixes containing limestone powder exhibit bending tensile strengths at least equal to that of the reference mix *0.25 CEM III*. The exception is the 28 day result from the mix *0.25 CEM III LS30*. Since the 7 days and the 56 days results are clearly higher then the reference mixture, this is defined as measurement inaccuracy. Limestone powder has a limited influence on early-age strength but offers significant benefits for long-term strength (28 and 56 days). Further, there is noticeable decrease in bending tensile strength after 28 days, for the the mixes containing LS and also for the reference mix.

Influence Silica Fume

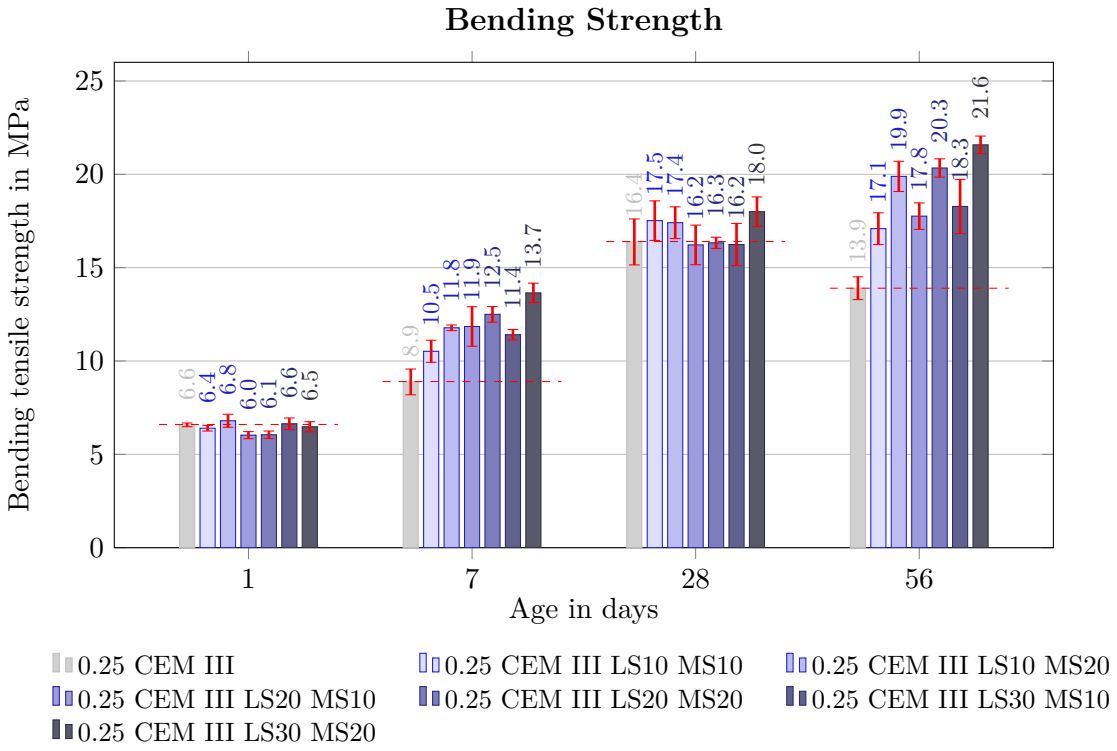

Fig. A.4: Bending Tensile Strength - Influence LS and MS Combined

Silica fume, or microsilica, is primarily used to enhance the workability of the mixture by improving packing density. However, it appears to have a negative impact on bending tensile strength after 1 day. From 7 days onward, the bending tensile strength of mixes including silica fume consistently remains in the same range or is higher than the reference mix. The bending tensile strength of the reference mix decreases between 28 and 56 days. This could be related to an increase in compression strength, which may make the mixture more brittle and prone to cracks from small imperfections. In contrast, the samples containing both LS and MS, maintain or even increase their bending tensile strength. Notably, mixes with 20% silica fume show significantly higher bending tensile strengths after 56 days, compared to those with 10 % microsilica, indicating a unique pattern of improvement with higher MS content.

Influences of Additives Compared

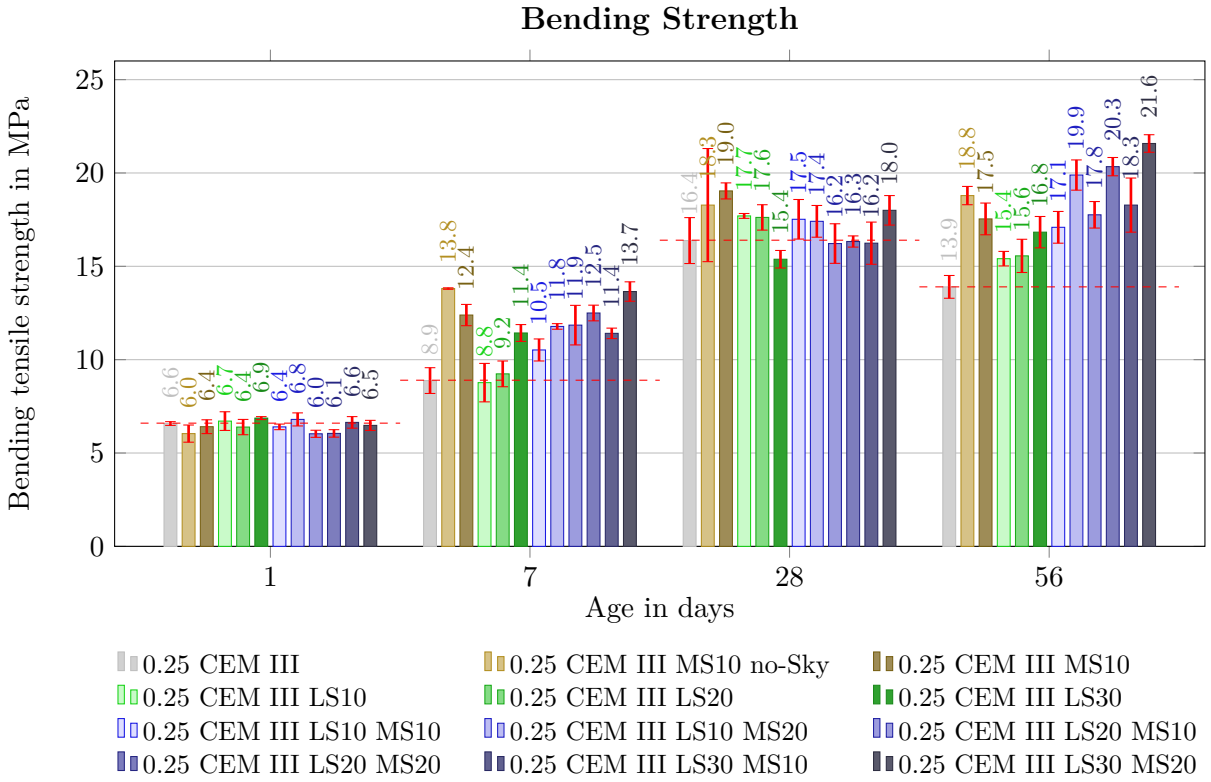

Fig. A.5: Bending Tensile Strength - Influences of Additives Compared

Fig. A.5 might appear overloaded on the first sight, but again provides a comprehensive overview of the influences of different additives on bending tensile strengths. The chart combined the three before mentioned bars into one chart. Similar to the observations for compression strengths, most mixtures that include LS or MS show higher bending tensile strengths compared to the reference mix *0.25 CEM III* without additives. Notably, mixes with MS significantly enhance early-age strength, and has a superior long-term strength compared to the reference mix, simply because it is not decreasing after 28 days. The bending tensile strength improves with increasing amount of silica fume, with the mixes containing 20% MS having a clear advantage over the comparable mixtures with 10% MS added, as can be seen after 56 days. For the 28-day values, the impact of additives on bending tensile strength is generally minimal, though other benefits of using additives, as previously discussed, are still present. As noted earlier, mixtures containing MS tend to exhibit higher early-age strength at 7 days, while long-term strength increases proportionally with the amount of limestone powder added.

Comparison of Mixtures Including 10% LS

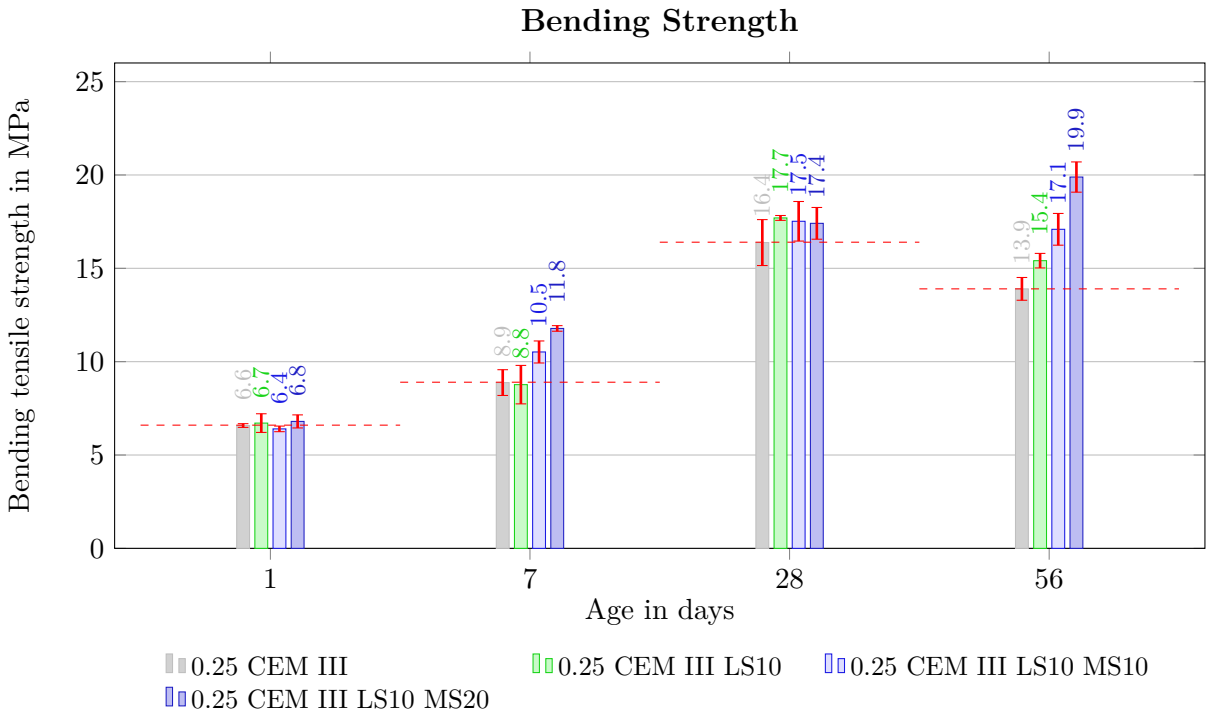

Fig. A.6: Bending Tensile Strength - Comparison of Mixes with 10% LS

For the long-term bending tensile strength, mixes containing 10% limestone powder, show a small improvement over the reference mix, though the difference is relatively modest. While the 28-day values for these mixtures are almost equivalent to the reference mix and show less than a 10% increase, the presence of MS seems to provide a slight advantage. However, the situation changes for the 56-day values. All mixtures with LS significantly exceed the reference mix in strength, with the addition of MS further enhancing this effect. Adding 10% limestone powder increases the bending tensile strength by approximately 10%. Incorporating an additional 10% microsilica raises the strength further, while doubling the amount of microsilica (to 20%) results in an additional 15% increase. Thus, microsilica has a substantial impact on bending tensile strength. For the short-term strength, the 7-day values show a significant effect of additives. After 7 days, limestone doesn't notably affect the results, but silica fume clearly improves the strength, leading to a 20% increase compared to the reference mix.

Comparison of Mixtures Including 20% LS

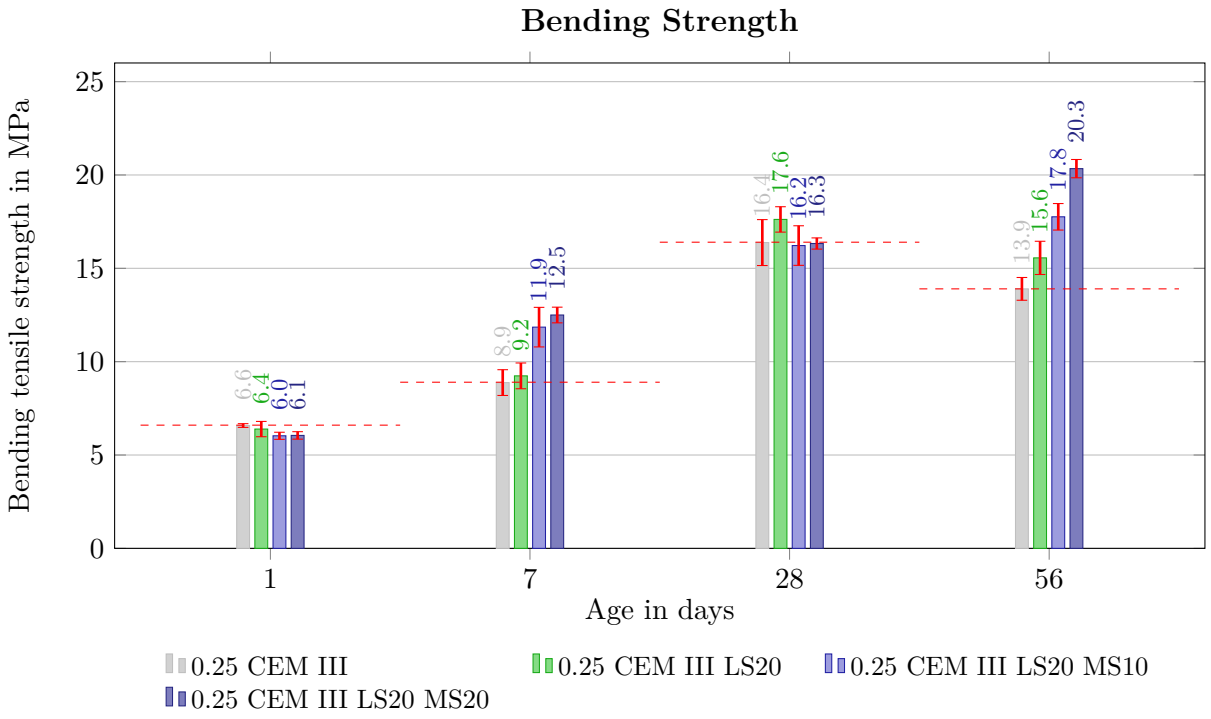

Fig. A.7: Bending Tensile Strength - Comparison of Mixes with 20% LS

The same trend with small differences applies to the mixtures containing 20% LS. In the short term, after 1 day, limestone powder has negligible impact on bending tensile strength, while microsilica shows a slight decrease in strength. After 7 days, limestone still does not have a significant effect, but silica fume notably increases the strength. For long-term performance, after 28 days, the mixtures with 20% LS show a small improvement over the reference mix *0.25 CEM III*, while the strength of mixes including microsilica remains comparable. After 56 days, the graph shows the same pattern as it is described already in the section *Comparison of mixtures including 10% LS*.

Comparison of Mixtures Including 30% LS

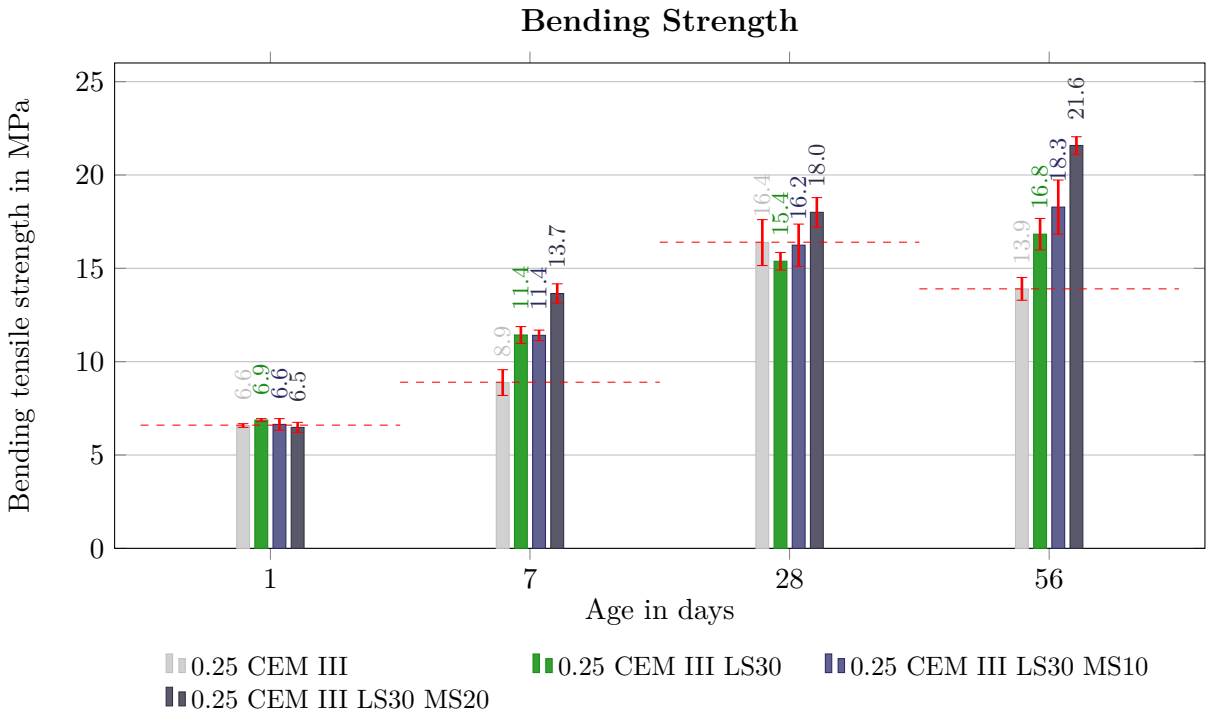

Fig. A.8: Bending Tensile Strength - Comparison of Mixes with 30% LS

One day after molding, no significant effect of limestone or microsilica on bending tensile strength was observed. However, at 7 days of age, LS significantly increases the strength, while 10% MS maintains strength at the same level as the pure LS mix. Adding 20% of microsilica notably improves the strength. At 28 days, mixtures containing only limestone delivers results clearly below the reference mixture *0.25 CEM III*. Adding 10% microsilica brings the strength approximately back to the reference level, and with the MS amount increased to 20%, the bending tensile strength clearly surpasses the reference mix. This trend continues for 56 days, where all mixes show a higher bending tensile strength compared to the reference mix. Specifically, the mixture *0.25 CEM III LS30 MS20* shows a strength over 40% higher then the reference mix.

Bending Tensile Strength Evolution - Influences of Additives Compared

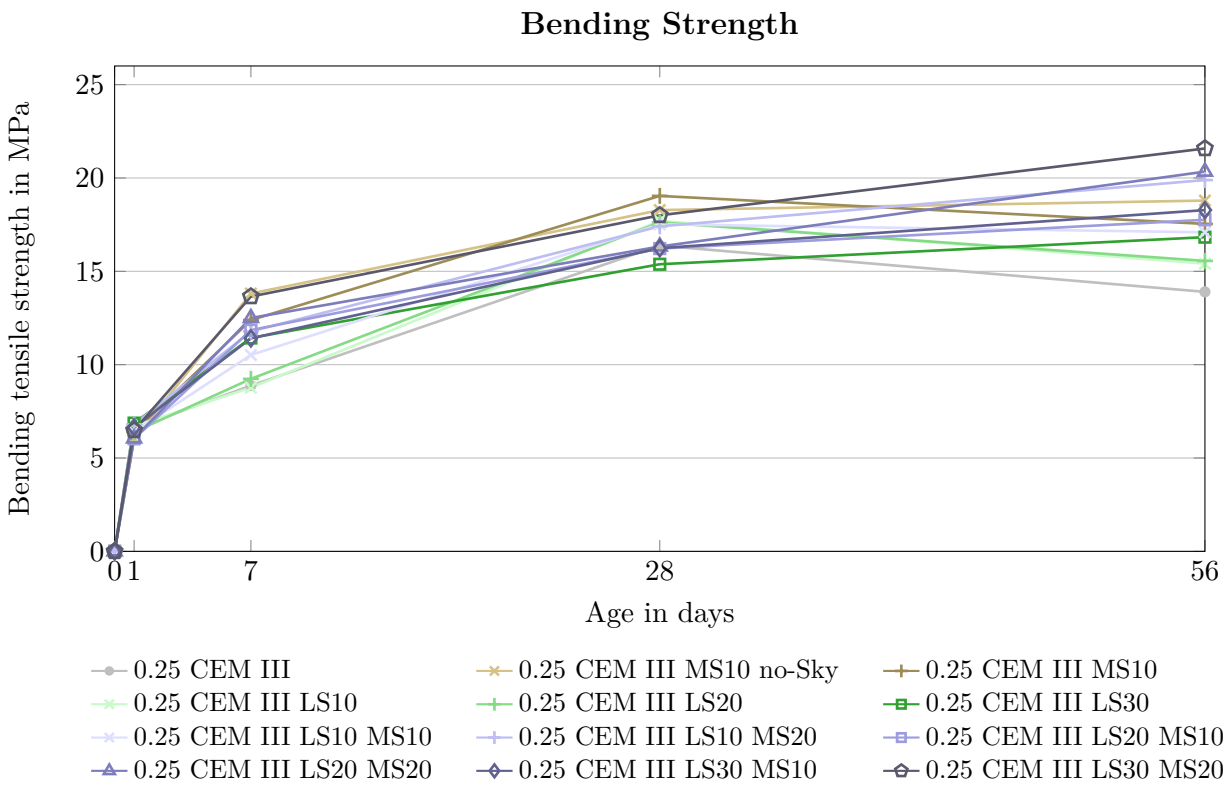

Fig. A.9: Bending Tensile Strength Evolution - Influences of Additives Compared

Figure A.9 illustrates the evolution of the bending tensile strength across different mixtures. It may appear overloaded at first glance, but it effectively demonstrates how the various additives impact both, early-age and long-term strength. After 7 days, microsilica noticeable enhances the strength, with a consistent increase over time, ultimately resulting in the highest long-term strength. In contrast, limestone exhibits a pattern similar to the reference mix *0.25 CEM III*, showing only a slight, negligible improvement at 7 days. Limestone positively affects long-term strength, although only marginally. It is important to mention that LS and MS have other positive effects as well, besides strength improvement. Regarding superplasticizers, mixtures without Sky, or a combination of ACE and Sky, show similar performance over time. While ACE only yields slightly higher early-age strength, the combination of ACE and Sky results in higher strength after 28 days before falling behind again at 56 days.

42d Bending Tensile Strength with Surplus Water Considered

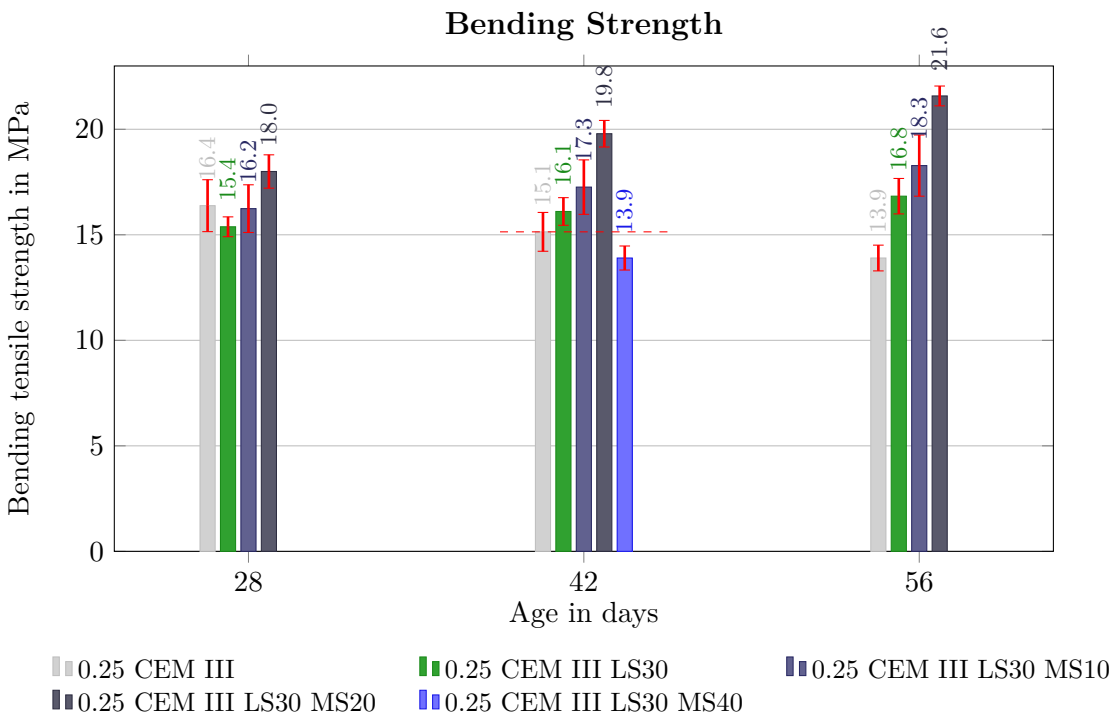

Fig. A.10: Bending Tensile Strength - with Considered Packing Density

To assess the direction of the mix with the significantly increased microsilica (*0.25 CEM III LS30 MS40*, a test was conducted after 42 days. While the other tests were performed after 1, 7, 28 and 56 days, this was not perfectly comparable. However, the 42-day data was approximated by linearly interpolating the values between 28 and 56 days. This approximation provides a reasonably accurate estimation. This plot indicates that the bending tensile strength of the mix containing 40% silica fume is almost 10% lower compared to the reference mix. This result should be cautiously questioned, since we can see a consistent rise of the bending tensile strength with an increasing amount of microsilica. In an upcoming thesis, it should be observed at which value of silica fume it has its maximum bending tensile strength, and if this result is trustworthy and correct. It can also be observed if the reduced bending tensile strength is negligible when there are steel fibres added to the mix that will attract the tension forces.